MANIPULATING FLUIDS: ADVANCES IN
MICRO-FLUIDICS, OPTO-FLUIDICS AND
FLUIDIC SELF ASSEMBLY

Thesis by

Saurabh Vyawahare

In Partial Fulfillment of the Requirements for the

degree of

Doctor of Philosophy

CALIFORNIA INSTITUTE OF TECHNOLOGY

Pasadena, California

2006

(Defended 16th May, 2006)

The efforts of most human-beings are consumed in the struggle for their daily bread, but most of those who are, either through fortune or some special gift, relieved of this struggle are largely absorbed in further improving their worldly lot. Beneath the effort directed toward the accumulation of worldly goods lies all too frequently the illusion that this is the most substantial and desirable end to be achieved; but there is, fortunately, a minority composed of those who recognize early in their lives that the most beautiful and satisfying experiences open to humankind are not derived from the outside, but are bound up with the development of the individual's own feeling, thinking and acting. The genuine artists, investigators and thinkers have always been persons of this kind. However inconspicuously the life of these individuals runs its course, none the less the fruits of their endeavors are the most valuable contributions which one generation can make to its successors....

-Albert Einstein in Emmy Noether's obituary (1935)[1]

---

[1] Quote in my graduate school application, circa 2001. I am happy to report that grad school has not blunted this belief, as yet.

ACKNOWLEDGEMENTS

ABSTRACT

This dissertation describes work in three inter-related areas – micro-fluidics, opto-fluidics and fluidic self-assembly. Micro-fluidics has gotten a boost in recent years with the development of multilayered elastomeric devices made of poly (dimethylsiloxane) (PDMS), allowing active elements like valves and pumps. However, while PDMS has many advantages, it is not resistant to organic solvents. New materials and/or new designs are needed for solvent resistance. I describe how novel fluorinated elastomers can replace PDMS when combined with the three dimensional (3-D) solid printing. I also show how another 3-D fabrication method, multilayer photo-lithography, allows for fabrication of devices integrating filters. In general, 3-D fabrications allow new kinds of micro-fluidic devices to be made that would be impossible to emulate with two dimensional chips.

In opto-fluidics, I describe a number of experiments with quantum dots both inside and outside chips. Inside chips, I manipulate quantum dots using hydrodynamic focusing to pattern fine lines, like a barcode. Outside chips, I describe our attempts to create quantum dot composites with micro-spheres. I also show how evaporated gold films and chemical passivation can then be used to enhance the emission of quantum dots.

Finally, within fluids, self assembly is an attractive way to manipulate materials, and I provide two examples: first, a DNA-based energy transfer molecule that relies on quantum mechanics and self-assembles inside fluids. This kind of molecular photonics mimics parts of the photosynthetic apparatus of plants and bacteria. The second example of self-assembly in fluids describes a new phenomena - the surface tension mediated self assembly of particles like quantum dots and micro-spheres into fine lines. This self assembly by capillary flows can be combined with photo-lithography, and is expected to find use in future nano- and micro-fabrication schemes.

In conclusion, advances in fluidics, integrating materials like quantum dots and solvent resistant elastomers along with 3-D fabrication and methods of self assembly, provide a new set of tools that significantly expand our control over fluids.

TABLE OF CONTENTS

LIST OF ILLUSTRATIONS AND/OR TABLES

NOMENCLATURE

PDMS   Poly (dimethylsiloxane)

MEMS   Micro electromechanical systems

FRET   Fluorescent Resonance Energy Transfer

BSA   Bovine Serum Albumin

PFPE   Photo curable Perfluoro polyether

Qdot   Quantum dot

DNA   Deoxyribonucleic acid

PL   Photoluminescence

3-D   3 Dimensional

Re   Reynold's number

Pe   Peclet's number

Ca   Capillary number

Chapter 1

INTRODUCTION

1.1 Manipulating Fluids: Overview

Manipulating fluids was once only a plumber's preoccupation, but not anymore - with the miniaturization of components, others want to manipulate fluids too, albeit at the micro scale. It might come as a surprise to know that micro-fluidic devices are already quite ubiquitous. Every time you send a document to be printed, you use a microfluidic device. In the same way that miniaturizing electrical circuits led to the electronics and personal computers, one may imagine a future where miniaturizing fluidics components will lead to many new technological benefits in medicine and biology[1, 2]. Naturally, then, the ability to control fluids and to manipulate objects inside them at the micro and nano scales has a recent explosion of work.

Micro-fluidics can largely be divided into two parts – micro-fluidics with hard materials like silicon or plastics, and micro-fluidics with soft materials like elastomeric polymers. For various reasons described later, soft materials have several advantages over hard materials[3]. In this dissertation, I will deal mainly with elastomeric micro-fluidics. Until very recently, most elastomeric devices were made with PDMS. However, PDMS swells up in organic solvents, making it impossible for use in many cases[4]. Newer fluorinated elastomers can replace PDMS, enabling use of organic solvents[5]. But due to problems with bonding, conventional fabrication methods are not suitable with these new materials. Three-dimensional solid printing can solve this problem by eliminating the bonding steps. Three-dimensional fabrication methods also have other advantages for integrating non-fluidic devices with chips, and I demonstrate a case where 3D structures enable incorporation of a silicon filter in a microfluidic chip.

Integrating non-fluidic devices with micro-fluidics is essential for broad applicability of these fluidic chips[6]. Opto-fluidics involves integrating these devices with photonic elements[7]. One essential element of this is the incorporation of light-emitting materials with

chips in the form of quantum dots or dyes. There are several ways to implement opto-fluidics, and I describe some of them in this thesis.

Moreover, manipulating fluids by themselves is not enough; control is also needed over substances inside the fluids. One attractive possibility is self-assembly – the marshalling of forces to automatically assemble structures[8]. I describe two cases involving self assembly at different length scales. In one case, molecular entities assemble by chemical recognition via DNA base-pairing[9]. In the other case, surface tension is used to assemble nano and micro particles[10]. Here, I combine the benefits of conventional micro-fabrication with fluidic self-assembly. Both of these cases demonstrate the utility of self-assembly for manipulating objects inside fluids.

Our ability to make micro-devices out of solids is unparalleled – semiconductor physics and MEMS allow exquisite control over their properties and function. In the future, we may hope for the same type of control over fluids. In a sense, we know this is possible because nature already provides us with extraordinary fluidic devices – marvels of fluidic engineering – that we otherwise know as cells.

1.2 Organization

Chapter 1 describes the current state of micro-fluidics and provides the required orientation to understand the remaining chapters. I describe how multi-layer soft-lithography works in the context of making chips. I also introduce the dimensionless numbers that are relevant for micro-fluidics and finally end by describing the properties of the elastomeric polymer – poly (dimethylsiloxane) (PDMS) that make it such a popular choice, as well its shortcomings.

Chapter 2 describes a number of advances in both in materials and in fabrication. I worked with Mike van Dam on many solvent-resistant materials to replace PDMS and this work is described here. I also discuss why 3-dimensional fabrication strategies are needed and two instances where they were indispensable – wax printing to make one-shot solvent resistant devices (work in collaboration with George Maltezos), and multi-layer photolithography to

incorporate silicon etched filters (work in collaboration with Sven Mathias and Emil Kartalov).

Chapter 3 tackles the new subject of Opto-fluidics, as well as work related to quantum dots. I discuss my attempts to make quantum dots composites (collaboration with Brian Zhou). I also show how the efficiency of quantum dots can be enhanced by either surface plasmon coupling to gold films (collaboration with Koichi Okamoto) or chemical passivation. Finally I describe how hydrodynamic focusing was used to write a quantum dot code (work in collaboration with Aziel C. Epilepsia).

Chapter 4 introduces self-assembling molecular photonic devices made of DNA. I discuss the physics of these devices and describe how I was able to create devices that try to mimic the photosynthetic machinery of bacteria and plants. This work involved collaboration with Shuli Eyal and Keith M. Mathews.

Chapter 5 deals with my discovery of self-assembling fluidic lines which can be used to assemble small particles like micro-spheres and quantum dots. This work was done in collaboration with Kate M. Craig.

Finally, in the appendix, I describe how current elastomeric microfluidic chips are designed.

1.3 Contributions

The original contributions in micro-fluidics, opto-fluidics and self assembly are detailed below:

First, in micro-fluidics, new materials were tested to replace PDMS. These new fluorinated polymers are described. Besides testing materials, I was responsible for coming up with a new material SIFEL, for making micro-fluidics devices. With 3-D fabrication techniques, we have been able to create solvent resistant microfluidic chips. This work has resulted in a patent[11], and a manuscript is in preparation. Work in incorporating silicon filters is also described. This is also a manuscript in preparation.

Second, in the area of opto-fluidics, I contributed to the spectrographic memory project by helping design micro-fluidics chips. This work is published in a conference proceeding[12]. I was also able to build on work done earlier by Aziel Epilepsia and myself to hydro-dynamically focus quantum dots in order to write a code. This work has not been published, but I hope to get it published in the near future. I also describe work on enhancing photoluminescence from quantum dots, a collaboration with Koichi Okamoto which recently resulted in a publication[13].

Third, in self-assembly, I describe how I was able to design 5-dye cascades where energy transferred from one end of the molecule to the other. This work resulted in a publication[9]. Then, I describe a previously unknown phenomenon that I discovered in which capillary flows to create line patterns. I show how these flows can be harnessed to assemble micro and nano particles. This work also resulted in a recent publication[10].

Chapter 2

MICRO-FLUIDICS

2.1 What is Micro-fluidics?

Micro-fluidics may be defined as the manipulation of fluids in channels less than 1 mm but greater than 1 μm in size, in any dimension. If the dimensions are smaller than 1 micron, then we enter the realm of nano-fluidics. Micro-fluidic devices will deal with nano-liters or pico-liter volumes, so the "micro" refers only to the smallest length dimension, not the fluidic volume.

The complete device containing the channels and other micro-sized elements is called a micro-fluidic chip. The control and detection systems are considered to be a part of the chip, unless they are large (> 1 cm), in which case they are usually, and quite arbitrarily, not considered to be a part of the microfluidic chip, although the chip could not function without them.
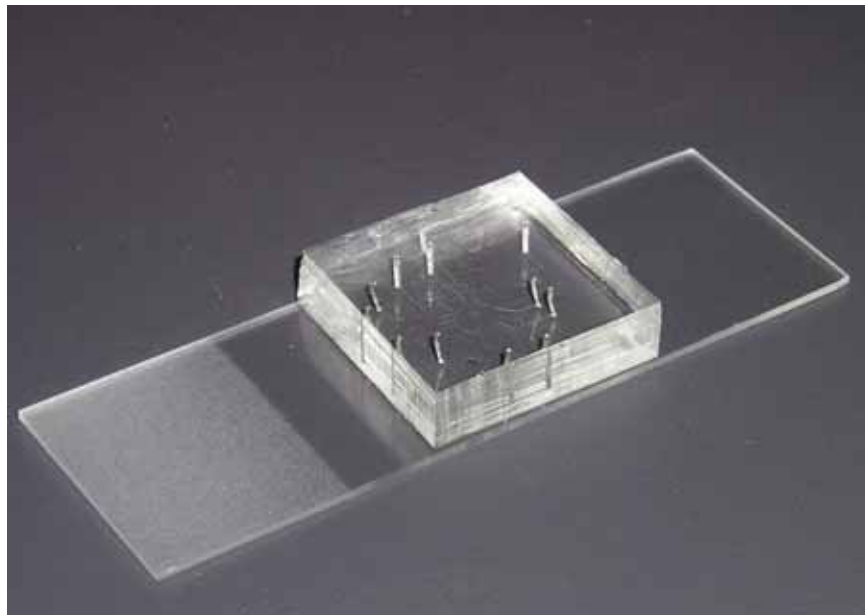
Figure 2.1 Microfluidic Chip. A typical microfluidic chip made by multilayer lithography – the chip is about 1 in square in area and has channels of 100 micron width and 10 micron height.

A large number of reviews on the topic are available, and the pressure to publish ensures that there are new ones written every year[14]. Last year, over 30 reviews with "micro-fluidic" in the title were published[15].

2.2 Brief History

The idea of micro-fluidic chips can be traced back to work done on micro-devices that combined mechanical and electrical elements or Microelectromechanical systems (MEMS). In 1990, Manz et al. designed devices in which analytic procedures could be carried out on fluid streams in microchips[16]. They called this μTAS – micro-total analysis systems - expecting that the chips would be useful in automating chemical analysis procedures. Arguably, this was the start of micro-fluidics. An explosion of papers on micro-fluidic MEMS devices followed, not just for chemical analysis but also in biology, sensing, drug manufacture, micro-reactors and other applications. The moniker "lab-on-a-chip" became very popular for such devices.

In 1998, Whitesides and co-workers described how soft polymers could be used instead of hard materials, and called this process soft-lithography[17]. Soon after, Unger and co-workers were able to design active valves and pumps using multiple layers of soft polymers[18]. Thorsen et al. were able to integrate many of these valves and pumps in ways reminiscent of computer microchips in 2002[19]. Micro-fluidics has now become a well-established field with annual conferences[20] and journals[21] dedicated to it. Figure 1.1 shows that in 2005, nearly two thousand papers on micro-fluidics were published.
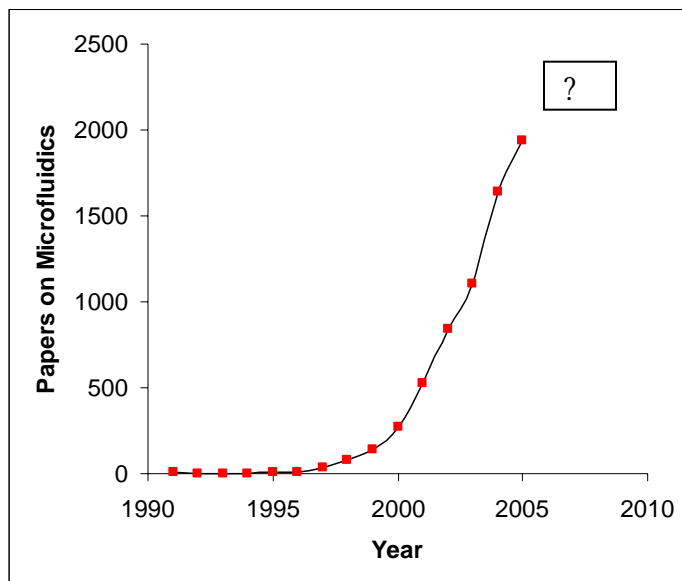
Figure 2.2 Annual Microfluidic Papers Microfluidic papers have seen an explosive increase, especially after 2000. Will this trend continue?

2.3 Soft versus hard materials

Micro-fluidics started out with chips made with hard materials like silicon, in part because the use of hard materials by the MEMS community was well-developed at that time. Recently, however, there has been a shift to soft elastomeric materials[3]. There are several reasons for this, but the biggest is ease of fabrication. The impetus to this change was the fabrication of active valves and pumps in elastomeric devices. Similar active devices in MEMS would require complex fabrication and tens of steps. Elastomeric polymers have other advantages in terms of ability to seal well because of their compressibility. MEMS devices also need high temperatures for fabrication, which may be problematic in many cases.

This change is not unique to micro-fluidics - polymers have started replacing metals and alloys in many industries. This is primarily due to economic factors. Polymers are far cheaper to produce weight-for-weight than alloys and metals. Similarly, elastomeric devices are presently far cheaper to manufacture than MEMS-based devices, sometimes by orders of magnitude.

2.4 Basic Fluid Physics at the micro-scale

Micro-fluidics is also of fundamental scientific interest because of the regime change with regard to physical laws that occurs as we go smaller[22, 23]. For this thesis, there are three important dimensionless numbers to consider[24]: Re - Reynolds's number, Pe – Peclet's number and Ca – capillary number.

In a beautiful talk, Purcell discusses the consequences for bacteria due to their size[25]. In micro-fluidic devices too, like bacteria, the micrometer scale means that flows are characterized by low Reynolds numbers,

$$\mathrm{Re} = \frac{\rho \upsilon l}{\mu} \leq 5$$

where ρ is the density, v the velocity, l a characteristic length scale, and μ the viscosity. This means that inertia becomes irrelevant at these size scales and flows are usually laminar. Turbulence is rare in micro-fluidics, and diffusive mixing is the main way to mix – which brings us to the second kind of dimensionless number, Peclet's number.

$$Pe = \frac{vl}{D}$$

Here, D is diffusion constant, v the velocity and l a characteristic length scale. It describes the competition between convection and diffusion. At low Pe, diffusion dominates over convection. The third dimensionless number is the capillary number, Ca:

$$Ca = \frac{\eta v}{\gamma}$$

where v is the velocity, η the dynamic viscosity and γ the surface tension. It represents the competition between surface tension and convection. We will have a chance to consider this in the future.

In a landmark paper, written in 1989, WSN Trimmer described how different forces scale as the size changes[26]. I summarize this in the table written below:

$[l^1]$	Surface tension; electrostatic forces where $E = [l^{-0.5}]$.
$[l^2]$	Electrostatics where $E = [l^0]$; pressure forces; biological forces; magnetic, where $J = [l^{-1}]$.
$[l^3]$	Magnetics where $J = [l^{-0.5}]$.
$[l^4]$	Magnetics where $J = [l^0]$.

Table 2.3 Scaling of forces with length. l is the length scale.
E the electric field and J the current density. Electromagnetism has
no length scale, so the scaling is dependent of heating effects,
maximum temperature allowable and electric breakdown.

As things become smaller, the forces that are applicable at the different length scales change. The ratio of surface-to-volume scales as the inverse of a length dimension, and this increases enormously as the size scale decreases. One consequence of this is that surface forces become very large at sub-micron scales compared to other forces. The ideal force for micro-devices would be surface tension, but surface tension is a hard force to manipulate. Current microfluidic devices work on a combination of pressure and electromagnetic forces. Both of these will face problems if the size of microfluidic chips gets smaller (i.e. in nano-fluidic chips) and the surface area increases.

In a paper by Jim Brody et al[27], the scaling of a number of important physical quantities is provided. I reproduce a modified version of the table here (Table 1.3):

Quantity	Scaling
Volume	$[l^3]$
Reynolds number	$[l^2]$
Length	$[l]$
Applied Pressure	$[l^0]$
Fluid velocity	$[l^{-1}]$

Surface tension pressure	$[l^{-1}]$
Evaporation rate	$[l^{-1}]$
Diffusion time	$[l^{-2}]$

Table 2.4 Scaling of physical quantities with length

As micro-fluidics becomes smaller, we can tell from this table that diffusion times will decrease, and evaporation rates will also scale up rapidly. Fluid velocities and surface forces will also increase. Pressure is not a strong force when size scale becomes smaller, and inertial effects can be completely neglected compared to viscous effects. These factors need to be kept in mind when thinking about micro-fluidic devices.

2.5 Applications of Micro-fluidics

An advertisement by Caliper[28] shows a couple with a troubled marriage[29]. Their problem: the husband, a post-doc is constantly thinking about work, which involves much pipetting. The solution suggested by their counselor: buy a microfluidic system! The ad shows the couple finally happy together, presumably after having brought the product. Now, microfluidic systems are not nearly so advanced that they can help troubled marriages, but in a number of biological and chemistry processes, they can end the "tyranny of pipettes."

In a review by Michell[30], three main advantages are listed, namely miniaturization, automation and integration. Making smaller channels means that smaller amounts of fluids may be used, leading to saving in cost. In some cases, due to the small amounts of materials available or the explosive nature of the chemicals involved, micro-fluidics may be the only recourse. Another advantage of miniaturization is that things are done faster; the time for an operation usually scales with the linear dimension with an exponent that varies from 0.5 to 1[26]. Heat, mass transfer and catalysis also benefit from miniaturization[2].

Automation allows computers to take care of tedious, mind-numbing tasks that researchers have to constantly perform. If larger amounts of samples are available, one can imagine

dividing them up into multiple parallel channels and automatically testing for thousands of conditions at the same time – in other words, using - parallel high throughput.

Automation also improves safety and reliability. In one case, one of my colleagues had a chemo stat hooked up to a phone[31]. The micro-fluidics system would grow E.coli cells automatically, periodically feeding the cells and cleaning away debris. It would call a phone regularly - one ring would mean everything was fine, two rings, something not quite right, and three rings was the equivalent of "the lab's on fire!"

The third benefit of integration refers to the possibility of integrating various functions on one chip – for instance, filtering can be combined with heating and cooling[32]. It also refers to the possibility of combining other kinds of small non-fluidic devices – microchips, C-MOS detectors, photonic crystals, solid-state lasers, etc. Later in the thesis I shall describe some efforts in this direction.

The fluid properties at the scale of microns also make possible devices that would be impossible otherwise – they involve taking advantage of diffusion and surface area. There are also advantages that accrue from the ability to use less floor space and the fact that smaller devices mean gentler forces on fragile objects like cells.

Irrespective of all these reasons, it is also the case that many researchers, including myself, work in this field for other reasons - not so much that they like the future application possibilities less, but like the intellectual challenges more – the joy of exploring a relatively unexplored nook of science.

Most devices produced till now have been one-paper wonders – rarely mass-produced or sold commercially. The most ubiquitous microfluidic devices are inkjet printers, which manipulate small amounts of fluids to print on paper. A few companies do sell complete microfluidic systems, including Caliper, Fluidigm, Gyros etc.

A literature survey will reveal that multi-layer elastomeric micro-fluidics chips have been used to grow cells[33] and manipulate cells[34], perform PCR[35], synthesize chemicals[36] and crystallize proteins[37] among many other applications.

2.6 Soft Lithography and Poly (dimethylsiloxane)

Soft lithography or replica molding, which came out of the work of Whitesides lab[38] , allows for the molding of structures down to 10 nm in size. This form of replica molding has been rapidly displacing hard materials for micro-fluidics, primarily because of cost and ease of use. The idea behind it is simple – just pour or spin a polymer on top of a mold, usually a two dimensional pattern on top of a flat wafer. The polymer is cross-linked or "cured." It can then be peeled off.

The main polymer used presently is poly (dimethylsiloxane) or PDMS for short PDMS has numerous advantages when used to fabricate microfluidic devices[39]. It is transparent in far UV, visible and near IR (240 nm – 1100 nm), and thus one has optical access to the channels embedded in it. PDMS is cheap (~$20/kg) because of use in the sealing and gasket industries. Being permeable, it allows air to diffuse through it – an advantage for dead-end filling. It seals well to glass and other materials, although this property must be engineered – by itself, PDMS has low surface energy and will not easily bond to other materials. It is bio-compatible and is generally considered safe to work with. Table 1.4 shows its major properties from the Polymer data handbook[40], unless otherwise noted.

Property	Value
Density	0.97 g/cm^3
Young's Modulus	360 - 870 KPa
Poisson's ratio	0.5
Thermal Conductivity	0.15 W/m K
Index of Refraction	1.4
Dielectric constant	2.3-2.8
Specific Heat	1460 J/K m
Magnetic permeability	0.6 x 10^6 cm^3/g
Electric conductivity	4 x 10^{13} ohm-m

Table 2.5 Properties of PDMS

2.7 Elastomeric Valves and Pumps

Multi-layer soft lithography has been extensively reviewed in other references[41], so I won't go into all the details, though I will cover the minimum necessary for a reader to understand this thesis without referring to anything else.

PDMS

A

B

cured PDMS with channel imprint

photolithographically defined relief in photoresist

mold

flat substrate
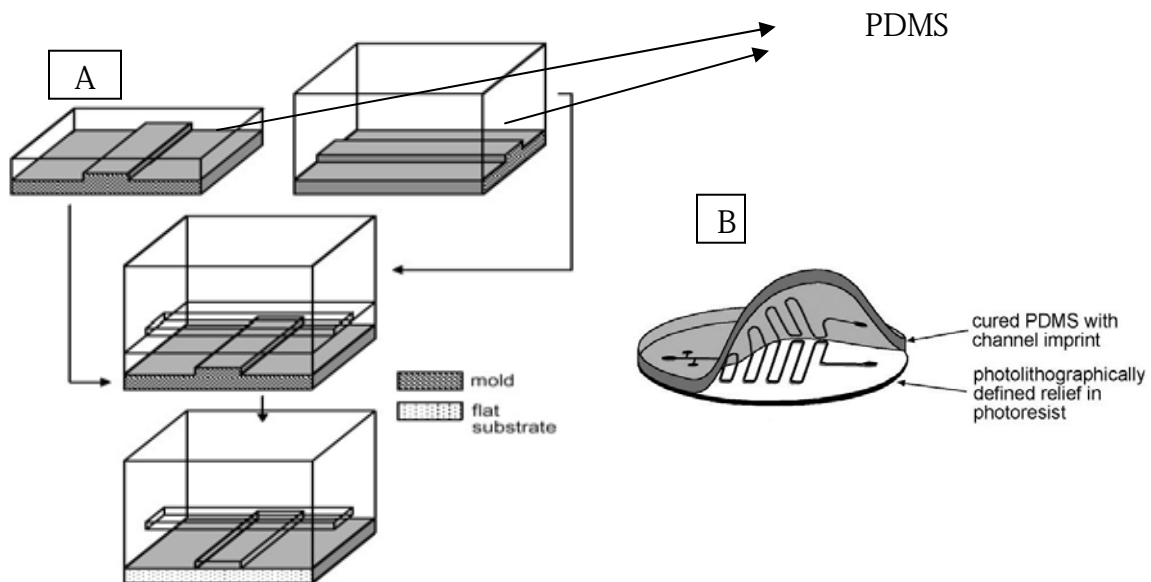
Figure 2.6 Multi-layer Soft Lithography A) Putting together two layers B) Replica Molding of PDMS (from Unger et al[18], copyright American Association for the Advancement of Science, 2000)

The idea is to bond multiple layers of elastomers with channels so that the channels cross each other. The bonding is achieved by using different amounts of a curing agent or an oxygen plasma. Then, if the separation between channels is small and the area overlap is large enough, pressurizing a channel will deflect the membrane between them and seal
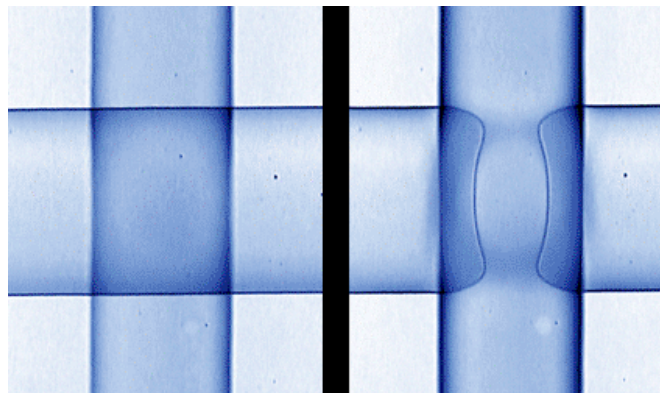
the channel with lower pressure. Thus, a valve is created[42].

One subtle detail is crucial for good sealing – if the channels being closed are square in shape, then the end will stick out, resulting in a leaky valve. So, the channels have to be rounded by resist reflow or other means to make non-leaky-valves[43]. This leaky valve geometry may be an advantage in certain circumstances if larger objects like beads or cells need to be contained, but flow of fluids needs to be allowed.
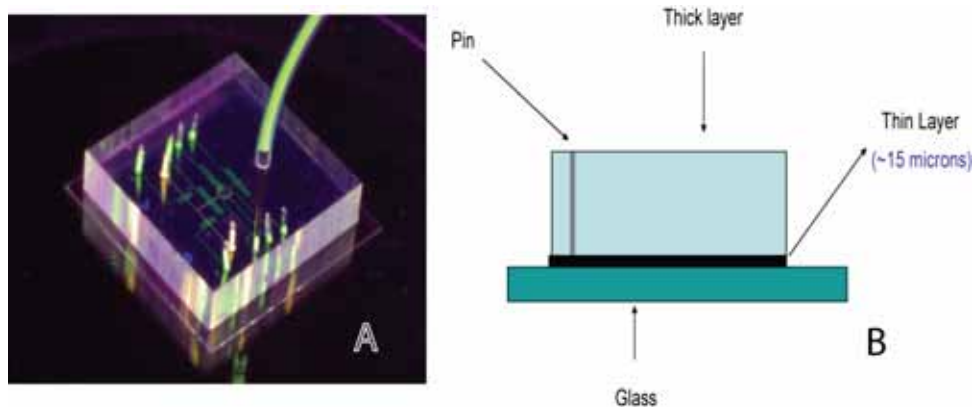
Figure 2.8 Geometry of a Chip. A) Microfluidic chip filled with fluorescent dye. B) Cross section of design with thin and thick layers

If the area of the crossing is not enough, then the channel will not close and we have a cross-over channel. This is useful in complicated geometries where we want channels to cross each other without actuating the valve action.

There are two possibilities for creating valves – the flow channels can be below or above the control channels. These geometries are shown below. In general, the push-down geometry requires higher closing pressures. The advantage that it provides is the direct access to the substrate below, usually glass on which a number or chemical treatments may

be carried out. The push-up geometry has the advantage of creating homogeneous channels surrounded by PDMS (we could also achieve this with push-down by bonding to a thin layer of PDMS on top of a cover-glass.)
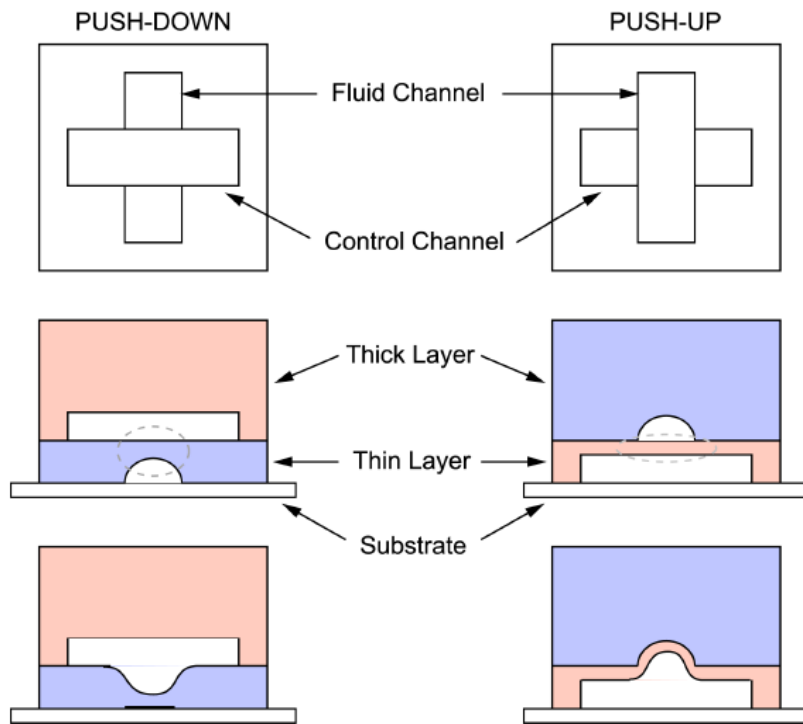
Figure 2.9 Top Down and Bottom Up Valves. There are two geometries possible for creating valves. Bottom up valves generally require lower pressures to actuate, but to down valves provide access to the cover glass. (Courtesy of Mike van Dam)

Having three valves in a row and operating them in a certain sequence (O=open, C=closed)

OCC

COC

CCO

OCC

allows for the creation of a peristaltic pump. With a combination of valves and pumps, a variety of devices can be built at high densities[19, 44].
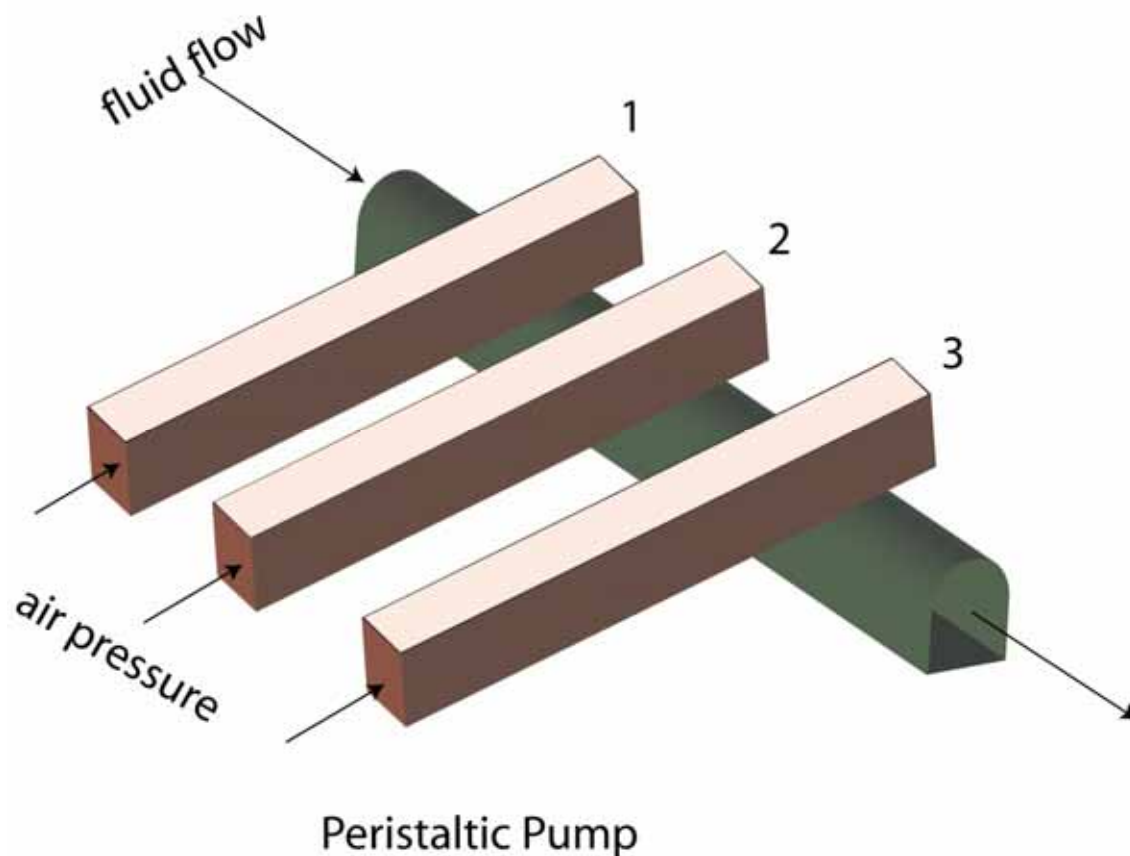
Figure 2.10 Peristaltic Pump. Pressurizing the channels in a specific sequence allows fluid to be pushed in the direction shown

2.8 Shortcomings of PDMS devices

If we try to flow dichloromethane inside a PDMS channel, something strange seems to happen – the liquid moves into the channel but then stops, and no flow appears although the liquid seems to be sucked in from the inlet port. After a while, the PDMS layer delaminates and the PDMS is seen to distort. What is happening is a classic case of partitioning of an organic solvent into two phases – in the polymer and in the channel. Because PDMS is cross-linked, it swells up, causing de-lamination and distortion of features.

Most organic solvents tend to swell PDMS (Figure 1.9) and cause other problems – like forming partitions and extracting un-reacted monomers, causing contamination. Some solvents even react with PDMS, changing its properties. The swelling can be considerable – many times the size of the device. The swelling causes de-lamination and closing of channels. The partitioning and extraction results in contamination of fluids inside the channels. These issues make it impossible to do most types of organic synthesis or combinatorial chemistry inside PDMS chips.
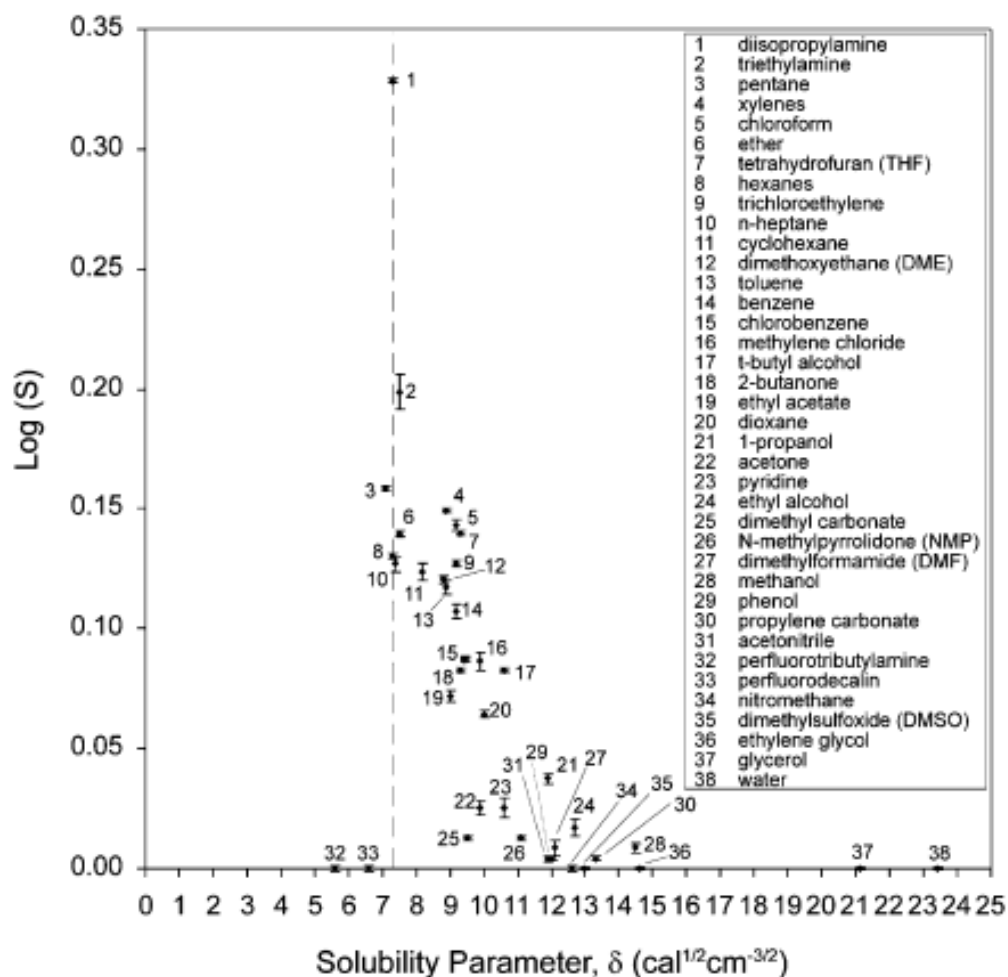
Figure 2.11 PDMS Swelling. PDMS swells in a number of organic solvents but does not interact much with aqueous solutions (reproduced from Lee et al[4], Copyright 2003, American Chemical Society)

In **Figure 1.9**, I have reproduced a graph from a paper out of George Whitesides's lab at Harvard[4]. The solubility parameter in the graph is the Hildebrand solubility parameter. Amine-containing solvents are the worst solvents for PDMS. Alkanes swell PDMS considerably, too. However, PDMS is compatible with most aqueous solutions and common acids and bases including hydrochloric acid, ammonium hydroxide and sodium hydroxide.

Having gone through this rapid introduction to elastomeric devices, I have set the stage for discussing new fabrication approaches and new polymers that help resolve some of the problems with PDMS. This is done in the next chapter.

NEW MATERIALS AND FABRICATION METHODS FOR MICRO-FLUIDICS

3.1 Where new materials are needed

Anyone familiar with the Challenger shuttle disaster will understand that materials fail –
often with tragic consequences. In the last chapter, the specific problems with PDMS that
needed to be overcome were mentioned. PDMS is good enough for most aqueous based
processes; however, a number of processes need the presence of organic solvents. For
instance, most organic synthesis, combinatorial chemistry, DNA and peptide synthesis
require organic solvents. Also, some reactions need higher temperatures and this makes
things more corrosive; PDMS cannot withstand high temperatures (>150 degrees) for long
periods of time.
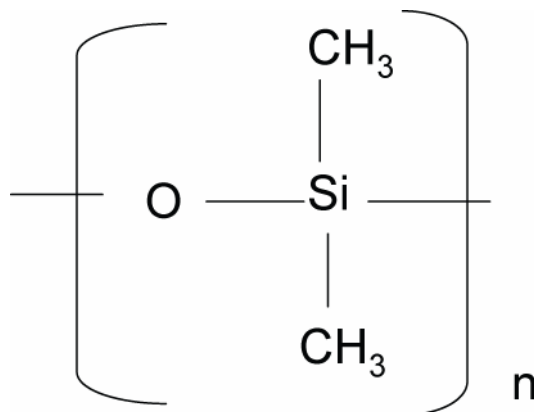
Figure 3.1 Structure of PDMS. PDMS is quite vulnerable to
attack by organic solvents that have affinity to the methyl groups.

This work described started as a collaboration with my colleague Mike van Dam (referred
to as Mike from now on), who wanted be able to synthesize DNA or peptides inside a
microfluidic chip with the ultimate aim of making a microfluidic universal array. More
details can be found in his thesis[45]. Here, I shall briefly describe work I have been involved
with; the detailed information may be obtained from Mike's thesis.

DNA synthesis (phosphoramidite route) involves using solvents like acetonitrile, tetrahydrofuran and dichloromethane. Peptide synthesis (F-moc synthesis route) needs dichloromethane, N,N-Dimethylformamide, Methyl-2-Pyrrolidone and Dimethylacetamide. All these solvents tend to swell PDMS, preventing devices from functioning. There are a number of possible alternatives that we shall survey next.

3.2 Survey of Materials

The preponderance of glassware in chemistry labs is an indication of the chemical resistance that glass (borosilicate or quartz) has to most chemicals. The only chemicals that attack it are hydrofluoric-acid-based derivatives. Similarly, silicon-based chips are also very resistant because of the silicon dioxide layer (SiO_2) found on all oxidized silicon. Silicon dioxide is the main component of glass. These materials are resilient because the very energetically-favorable oxide bond is hard to break.

Another resistant material is Teflon, invented by the DuPont Corporation. It is even more resistant to chemicals than glass because the fluoride bonds are stronger than oxide bonds. We see Teflon used increasingly more often for piping and cookware. Ceramic materials can also be tailored to be very resistant to chemicals.

All these materials have been used to make chips[46]. However, they suffer from all the disadvantages of hard materials outlined in the previous chapter - it's hard to create active elements because many complicated fabrication steps are needed that require lots of time and money. Ideally, one would like to have a material similar to PDMS in every way, except having better chemical resistance. Chemical resistance is primarily determined by bond strength and steric effects or how easy it is to access the vulnerable chemical bonds.

Bond	Energy (kJ/mol)
C-C	284-368
C-H	381-410

C-Cl	326
C-F	452
C-O	350-389
C-N	293-343

Table 3.2 Strength of Bonds. The C-F bond is the strongest bond, and this makes fluorinated materials very resistant to chemical attack.
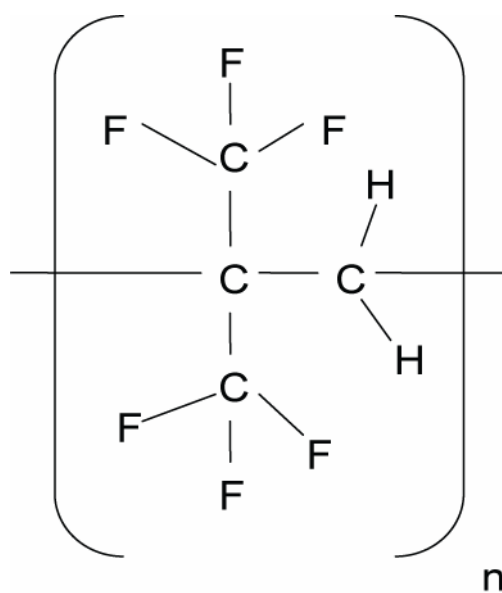
Figure 3.3 Steric effects. Steric effects protect the hydrogen in this polymer from attack of solvents.

PDMS is an elastomer – a polymer with glass transition temperature below room temperature. Elastomers are amorphous rubber-like polymers. They are used in seals, shoes, o-rings, pipes, etc. and are part of a multi-billion dollar industry. The American Society for Testing of Materials (ASTM) has designed a test for these materials that acts as a guide to selection of materials. The test D2000-06 involves dipping these polymers in special oil for

70 hours under controlled temperature and humidity, and measuring the swelling. The material is classified with a code depending on its performance. The most universally-resistant materials turn out to be the FFKM (perfluoro-elastomers) and FKM (fluoro-elastomers) class of materials. Both of these materials are highly fluorinated.

Initially, the plan was to make the fluoro-materials ourselves[47]. However, this idea was quickly abandoned when we realized that the chemistry is potentially explosive, and this is the reason that only a few large corporations make these polymers. An apocryphal story involves a grad student who produced a fluoro-compound in a test-tube and then ran to his professor's office to tell the happy news, only to have the test tube explode. The student lost a finger [48]. Upon hearing this, our enthusiasm for producing fluoro-elastomers suffered a setback, so we decided to stick with commercially-available materials.
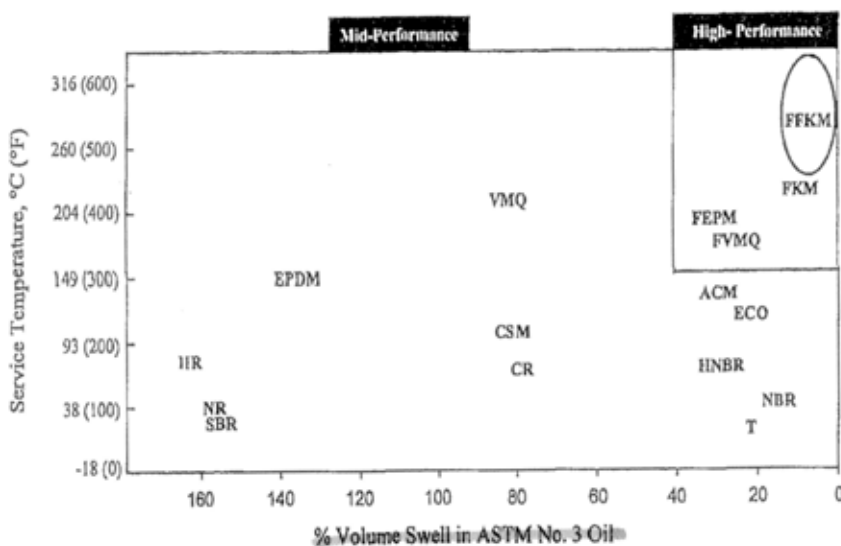
Figure 3.4 Swelling of Rubbers. FFKM and FKM class of rubbers provide the highest chemical resistance (copyright being sought)

One of the problems with commercially-available materials is the unreliable chemical resistance guide that most manufacturers provide. Usually, a material is given a letter or number grade. However these grades are usually incompatible between different manufacturers. Also, the same material may have multiple commercial names, and the formulations are often proprietary.

There are various possibilities in fabrication with fluorinated materials – we could use thin films, coat PDMS using soluble fluoro-materials[49] or simply replace PDMS with the new material elastomer entirely. I shall explore some of these options.

3.3 Coatings

One idea on conferring solvent resistance to PDMS is to coat it with something solvent-resistant. This is a common theme in semi-conductor fabrication. Mike performed many experiments involving a number of coatings, and I helped him with some of them, which I will describe below. There are two ways to create coated devices – one method is to coat the layers before the device is made, and the second alternative is to do it after the device is made by flowing the materials in through the channels. Flowing the coating has the advantage of not having to deal with the fabrication of the actual chip, which may involve high temperatures or incompatible solvents, but it usually also results in patchy coverage because it is hard to get the conditions right for coating the often-complicated fluidic channel structures inside chips. Also, the type of device makes a difference – a top-up device has to have fluid channels surrounded by polymer, unlike top-down valve architecture, and the extensions experienced in the bottom-up are also larger than in top-down architecture.

Various coatings were tried out with varying degrees of success, including fluorinated polymers like paralene, Viton, Chemraz, Teflon powders and sprays and metals like gold. None of them were completely successful. The complete experiments are given in Mike Van Dam's dissertation[45]. Here, I shall describe Cytop coatings.

3.4 Cytop

Cytop is a cyclic fluoro-polymer - poly(1,1,2,4,4,5,5,6,7,7-decafluoro-3-oxa-1,6-heptadiene) made by Asahi chemicals and used in the electronic industry[50, 51]. It is a hard but amorphous material with $T_g \sim 108^0$ centigrade. The table below gives its properties. One possibility for resistance was to coat PDMS with Cytop[46]. Cytop is soluble in very few solvents, notably the Fluorinert series of solvents from 3M and perfluorotributylamine. Commercial-grade Cytop comes in different varieties – we used Cytop 809A (Sigma Aldrich). For a solvent, we used FC-43 Fluorinert (sample from 3M). Using a 1:10 ratio of

solvent and polymer, we can spin Cytop onto a flat surface. This is followed by solvent evaporation at 80^0 degrees. The film can then be annealed at temperatures higher than the glass transition temperature. The films are generally less than 100 nm thick. The thinness of these films is essential because the height of the micro-fluidic channels is between 10-50 microns and the coatings must be thin enough not to interfere with the fluid flow or the valve-closing mechanism.
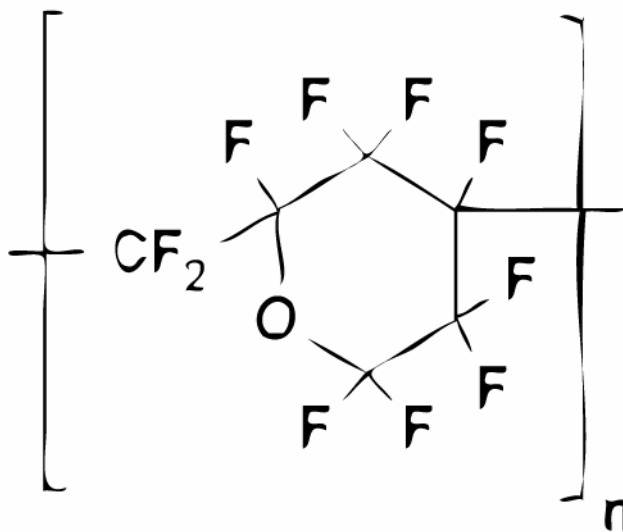
Figure 3.5 Cytop structure. The complete fluorination makes it very resistant to chemical attack

Property	Value
Density	2.03 g/cm^3
Young's Modulus	1200 MPa
Glass Transition temperature	108^0 centigrade
Thermal Conductivity	W/m K
Index of Refraction	1.34
Dielectric constant	2.1
Specific Heat	J/K m
Magnetic permeability	cm^3/g

Electric conductivity	4×10^{17} ohm-m

Table 3.6 Cytop properties.

Devices could be made both in the top-down and bottom-up format. Attempts to flow Cytop through channels to coat the device never succeeded because of the patchy coverage. Further details are available in Mike's dissertation[45].

In all cases, Cytop coatings could only provide temporary resistance. Moreover, due to the thermal mis-matches, the membrane would wrinkle up inside channels (Figure 3.6).This results in faster failures.

Figure 3.7 CYTOP coating on PDMS. This is micro-valve geometry of channels crossing each other. Notice the wrinkle due to the thermal mismatch between PDMS and Cytop.

In general, coatings don't seem to be a complete solution – they protect PDMS for a while, but the devices eventually fail. The coatings need to be thin enough for elastomeric chips to function, but the thinness also means that the solvents diffuse through the coating easily. Thin films also result in a greater number of defects and patchy coverage. Other coatings that we tried include paralene, Viton (Dupont), Chemraz, Teflon powder, CF_4 (plasma treatment), and various metals. All failed after a few minutes or a few hours.

We realized that fluorinated elastomers are the only complete solution to the problem, and many commercially-available polymers were tried out. These polymers are available in the final cured form, usually processed by injection molding into thin films or o-rings.

3.5 Perfluoroelastomers

We can try to replace PDMS completely with another elastomer. As mentioned earlier, the highly-fluorinated FFKM or perfluoroelastomers are the best suited for this[52, 53]. They have resistance similar to Teflon but not the crystallinity – instead, they are rubber-like elastomers.

Conventionally, these polymers are used in O-rings, which are produced by injection molding. They have the best chemical resistance of nearly any known material[54]. A number of companies produce them – Dupont, Greentweed, Shinetsu etc. - and sell them under various names, such as Chemraz, Kalrez, Aflas, etc. However none of them are suitable for use in the form in which they are available, because it is hard to form thin layers with them. High pressure and high temperature injection molding machines are required to shape the polymers, and then sizes of features cannot be reduced to the micro scale - the sizes of features produced in other ways are larger than replica molding. What is required is a liquid polymer that can be cured under mild conditions to an elastomeric solid.

Three elastomers were found that could satisfy the requirements of soft-lithography – PFPE (photocurable perfluoropolyether), SIFEL (elastomer sold in Japan by Shinetsu) and FNB (Fluoro-norbornene). In this dissertation, I shall discuss only SIFEL and PFPE, two polymers I worked on. More details on all the three elastomers can again be found in Mike's thesis and a recently published paper[45, 55].

3.6 PFPE

PFPE was first made by the DeSimone group in North Carolina state university[55]. It is made from Poly (tetrafluoroethylene oxide-co-difluoromethylene oxide) α,ω diol or

ZDOL (Sigma Aldrich). This precursor is used in the lubrication industry under harsh chemical conditions. We could only obtain a few grams of the PFPE material a time. This was used to make devices. Mike and I performed extensive solvent testing and the solvent testing table is reproduced below. The error in the table is expected to be of the order 0.5%. PFPE shows good solvent resistance.

Solvent	Weight change	
	3 days	7 days
Acetone	4.3%	4.11%
Xylene	1.8%	1.70%
Toluene	1.9%	2.04%
Fluorinert-75	39.7%	66.35%
Pyridine	4.8%	5.21%
DMF	3.9%	4.22%
Chloroform	10.3%	8.33%
Diisipropylamine	2.3%	2.30%
Hexane	1.1%	0.79%
Triethylamine	2.7%	2.60%
Formaldehyde	0.4%	0.69%
Trichloroethylene	6.8%	6.70%
Acetonitrile	1.9%	2.03%
Nitric acid	4.6%	4.52%
Ether	3.8%	3.56%
Chlorobenzene	2.8%	2.64%
Isopropyl alcohol	2.3%	2.31%
Ammonium Hydroxide	0.7%	0.37%
THF	6.0%	5.27%
Sulphuric acid	7.4%	10.34%
Cyclohexane	1.5%	1.56%
DMSO	2.3%	3.02%

Figure 3.8 Solvent resistance of PFPE. PFPE is quite resistant to many solvents. We noticed color changes with trithylamine, trichloroethylene diisipropylamine and sulphuric acid.

Several devices were made with the material. One such device is shown in **Figure 3.9**. The main problem with the PFPE was the fact that it is hard to bond two layers of PFPE. By adding different terminal chemical group to the layers[45] that tend to react with each other, some improvement was achieved in the bonding and we were able to verify that the devices were indeed solvent-resistant. However, the small quantities of PFPE and its high cost have prevented extensive testing. More recently, a new company called Liquidia has been formed that is trying to commercialize this technology[56]. Further details about our experiments with PFPE are available elsewhere[45].
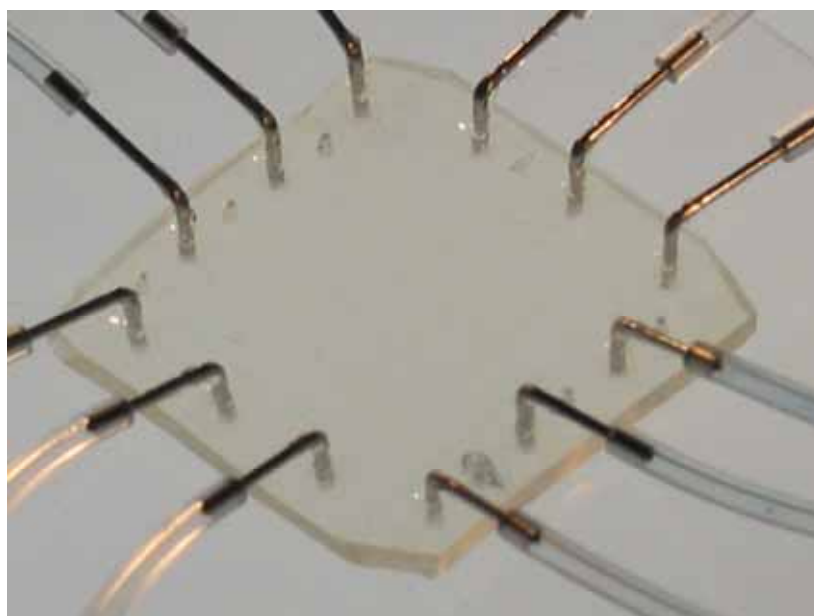
Figure 3.9 PFPE Microchip. PFPE is designed to be as similar as possible to PDMS in physical properties.

3.7 SIFEL

SIFEL is a new polymer invented by chemists at Shinetsu Corporation (Tokyo, Japan)[57]. At present, it is not available in the United States though this is expected to change soon. I was able to obtain small samples through Claude C. McClure of Shinetsu. SIFEL is also a liquid fluoro-elastomer. It is sold in different formulations. Shinetsu describes it as combination of a perfluoropolyether backbone with a terminal silicon-based cross-linking group.
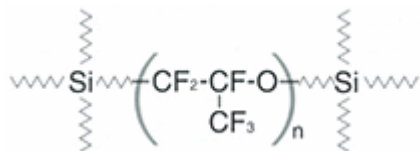
Figure 3.10 SIFEL structure

Initially, we attempted to try the potted gel formulation of SIFEL 8070 A/B. It comes in two parts, A and B, which need to be mixed together. The curing is done thermally at 150^0 centigrade. It was spun on a wafer that can be treated [vapor phase coating of (Tridecafluoro-1, 1, 2, 2-tetrahydrooctyl)-1-trichlorosilane] to be less adherent. I found SIFEL potting gel to be extremely sticky even after curing, and thus unsuitable for use with micro-fluidics.

We had better results with the one component adhesives SIFEL 6030, SIFEL 610 and experimental product SIFEL X71-0603. They need to be stored in a refrigerator at $< 4^0$ centigrade or less and cure at 150^0 centigrade. SIFEL adhesives are significantly elastic. Curing results in a milky white solid.

Solvent testing with dichloromethane over 3 days revealed swelling of about 10-15%, which shows significant resistance. The adhesives are designed to have strong bonding with glass, silicon and metals. To make multi-layer devices, we need to be able to bond two layers together. However, all attempts with these also failed – SIFEL layers do not stick to each other on curing, and we could never succeed in partially curing two layers and sticking them together. The timing of partial-curing seemed to be very finicky and varied batch to batch. It may be that curing occurs very quickly, leaving no way to partially cure SIFEL adhesives and stick them together. On pouring uncured SIFEL on top of cured SIFEL, we did obtain some adhesion. However, without partial curing, we can't mold features on layers, making multilayer device fabrication impossible. Oxygen plasma made no difference to the adhesive ability.

One-layer SIFEL is able to perform replica molding as well as PDMS. We found that we could spin SIFEL onto a mold and it seemed to follow a power law for the thickness. SIFEL adhered significantly to the mold, so releasing it was a problem. Holes could be punched into the SIFEL without any difficulty.
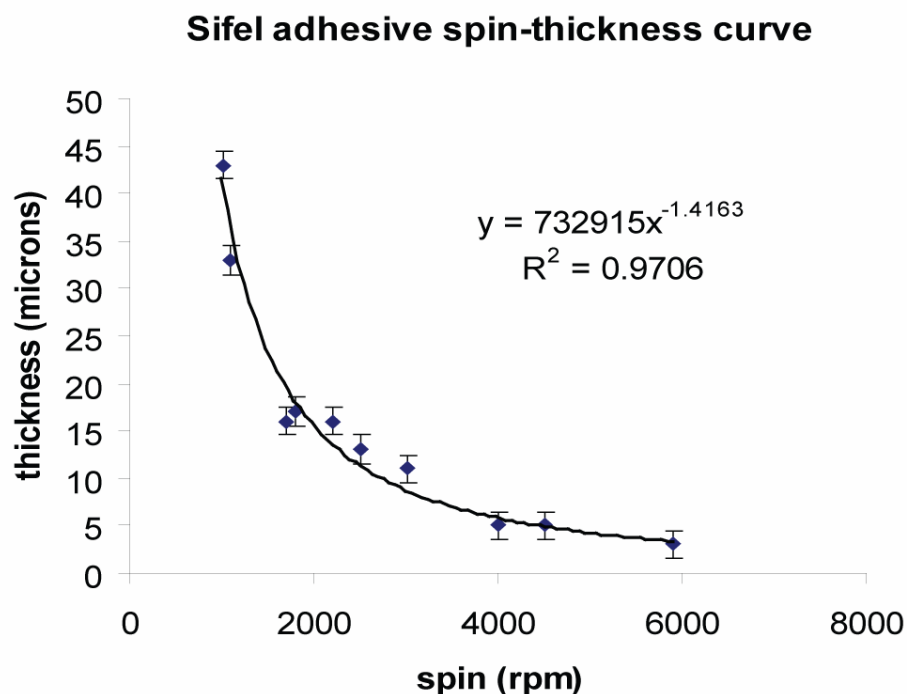
Figure 3.11 SIFEL Spin Curve. SIFEL adhesives on silicon wafer seem to follow a power law with film thickness.

SIFEL is a very promising material for microfluidic fabrication. Due to the small amounts of samples available, we were able only to do limited testing. However, we can expect that with further experiments, SIFEL will be a viable material able to compete with PDMS.

3.8 Outlook on Solvent Resistant Materials

Having worked on many materials it is clear that perfluoro materials are the best materials for solvent resistant microfluidic devices. The main problem has been the lack of availability of liquid fluoro materials that can be cured on a mold. Their solvent resistance

also makes it hard to bond different layers together to make multi layer devices because of their inertness. Both of these problems have been solved to an extent, and solvent-resistant devices can be made. However, these elastomers are expensive, and unless they are produced in mass quantities, they are likely to be used solely in niche applications.

The other problem has been the mesh of patents and proprietary technologies that prevent widespread adoption of these perfluoro-elastomers. It increases the cost and makes it hard to obtain materials without signing a lot of papers and paying a lot of money. At present, SIFEL is the only material available somewhat freely (though only as samples); all other materials are tied up in licensing agreements and patents. This situation is rather unfortunate because the new materials have so much promise for use in micro-fluidics.

3.9 Alternate Fabrication strategies

With the lack of success with conventional multi-layer lithography, we started to look into alternatives. If we look at semi-conductor fabrication strategies, then one realizes that 3-D fabrication with multiple layers is needed to make successful designs. Possibly, similar processes could be required for micro-fluidics. By 3-D, I mean that different layers are interconnected by channels that could point in any direction in space instead of just being in a plane. There are two ways to create 3D micro-fluidics – to build things layer by layer, or to build things directly in 3D. The first type includes solid printing and multi-layer lithography. The second method includes laser ablation machining and stereo-lithography. Here, I will describe 3-dimensional wax printing and 3-D photolithography. There are other 3-D processes possible including stereo-lithography, laser ablation, etc.[45], but as of yet these are still not very mature from the point of view of elastomeric microfluidics.

In fact, I will demonstrate two cases where 3-D architectures were indispensable for success. Before I discuss the two cases, I will mention here another possibility where a thin membrane is sandwiched between two flow channels etched in a solvent-resistant material like glass or a silicon wafer. This kind of device could overcome the problem of solvent resistance provided that we used a solvent-resistant material for the membrane. The idea originated in realizing that thin films of fluoro-elastomer films were readily available from various manufacturers[52]. The design architecture is shown in the Figure 3.12. A few

experiments with PDMS were attempted and are described in Mike Van Dam's thesis. Unfortunately, most of these trials were unsuccessful in producing solvent-resistant devices, primarily because thin enough films were not available. Moreover, there are few established techniques to handle thin-films. However, this remains a possibility that may be implemented in the future.
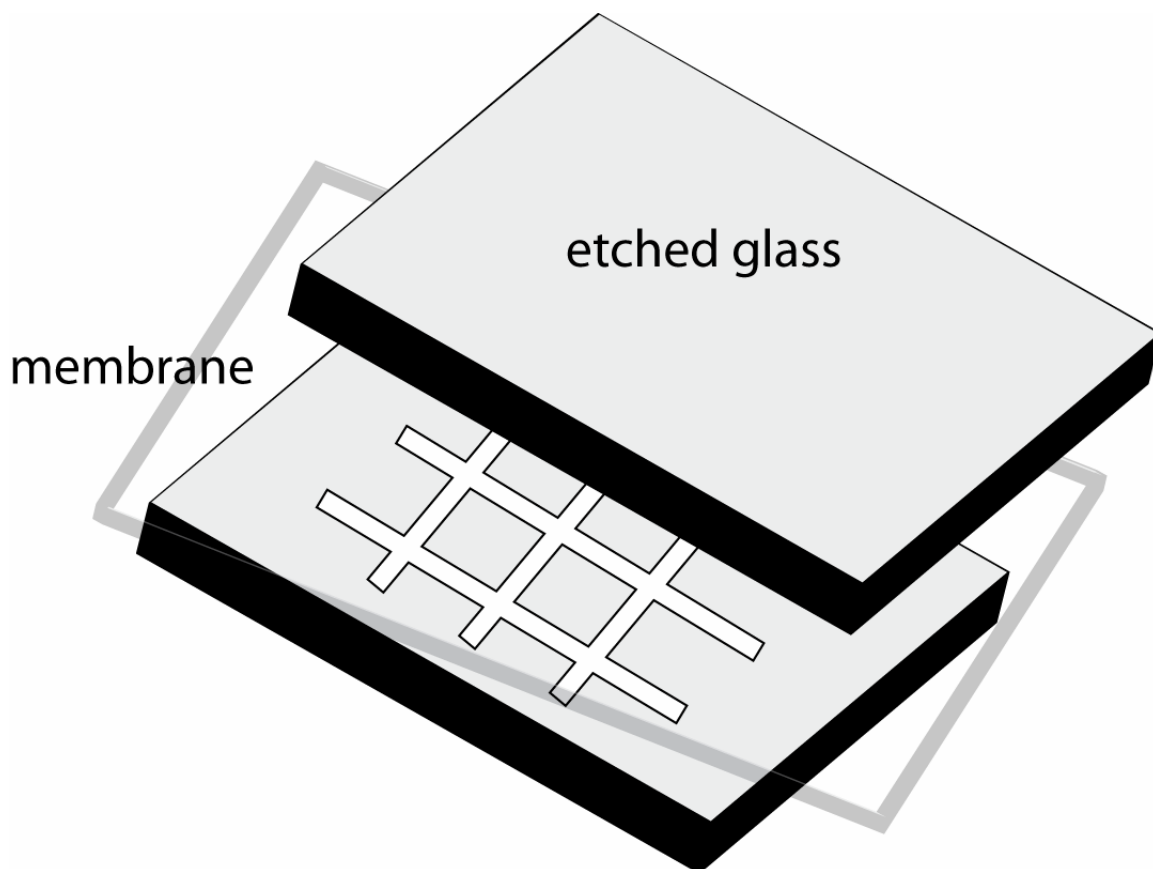
Figure 3.12 Membrane sandwiched between channels. If thin-enough membranes could be produced that bond to etched silicon or glass, this may provide another route to solvent-resistant devices with valves.

3.10 3-D fabrication

With all the things possible with two-dimensional planar systems, it begs a question as to why a 3-D chip is needed. To understand why, we need to look at the semiconductor industry. Most microchips are thought to be planar; however, the final chip often takes advantage of complicated 3-dimensional geometries as shown in **Figure 3.13**. Not having the ability to make connections in 3 dimensions would severely impact the type of chips

that could be built. Similarly, one can expect that as microfluidic technology matures, more and more chips will use some kind of 3-D fabrication. I will describe two examples of how 3-D fabrication helped solve problems that may have been insurmountable in 2D.
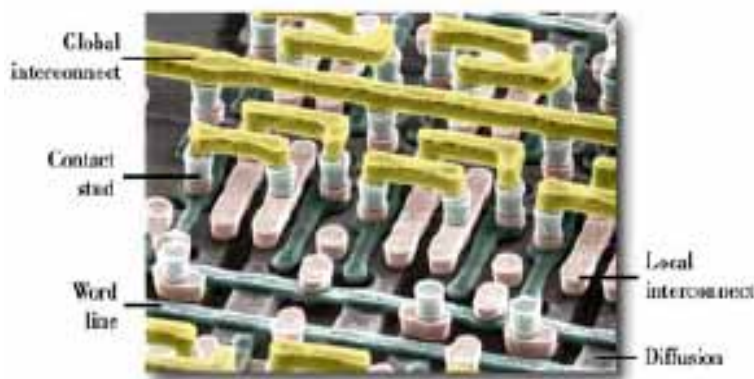
Figure 3.13 CMOS 3-D Architecture. Note the interconnections between layers. Although the fabrication is done layer by layer, the final product is 3-D. Image is in false color. (from a presentation by Paul Nealey, University of Wisconsin)

What are the advantages of having access to the third dimension? One obvious advantage of 3-D is the possibility of easier connections and new structures like vias or coils around channels. Thus, the phase space of structures that can be made expands. Another advantage is the whole chip may be built at once without need for multiple layers, eliminating the problem of delaminating. The disadvantage of most 3D fabrication methods is that it is hard to scale them up. It's easy to make a few devices, but at present, producing a million of them would be too time-consuming and there is no clear path to parallelization.

3.11 Solid Printing

With the widespread ability of 3-D rapid prototyping printers, it has become possible to create shapes and then use them to mold[58-60]. In early 2005, on meeting with George Maltezos, who was working with a 3-D wax printing machine, Mike and I realized that we could solve the problem of bonding between elastomer layers by simply making the chip in

one shot with the 3-D wax printing machine. All of the channels can be embedded inside the polymer, and there is no need to bond the elastomer to any substrate or one layer to another. The main problem with wax printers is that the sizes of structure being used are still large compared to conventional photolithography, but this may not be an issue in many applications.

We used a Solidscape T66 bench-top machine, which uses the Sanders prototyping method to build features. This involves the use of two different waxes – a build wax (blue wax or "InduraCast" and a support wax (red wax or "InduraFill"). These proprietary waxes have different melting temperatures – 45-70 degrees for the red wax and 95-110 degrees for the blue wax. The support wax ("red" wax) can be dissolved in a proprietary solvent provided by the Solidscape (BioAct VSO), leaving behind the mold wax ("blue" wax)
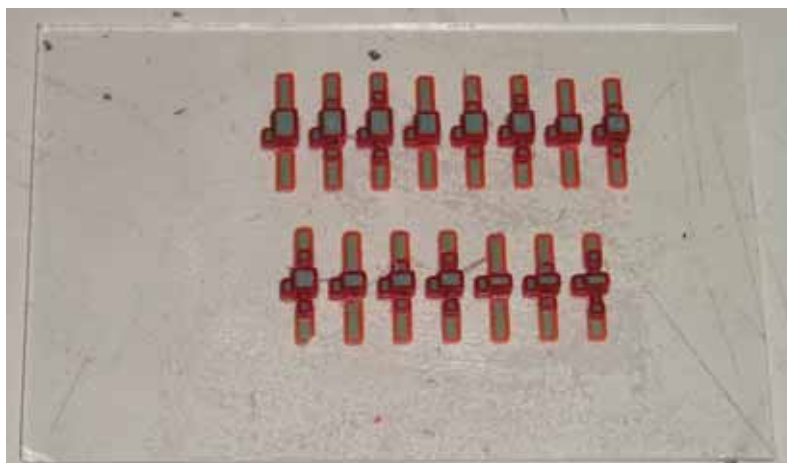
Figure 3.14 3 D printing on glass. The red wax is the support wax and the blue wax is the actual mold.

The machine accepts .STL files (stereo lithography), which is a standard for 3-D printing. The designs are made using SolidWorks software. The machine itself works by putting drops of the two waxes on a substrate and building layer by layer. Sander's innovation is the presence of a milling head that sweeps by after a layer is complete to smooth the surface. The machine deposits drops of wax about 75 microns in size every 5 microns. The final roughness of the features is <10 microns. Once the mold is made, it is put into a vat of BioAct VSO to dissolve the red wax.
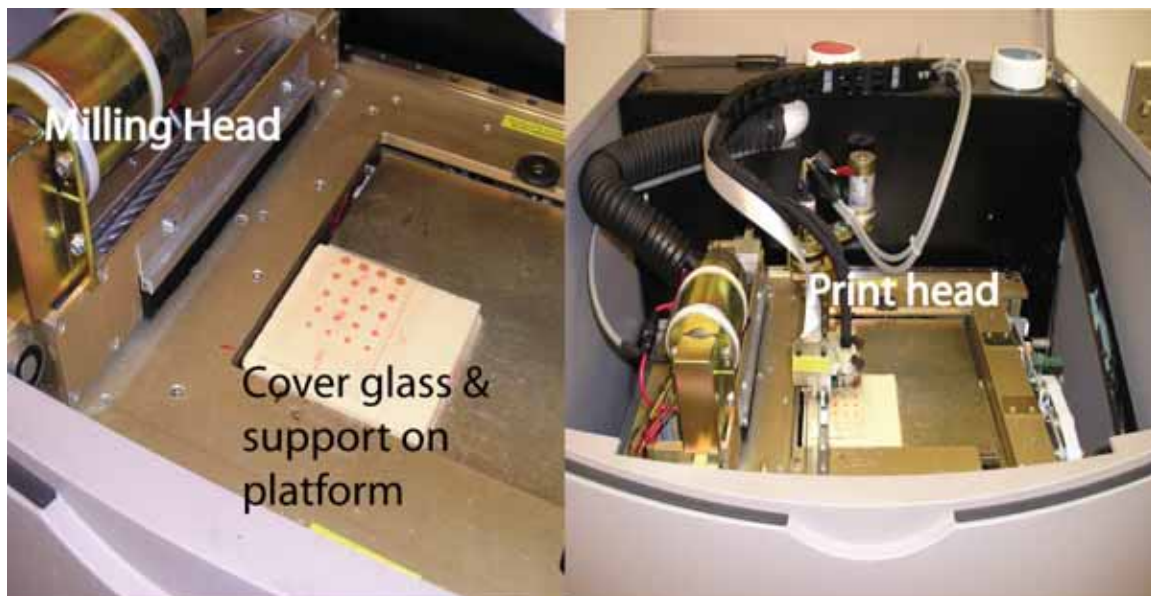
Figure 3.15 Solidscape T66 machine. This machine uses the
Sanders rapid protyping method involving two waxes to do solid
ptinting. Use is made of a milling head to smoothen each layer
after printing. The shapes can be built directly on a cover glass or
a silicon wafer.

Once the red wax is dissolved, the polymer may be pored on top of the mold. We found
that it is very important to have the solvent completely evaporate and leave no traces;
otherwise it interferes with the curing of the polymer. Low-temperature thermal curing or
UV curing is then used to cure the polymer. The blue wax is subsequently melted and
removed.
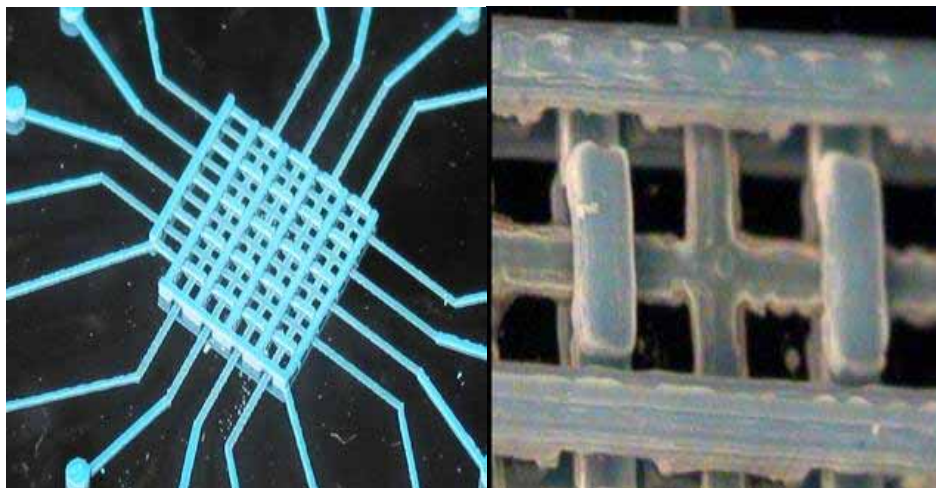
Figure 3.16 Solid Wax Mold. Notice the three dimensional pattern.

A number of ways of designing valves was tested with PDMS, including the tube valves (by George Maltezos), cross channel valves and H valves. I will not attempt to describe the details here, because they are available in Mike's dissertation[45].
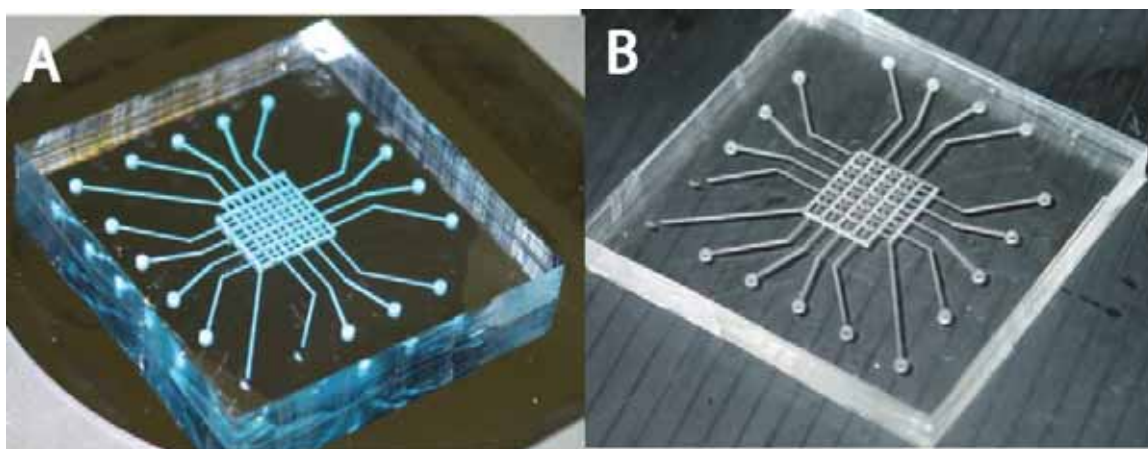
Figure 3.17 Wax Molding A) PDMS on a wax mold B) Wax is melted leaving the embedded channels.

Valves can be made by with crossing channels or by coaxial geometries. Both of these geometries have been tested and can provide valve action. However, these valves are not as good as the multi-layer lithography valves. The reason for this is the larger size leading to higher pressure and stretching of the elastomer before the valves close, and the roughness

of the wax molds. Nevertheless, the valves do work and offer a possibility where none existed before.
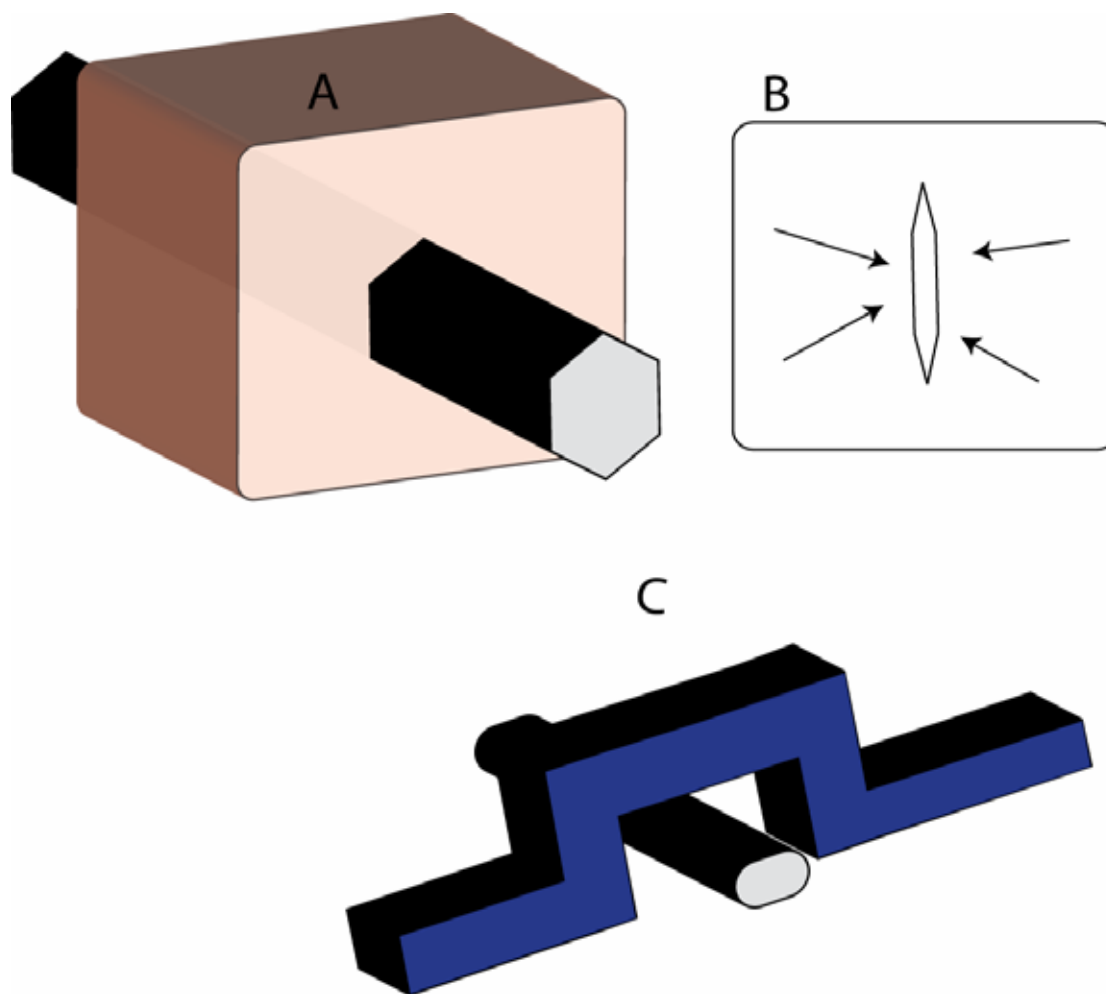
3.18 3D valve geometries A) Coaxial valves B) Hexagonal channels collapse well C) channel crossing geometry

The main reason for making these valves was to use solvent-resistant materials to be able to make chips in one shot, eliminating the bonding steps. We had only a limited supply of solvent-resistant materials and only limited testing was possible. The molds were surrounded by a PDMS hollow cylinder so as to conserve the solvent-resistant elastomer, either SIFEL or PFPE. With PFPE, the material was poured on the mold and UV cured. The orientation had to be changed often because the wax blocked the UV radiation. Then, the wax was melted at 120^{0} degrees and easily flowed out. In the case of SIFEL, the same

procedure was followed except that thermal curing is done at 60^0 overnight. In both cases, we got the valves to work.
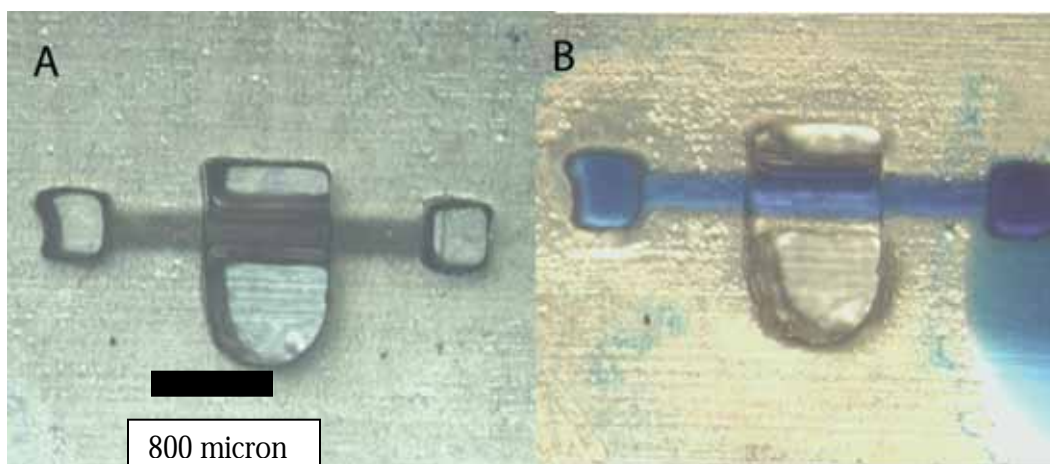
Figure 3.19 3D molding of solvent resistant elastomers. Here PFPE is shown molded into a coaxial micro-valve. A) Valve with no flow B) Flow of methanol with blue dye xylene cynol FF through the channel.

In conclusion, solid printing allows us to make devices in one shot, getting rid of all the bonding steps. We have been able to use it to make proof-of-principle solvent-resistant devices with new liquid perfluoro-elastomers.

3.12 3D hybrid molds

Another way to get 3D dimensional structures is with the creation of hybrid molds – molds that use more than one photo-resist, thus allowing structures of varying height on the same mold. Again, this is not a new concept[58, 61-63].

The reason for interest in this is the problem that one encounters when trying to incorporate non-fluidic elements with these microfluidic chips – sensors, filters, CCD chips, heaters and coolers, etc[6]. The planar fabrication of multi-layer microfluidic chips does not allow for incorporation of other devices unless they are fabricated completely flat on a surface. Without a flat surface, there will be leaks when a channel crosses the boundary of the device. This is clearly inconvenient for integration.

One way to solve this problem is to create channels like shown in **Figure 3.20,** where channels go down in the third dimension to interface with the sensor, whereas the remaining channels are at another level isolated from the sensor. Instead of a sensor, we could use a heater or a cooler, allowing us to heat or cool parts of a chip simultaneously.

elastomeric multi-layered chip
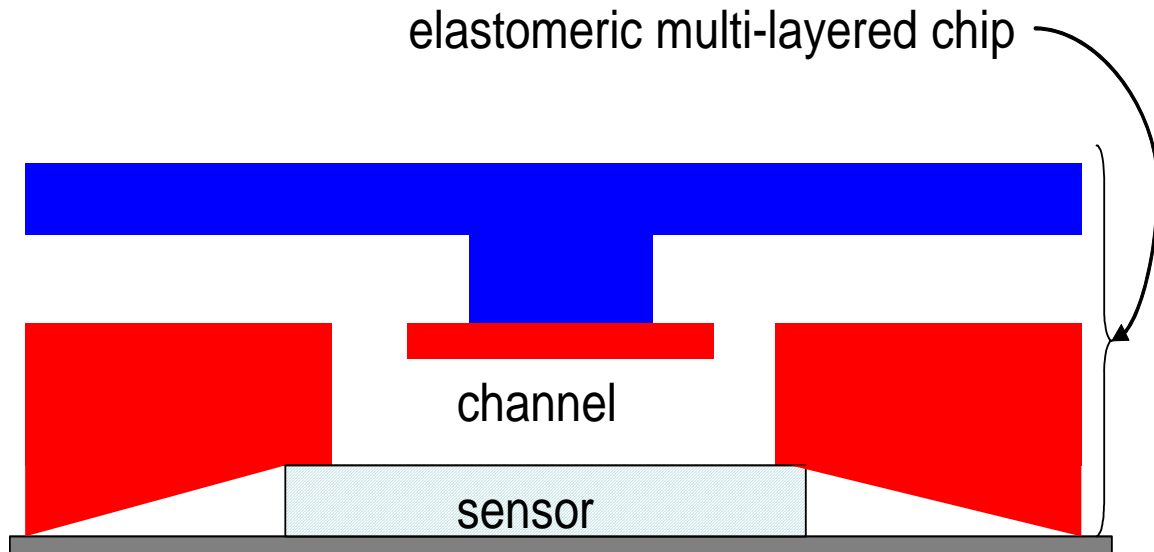
channel

sensor

Figure 3.20 Integration of a sensor with a 3D chip. Notice how the channel goes down to meet the sensor. The rest of the channels are at another level. This ensures that the air gaps next to the sensor due to its thickness do not cause any leaks.

These kinds of chips can be made by creating hybrid molds using a process that was first used by Whitesides' group at Harvard[64] and further developed by Emil Kartalov[65]. The procedure involves using photo-resist SU8 (Microchem) to create a pattern and then following up with a thick positive resist like AZ50 (AZ-electronic materials) to create larger structures that will serve as interconnects. The entire fabrication procedure is shown in **Figure 3.21**. SU8 is used as the first resist because it can be hard-baked, resistant to future processing. We can now put in a sensor or other micro-devices as shown in **Figure 3.20**.
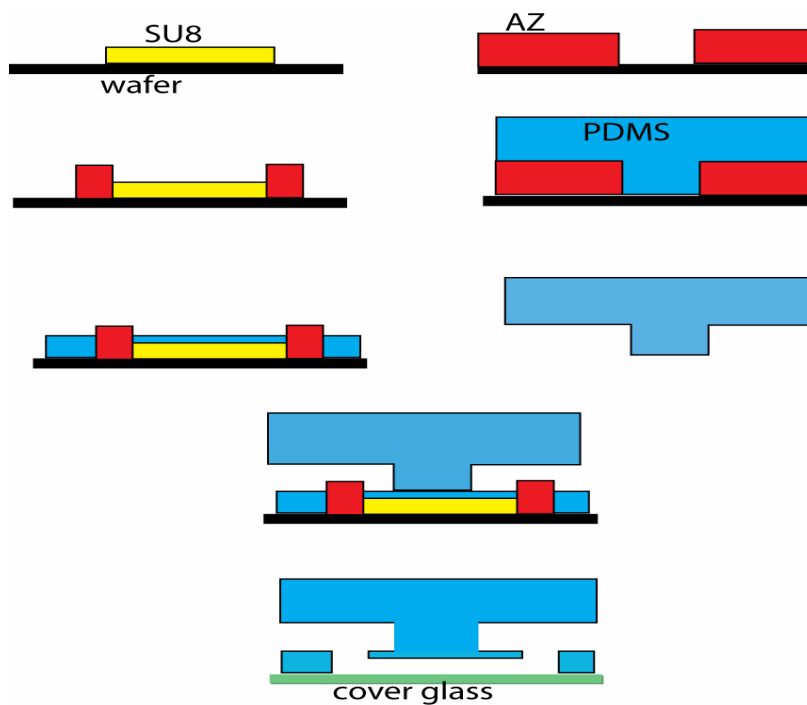
Figure 3.21 Fabrication of interconnected channels.

In collaboration with my colleague Sven Mathias, this design was used to integrate a electrochemically-etched filter[66]. We designed chips similar to ones displayed in **Figure 3.20** and then put the filter in between them. In principle, any micro-fabricated planar device could be inserted instead of the filter.

A design like this could, in principle, allow for the tight integration of a number of micro-devices with a microfluidic chip. It demonstrates the power of being able to use the third dimension.
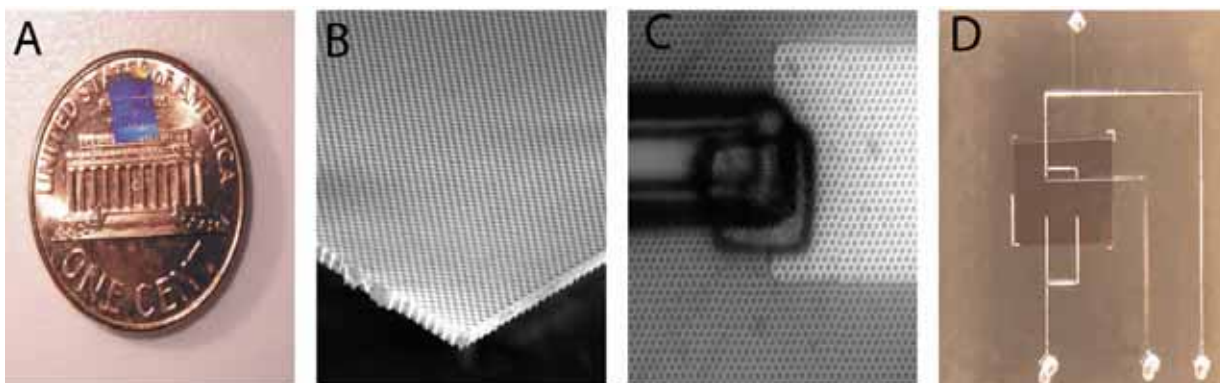
Figure 3.22 Integration of Filter using Hybrid Molds A) Silicon electrochemically etched filter B) Close up of filter B) Channels interfacing with filter D) The final microfluidic chip. Notice that channels vanish because they go down to interface with the filter.

Testing this filter for use is a work in progress that involves using beads of different sizes – one capable of passing through the filter, the other unable to pass through. Flow tests have shown that at the 3D junction, some beads can get jammed, and a new design is being developed to overcome these difficulties[67]. However, the important point is that any kind of planar device can be incorporated in this manner, rather than the specific details of this case.

From the two cases of 3D fabrication provided, it is clear that being able to use the third dimension provides many advantages. In using it, we have a clear path to integrating many non-fluidic devices with microfluidic chips, something that is hard to do otherwise. I believe that as chips get more and more complicated, it will be hard to avoid some kind of 3-D connection between layers. One can imagine a future where an integrated device is able to heat and cool streams of fluid simultaneously while also making various kinds of measurements. These devices will be able to withstand any kind of solvents and be able to perform high throughput analysis using the parallelism intrinsic to microfluidic chips. Perhaps they sequence DNA, or synthesize peptides, or test hundreds of targets for drug efficacy. These devices will be the fluidic equivalent of today's Pentiums and Athlons.

3.13 Acknowledgement

I like to thank both Mike Van Dam and George Maltezos. Work on solvent resistance was initiated by Mike Van Dam, who wanted to have a microfluidic device to synthesize DNA.

I helped him with many experiments, some of which are described here. More details may be found in Mike's thesis. When I joined Axel Scherer's Nanofabrication group, I realized upon meeting George Maltezos the ability to use his solid printer for the solvent resistant device – this started a fruitful collaboration between George, Mike and me.

Emil Kartalov came up with methods for vias, and that helped Sven Mathias and me in integrating Sven's electrochemically-etched filter. This also made me realize the power of 3D structures. Thanks are due to both Emil and Sven.

Finally I would also like to thank Claude McClure at Shinetsu for his help in obtaining Shinetsu SIFEL products from Japan, some of which are experimental products not yet publicly available.

Chapter 3

QUANTUM DOTS & OPTO-FLUIDICS

4.1 Introduction

This chapter is divided into two parts first, I introduce work on quantum dots: how to make composites of quantum dots and micro-spheres, and how light from quantum dots can be enhanced through different means – through evaporated gold films and through chemical means. The second part introduces concepts of Opto-fluidics, combining fluidics with photonics. I describe work done with hydro-dynamically focusing quantum dots to write a barcode in a channel.

4.2 Quantum dots

In the '80s, Alex Effimov in the former USSR and L. Brus at Columbia University (and their collaborators) found that the optical properties of semiconductors changed when their size was about 10 nm[68]. They realized that the reason for this was quantum confinement. As electrons in these "nano-crystals" were confined, the energy levels changed – a consequence of the quantization of energy in a confined well. Thus, engineering the size meant that the optical properties could be tailored[69].

 It took over fifteen years to figure out how to conveniently make these nano-crystals as small colloidal particles. There are many reviews available on the chemistry involved[70]. Today, there are two companies that commercially sell quantum dot products – Invitrogen (which bought the company formerly known as Qdot Corporation) and Evident Tech. Most academic groups, even the originators of the process, prefer to buy the quantum dots from these companies if they need high quality nano-crystals. In other words, the quantum-dot making process has been out-sourced, just like many processes in the semiconductor industry[71].
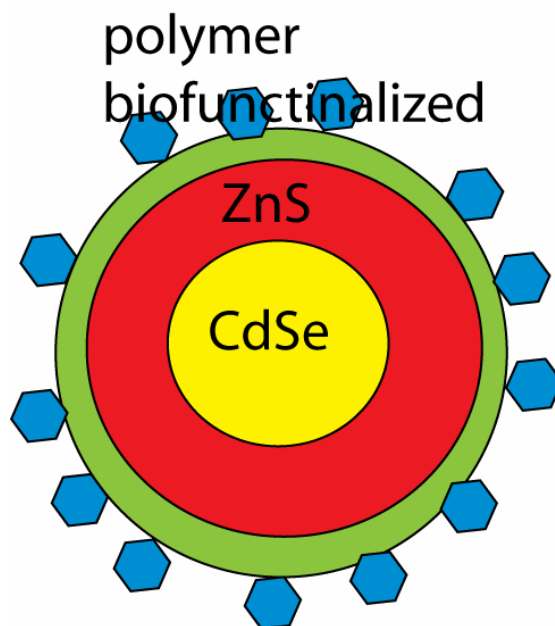
Figure 4.1 Structure of Core-shell Quantum Dot

Most visible-range quantum-dots are made using Cadmium Selenide (CdSe) or Cadmium telluride. Usually, to improve the quantum efficiency, a proprietary coat of ZnS is added to these dots. The ZnS, which has a larger band-gap serves to plug the defects on the surface of CdSe which would otherwise cause non-radiative recombination. To this particle, a coat of an inert polymer may be added, and then the particle can be functionalized with various bio-ligands like biotin and streptavadin[72]. If not functionalized, a surface coating of tri n-octylphosphine (TOPO) is used to allow organic solvents to solvate them. Quantum dots are also available in the NIR or mid-IR range, made with PbSe or PbS – however, their conjugation chemistry is not as developed compared to the CdSe dots, making them less useful at present.

Quantum dots have found many applications in bio-labeling, solar cells, counterfeit detection, organic light emitting diodes etc. They have been used to make lasers[73] – although their use in lasers is restricted to high-concentration films, because at low concentration it is hard to obtain gain from these quantum dots.

4.3 Comparison to Dyes

The best way to understand quantum dots would be to compare them to fluorescent dyes. Fluorescent dyes have been used in a number of applications for a long time. Like quantum dots, these are also light emitting particles. I believe that quantum dots will gradually replace dyes in a large number of applications.

	Dyes	Quantum Dots
Size	<10 nm	Core dots < 10 nm but with coatings can be as large as 50 nm
Bleaching	Photo-bleach irreversibly	Blinking reversibly
Switching (on and off)	Can be turned on or off via FRET	Not possible presently
Biological compatibility	Many dyes like GFP etc do not poison cells	Generally poisonous, however with coatings may become safer.
Brightness	~100 times less brighter than dots	~100 times brighter than dyes
Absorption/Emission Spectra	Mirror absorption, emission spectra separated by < 100 nm usually	Absorption spectra very broad, emission spectra narrow, widely separated.

Table 4.2 Quantum Dot and Dye comparison

4.4 Quantum Dot Composites

In many applications, the small size of quantum dots can be a disadvantage. For instance, optical tweezers need particles of larger volumes. Moreover, this allows the multiplexing of quantum dots using a mixture of quantum dots[74, 75]. One way around this is to create composites of quantum dots with other micro-particles. There are three ways to conjugate micro-particles with quantum dots.

1) Quantum dots inserted inside pores of beads

2) Quantum dots inserted inside shells of beads

3) Conjugation via bio-ligands like biotin/streptavidin.

Here I will describe the first two methods, which we attempted in order to create composites. Most of this work was done in collaboration with Brian Zhou initially, and then later with Sven Mathias.

4.5 Quantum dots inserted inside pores

This relies on the fact that the coordinating ligand around quantum dots is hydrophobic as is the interior of polystyrene beads[75] . The procedure involves swelling polystyrene beads in chloroform. The polystyrene beads may either be produced in the lab using emulsion polymerization procedures, or bought commercially (Bangs Labs). Polystyrene beads in aqueous solution are solvent-exchanged into n-butanol or n-propanol by centrifuging at low speed and exchanging solvent. This procedure is repeated at least 3 times to ensure complete exchange. Chloroform is added to the solution, up to a 5% concentration by volume. The soaking is done for 30 minutes at the minimum. During this time, the polystyrene beads expand and the pores become accessible. To this, a solution of quantum dots in n-butanol is added. The quantum dots, due to their surface coating, like preferentially to get into the pores of the beads. Finally, the solvent is exchanged back to an aqueous one. Again, this is repeated at least three times to ensure complete exchange. Beads as small as 100 nm and as large as 10 microns can have quantum dots incorporated into them.

This procedure needs to be modified if the beads have carboxyl (-COOH) functionality – in that case, ethanol is added instead of n-butanol, and the final result is still the same. The result is beads with quantum dots embedded in them. Different colors of quantum dots may be added in different ratios to encode information spectrally. More recently, a company has started to sell these types of beads, commercially. The beads have applications in biology[76].
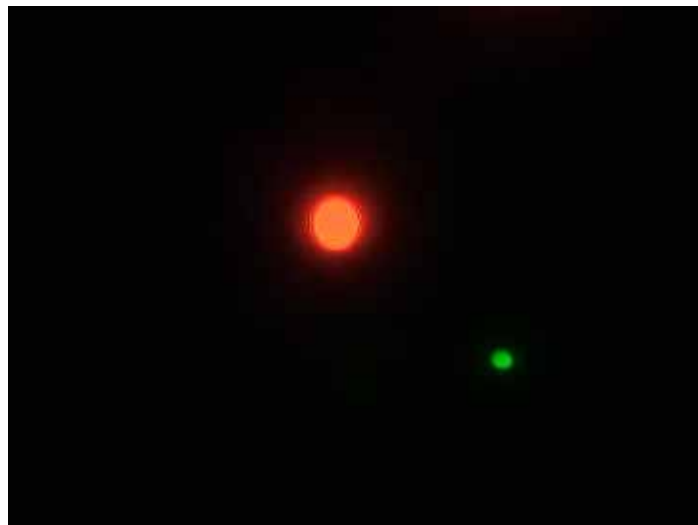
Figure 4.3 Polystyrene Micro-spheres Embedded with Quantum Dots. The large sphere is 8 micron and the small 2 microns. The quantum lost emit at peak wavelength of 620 nm and 525 nm.

4.6 Shell growth

Another way to create composites is to grow silica shells – a method devised by the Bawendi group[77]. The idea behind this method is to grow a silica shell while quantum dots are present in the solution, allowing the dots to be incorporated with the shell. This method is an adaptation of the method used to incorporate dyes in silica shells[78]. Briefly, the procedure involves functionalizing both beads and quantum dots with 3-amino propyltrimethoxy silane (APS) and 5 amino 1-pentanol (AP). Quantum dots in toluene are precipitated using 5% methanol (by volume). This is followed by a cap exchange where TOPO groups are exchanged for AP in ethanol. AP makes the quantum dots soluble in ethanol. A few cycles of cap exchange may be necessary. These quantum dots are added to a ethanol solution of the silica particles along with AP, tetraethoxysilane (TEOS) and hydropropyl cellulose. A small amount of ammonium hydroxide and water is added and entire solution is heated at 75^0 degrees for 4 hours. As the shells grow, the quantum dots are incorporated in them. The silica beads can be recovered by a few repetitions of centrifugation/precipitation and re-suspension in ethanol. In this procedure, it is essential that the concentration of beads is dilute, or they may aggregate.

Figure 4.4 Silica with quantum dots. 2 micron silica beads embedded with quantum dots that emit at peak wavelength of 620 nm. There is some aggregation.

This method does not work as well as the previous method, but on the other hand, if silica beads are needed, it must be used. In both of these cases, the beads were obtained from Bangs Labs and the quantum dots from Qdot Corporation. All chemicals were obtained from Sigma Aldrich and used as obtained. A rapid thermal cycler PTC 150 Minicycler (MJ Research) was used to heat.
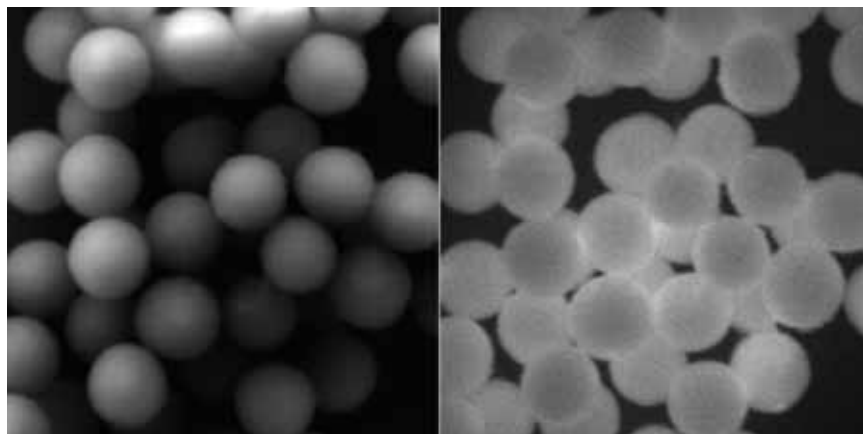
Figure 4.5 Cathode-luminescence of Silica Beads. We found significant cathode luminescence from 2-micron silica beads coated with quantum dots – however later, light was later shown to be coming mostly from the micro-spheres themselves. On the left is the SEM image and on the right is the cathodeluminesce

We did some cathode luminescence measurements with these quantum dots coated with beads and found significant amounts of light from both the silica and the polystyrene beads – however, it seems like most of the light was later determined to be in fact coming from the beads themselves rather than the quantum dots. As an aside, it may be interesting to use these beads for imaging cells inside a SEM equipped with cathode-luminescence. The CdSe quantum dots themselves do show some cathode-luminescence, but they become dark in a matter of a few seconds. Other kinds of dots may be designed in the future with better cathode-luminescence properties for imaging. All imaging was done using a FEI Quanta SEM equipped with a GATAN photoluminescence probe.
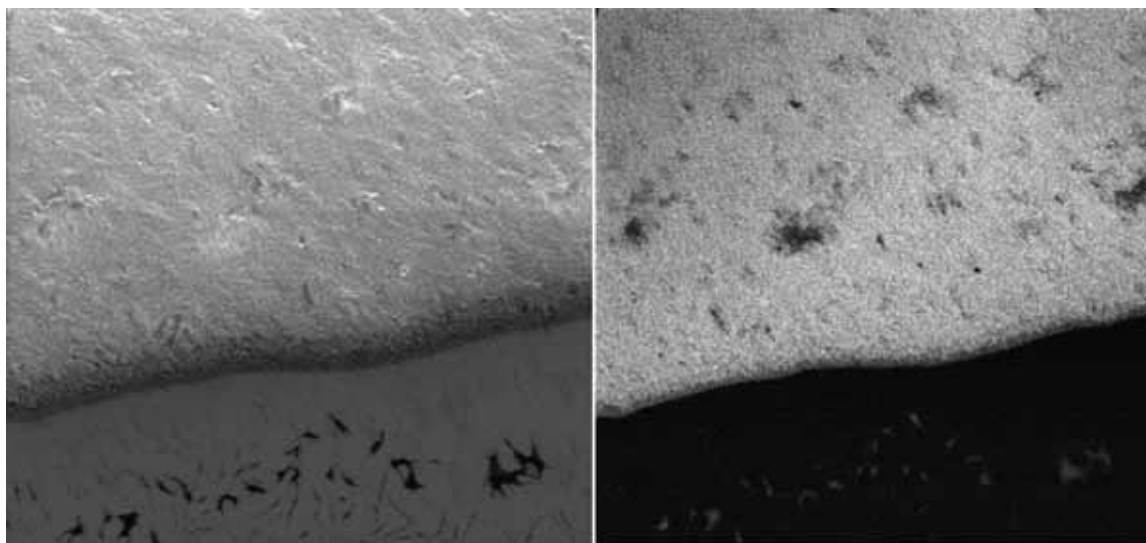
Figure 4.6 Cathode-luminesence from Core Shell Qdots. Left picture shows Cdse/ZnS qdots under SEM, and right shows the corresponding CL image. This is the edge of a drop of avce qdots evaporated on a surface.

4.7 Plasmonic interactions with quantum dots

Recently, there has been a surge of interest in plasmonic interactions with dyes and nano-crystals[79] because of the possibility of enhancing light emission by improving efficiency. This would impact many fields ranging from solar cells to sensitive biological assays[80,81, 82]

My colleague, Koichi Okamoto, has been successful at using gold films to enhance emission from indium gallium nitride wells[83] as well as dyes[84]. Surface Plasmon-based

enhancement has been demonstrated in a number of cases[85, 86]. We wondered if a similar enhancement could be achieved in quantum dot emission using evaporated gold films.

In our experiments, we found that a simple evaporated gold film can enhance emission 23-fold. This is nearly one order of magnitude.

The experimental setup is shown in Figure 4.7. On a quartz cover glass, we thermally evaporated a 50-nm gold film. Core shell and core quantum dots were dispersed on the surface. These dots were CdSe core ZnS shell with a photoluminescence peak close to 620 nm. They are suspended in toluene, have a diameter of about 4 nm and were obtained from Evident Technologies (Troy, NY).
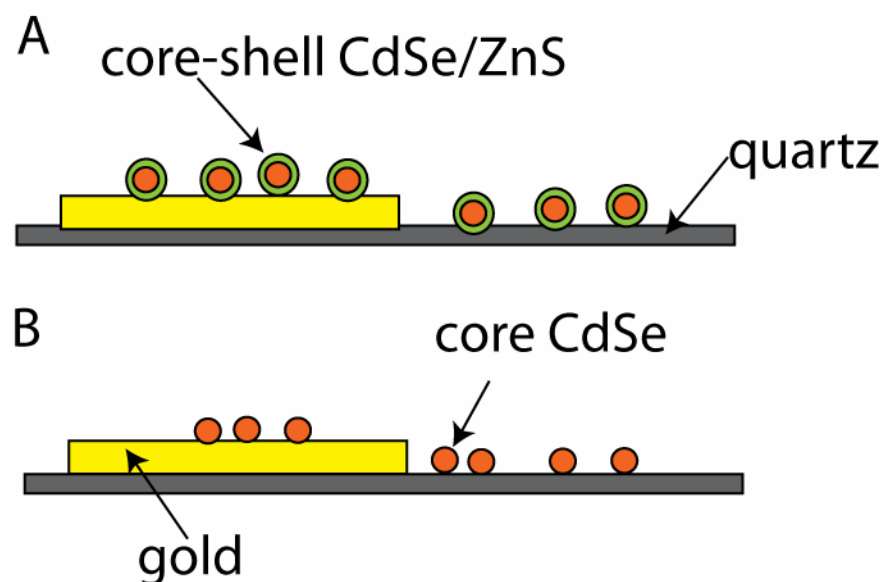
Figure 4.7 Quantum dots on gold films. A) Core shell CdSe/ZnS quantum dots dipersed on gold film b) Core CdSe quantum dots dispersed on gold film.

These cover glasses were illuminated with a solid state blue laser at 400 nm, and the photoluminescence was measured using a cooled CCD (Princeton instruments) that had a 10 micron slit width and a 300 mm^{-1} grating. We noticed a significant enhancement for the core dots, but not for the core shell qdots.
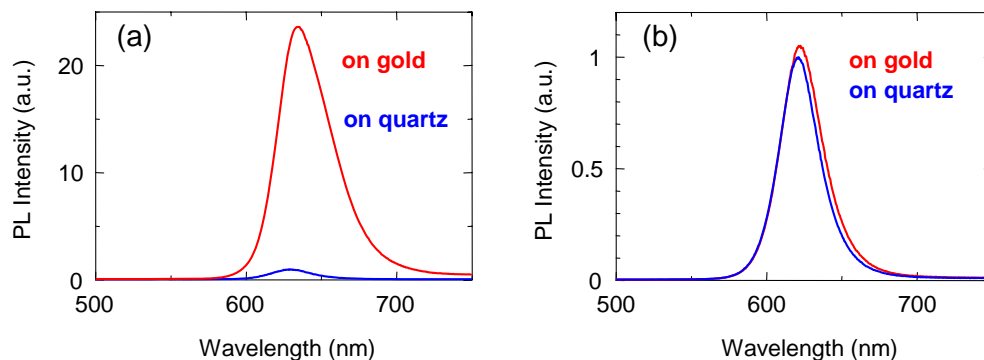
Figure 4.8 Pholuminescence spectra a) Core CdSe qdots on quartz normalized b) core-shell CdSe/ZnS on quartz normalized.

A 23 fold enhancement is quite remarkable and implies some kind of coupling between the gold and the qdots. I must mention that the normalization is from the graph; we should not compare the core shell and core qdots, because they have been normalized separately. We can only compare them with themselves – either on gold or on quartz.

The same samples were then taken for time-resolved measurements. We use a Ti- sapphire mode locked laser. The wavelength had to be doubled to get the correct excitation wavelength for the qdots – about 400 nm. The pulse width was chosen to be 100 femto-seconds with 80 MHz repetition rate. The signal was fed to a Hamamatsu streak camera (Hamamatsu Photonics C4334), which can resolve signals to 5 pico seconds.
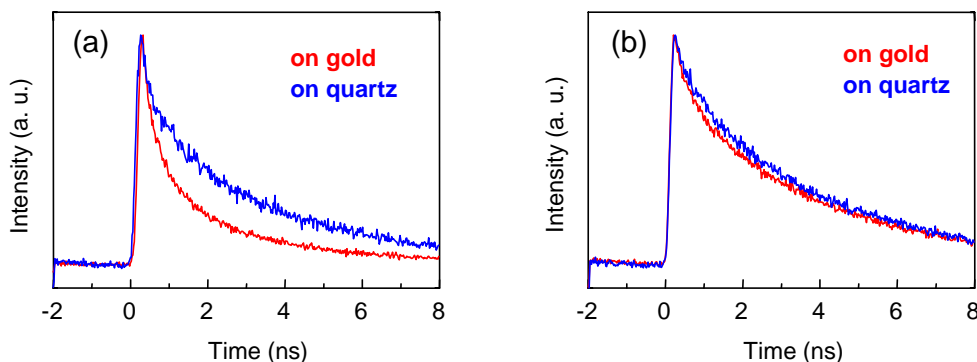
Figure 4.9 Time Resolved Measurements of Qdots. a) CdSe core dots b) CdSe core shell dots.

Other groups have demonstrated the coupling of quantum dots to surface plasmon modes - for instance, with colloidal gold or with silver nano-arrays[79, 87, 88]. However, this method is rather simple to implement compared to others, and we are able to show considerable enhancement without any attempt at optimization.

To understand the difference between the two types of qdots, we obtained the dielectric functions of CdSe and ZnS from previous literature[89, 90]. The surface plasmonic mode at the metal dielectric interface can be written as:

$$k = \frac{\omega}{c} \sqrt{\frac{\varepsilon_1 \varepsilon_2}{\varepsilon_1 + \varepsilon_2}} \qquad [4.1]$$

From this we can calculate the dispersion diagram, and from that we can calculate the surface plasmon frequency to be 2.2 eV for the CdSe/gold interface and 2.3 eV at the ZnS/gold interface. This difference is small, and moreover the ZnS is a very thin layer, much smaller than the surface penetration depth of surface plasmon, implying that this is not the reason for the discrepancy between the core and core shell qdots.

Quantum efficiency of an emitter η is calculated as:

$$\eta = \frac{k_{rad}}{k_{rad} + k_{non}} \qquad [4.2]$$

where k_{rad} and k_{non} are the radiative and non-radiative rates. With surface plasmon coupling we have an extra rate term k_{sp} changing the expression for efficiency to:

$$\eta^* = \frac{k_{SP} + k_{rad}}{k_{SP} + k_{rad} + k_{non}} \qquad [4.3]$$

The presence of the ZnS shell is to reduce k_{non}. By providing a higher energy barrier, it confines the excitation, reducing the non-radiative losses through the surface. In fact the CdSe efficiency increases from ~2% to ~40% due to the shell. The surface plasmon coupling works in a completely different way, changing the radiative rate by adding an extra way to couple light out.
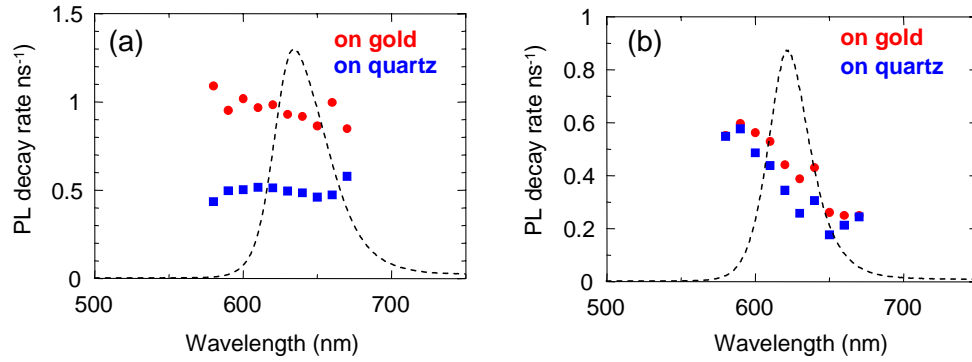
Figure 4.10 PL decay rate a) for core qdots b) for core shell qdots.
The dotted line is the photoluminescence

The effect of the shell is clearly seen in the photoluminescence rates, calculated from the streak camera data and plotted in Figure 4.10. The photoluminescence decay rates may be given as $k_{pl} = k_{rad} + k_{non}$. For the coupling with surface plasmon, this changes to $k_{pl}^{*} = k_{rad} + k_{non} + k_{sp}$. The Purcell enhancement factor may be calculated as $E_{pur} = k_{pl}^{*}/k_{pl}$. We can calculate the Purcell factor as:

$$E_{pur} = \frac{1-\eta}{1-\eta^{*}} \quad [4.3]$$
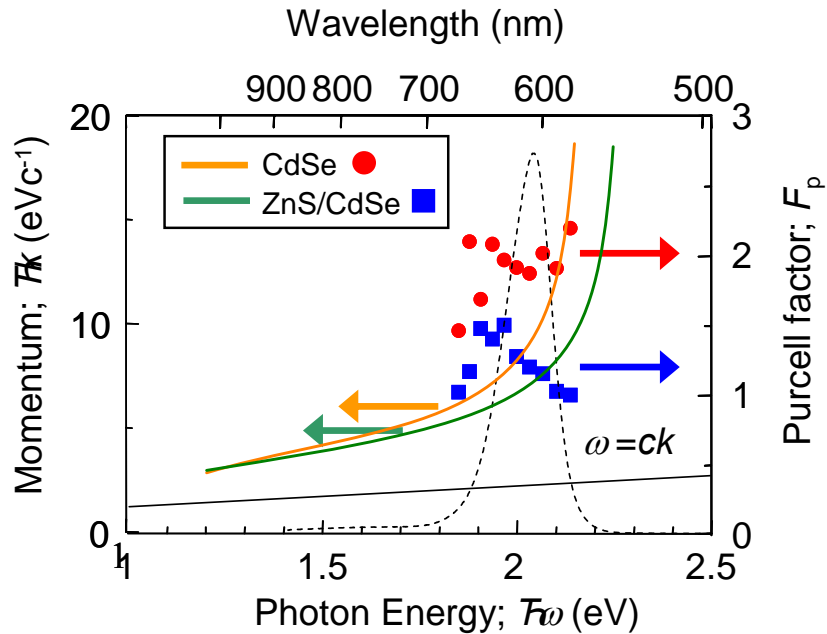
Figure 4.11 Purcell factor and the dispersion curve. Core and core shell qdots on gold - both the dispersion curve and the Purcell enhancement factors are plotted.

The Purcell factors are calculated and plotted along with the dispersion curve in **Figure 4.11**. From these diagrams and Equation 4.3, we can start to discern the reason for the difference between CdSe core and Cdse/ZnS core-shell quantum dots. A Purcell enhancement factor of about 2.2 makes a large enhancement to the emission of a low-efficiency emitter like CdSe core dots – from 2% to about 51%. On the other hand, in CdSe/ZnS core-shell dots, the enhancement is from 45% to 75% with enhancement factor of 2. Thus, the enhancement is about 20 fold with Cdse and <2 fold with CdSe/ZnS.

In conclusion, this method represents one of a few ways to enhance the emission from low-efficiency emitting materials. Instead of reducing non-radiative transition it works by coupling to surface plasmons, enhancing the radiative rate. This could be used as a simple way to enhance emission from indirect band-gap materials like Si, Ge, SiC etc. It will not be that useful for bright materials. With regard to quantum dots, it suggests that we can also use gold as a cladding layer instead of ZnS and get bright emission.

4.8 Enhanced emission though chemical means

While working with quantum dots, I had a meeting with Mohan Sankaran, who was producing silicon quantum dots using a plasma processing method[91]. The quantum dots he produced showed low efficiency. Quantum dots tend to have non-radiative recombinations through defects on the surface, causing blinking[92]. A paper published by T. Ha group at UIUC [93] was able to show that beta-mercaptoethanol (BME) was able to suppress blinking completely in quantum dots. The explanation offered was that BME was a strong electron donor and on attaching to the surface plugged the defects, making them ineffective.

We wondered if it was also possible for that this mechanism to work for Si quantum dots. In T.Ha's experiments, the quantum dots were CdSe/ZnS quantum dots coated with streptavadin – very different from Si quantum dots in toluene. The Si dots would rapidly become dark in a few seconds when exposed to UV light from a 200W mercury lamp attached to the microscope (Nikon TE 200).
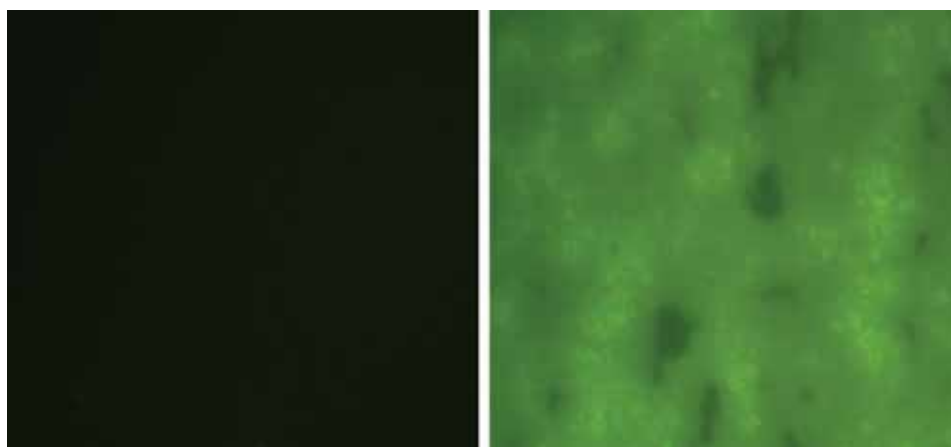
Figure 4.12 Si quantum dots passivated with BME. On the left is a picture of a sample after 1 minute of UV illumination. The sample on the left after a minute but this time with BME added.

In our experiment, we found clear evidence that BME seems to prevent blinking in quantum dots and prevents the dots from going into a dark state. This experiment shows the interesting ways in which passivation of quantum dots can influence its properties strongly and provides another way to enhance quantum dot emission.

Both these methods – gold films and chemical passivation - provide a way to enhance the emission of quantum dots if they don't have high quantum efficiency. It is likely that they will find use mainly in future light emitting diodes and solar cells.

4.9 Optofluidics: Hydrodynamic focusing

A width of a microfluidic channel does not necessarily determine the width of fluid stream. It is possible to have streams of fluid that are much smaller than the channel. There are two ways to do this. One way is to pattern hydrophobic and hydrophilic pattern on the surface of the channel – then, fluids will remain on the surface that they wet. Another option is to use hydrodynamic focusing, which relies on the fact that at the scale of micro-fluidics, flows are mostly laminar, so the only mixing that happens is via diffusion unless special mixers are designed[94].

Here we shall describe attempts to write a pattern of quantum dots inside a microfluidic channel by hydro-dynamically focusing a mixture of quantum dots on a surface. The applications of this method could lie in memory barcode devices as well as protein patterning. Initially, this work was done in collaboration with Aziel C. Epelepsia.
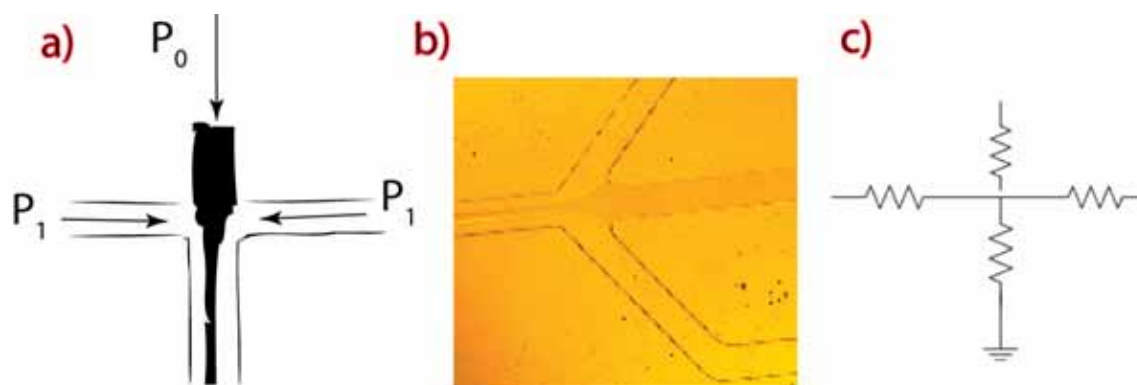
Figure 4.13 Hydrodynamic Focusing a) schematic of the chip b) A picture of a focused stream c) electric circuit model of the focusing.

Hydrodynamic focusing is the idea of having two different streams of fluids meet at a junction, as shown in **Figure 4.13**. By varying the pressure of the streams, we can change the width of the center stream. Widths as small as 50nm have been reported[95].

Hydrodynamic focusing has applications in measuring reaction dynamics, separation of molecular species and cells and patterning[96-99]. Three-dimensional hydrodynamic focusing has also been reported[100].

The fluid flow can be modeled as a resistive circuit shown in the Figure 4.13. Each line has its resistance to fluid motion and the current represents the flow. The expression that gives the
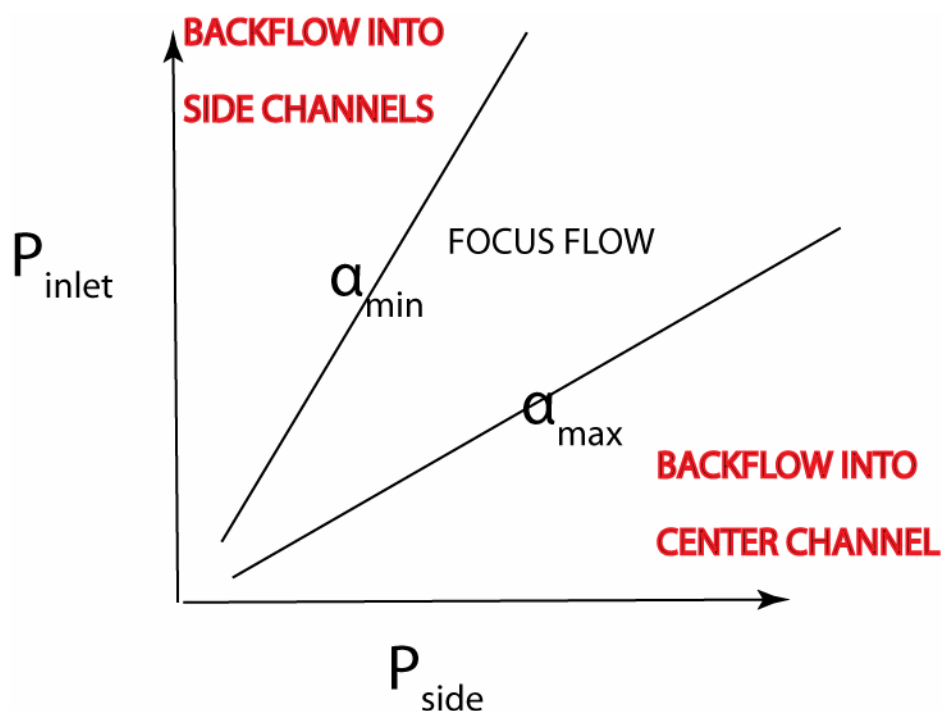
Figure 4.14 Focus flow. Focus flow occurs only for a range of pressures. At other pressures there is backflow.

width of the stream (assuming low Re and large lengths of channel relative to the width) is fairly complicated[95]. If the ratio pressures between the central channel and side channels is $\alpha = P_{side}/P_{center}$, and the ratio of fluidic resistances between the side and central inlet is β and the outlet channels and the side channel is γ, then the width w is proportional to:

$$w \propto \frac{1 + 2\gamma - 2\alpha\beta\gamma}{1 + 2\alpha\beta\gamma}$$

This assumes that spreading by diffusion is negligible and applies only to the center of the channel. Focus flow occurs only for a center range of the α parameter, as shown in **Figure 4.14**.The α parameter range can be changed by changing the angle of the junction. We found that an angle between 45 and 60 degrees was the best for the range of pressures we could operate at.
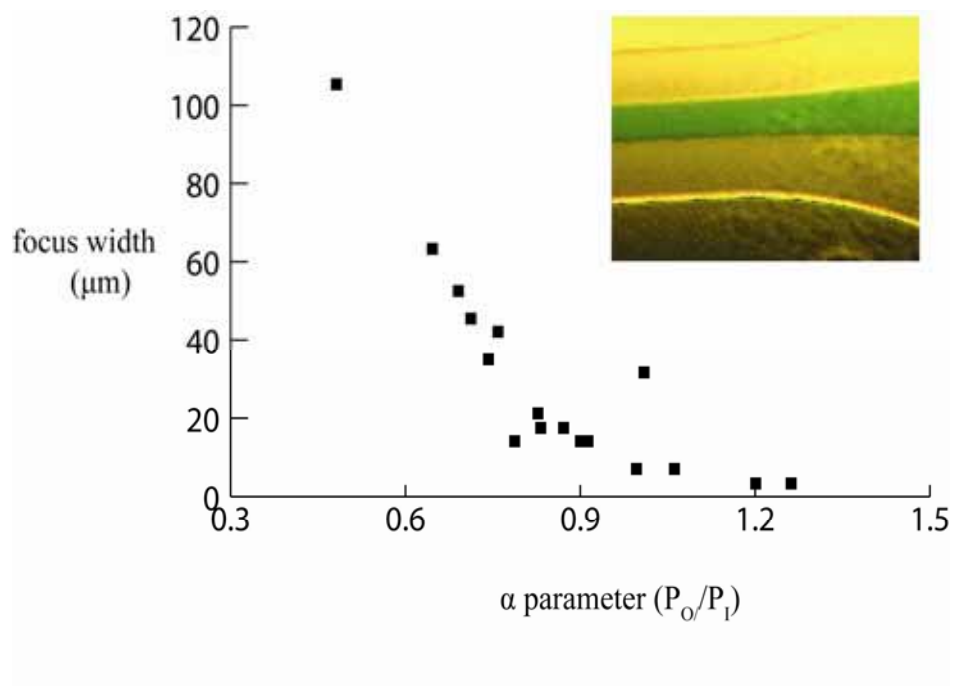
Figure 4.15 Focus widths with pressure. In one microfluidic chip we tested this was the width we obtained for different values of pressure.

In a paper that involved two streams mixing in a T- junction, it was shown that while at the center of the channels, the spreading transverse to flow scales as expected to a power law with exponent ½ down the channel[101, 102]. However, near the walls, the scaling exponent changes to 1/3 – this time both with distance down the channel and the inverse average velocity.
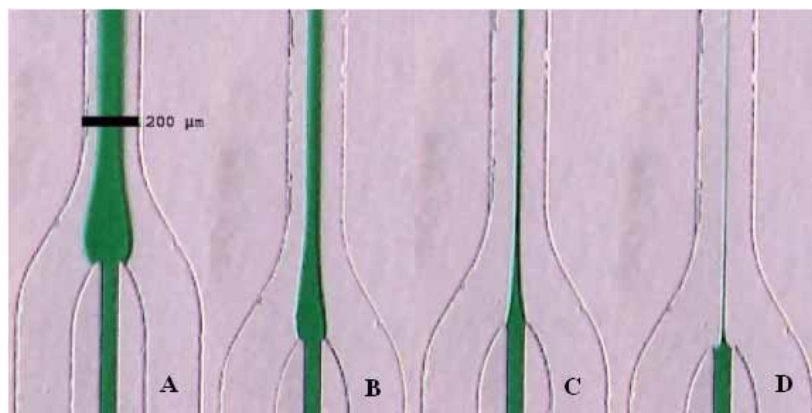
Figure 4.16 Focus width change. Green food dye is used here to show the change in focus.

There are two possible regimes of operation – if Pe (Peclet number) (= vH/D where v is the average velocity, H the height of channel and D the diffusion constant) is much greater than z/H – where z is distance down the outlet channel, then the difference between the diffusion boundary at the top and center of the channel is significant. Otherwise it is insignificant. Of course, Pe must be >1 to insure that convection dominates over diffusion.

We were also able to vary the position of the stream by varying the pressures in the side channels as shown in Figure 4.17.
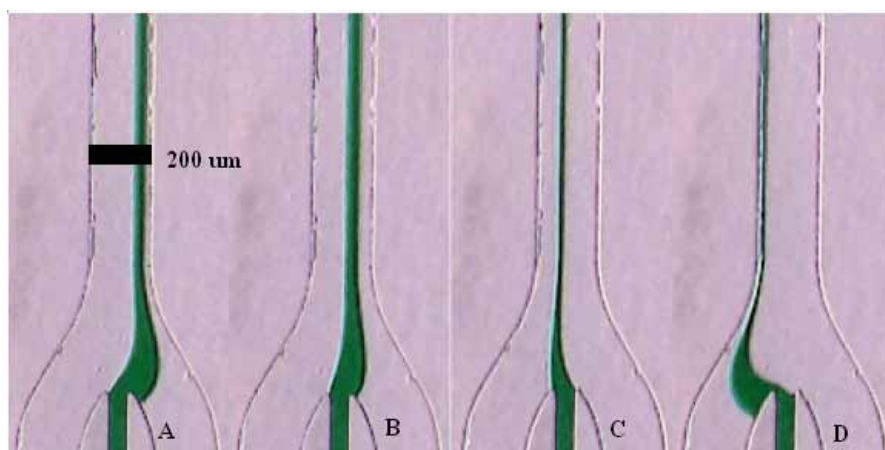
Figure 4.17 Moving the Focused Stream

The width of the focus changes a bit as we move from the center of the channel to the sides, as seen in the **Figure 4.17**, but it is still a focused flow. In all of these experiments the channel height was about 10 microns and the flow rate was about ~1000 micro-liters/hour, implying a Pe > 1000.
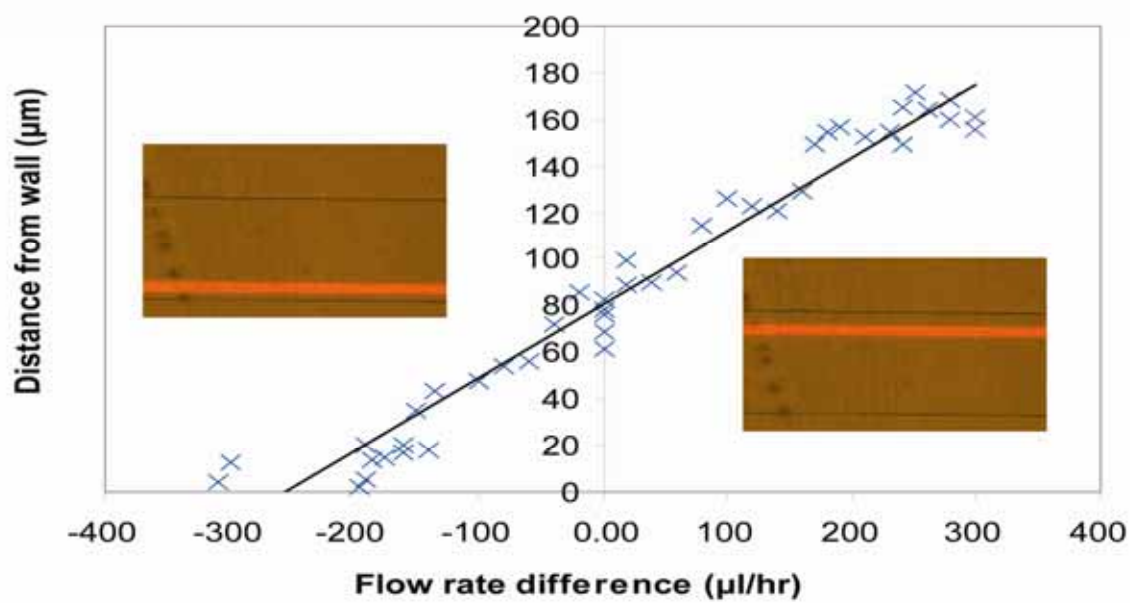
Figure 4.18 Adjusting Pressures to Move Focus.
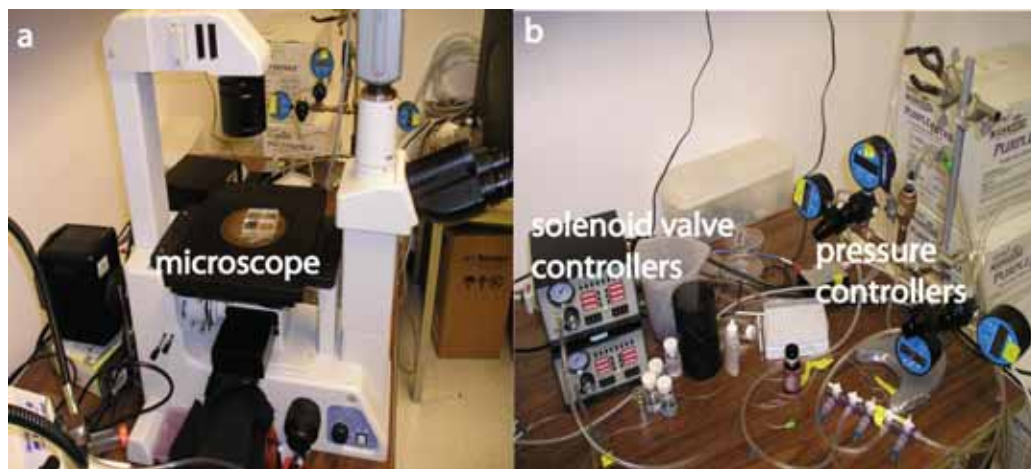
Figure 4.19 Apparatus to change pressure a) Nikon TE 200 inverted microscope equipped with a quantum dot filter and mercury lamp. B) pressure and valve controllers.

4.10 Writing a line

With the setup, we tried to flow quantum dots coated with streptavadin on a biotinylated surface. The biotinylated surface was produced by coating a cover glass with amino silane groups and following that with biotinylation. Another alternative is to use biotinylated BSA and get it to stick to the surface.

Initially, I would flow plain water into the side channels and buffered quantum dots into the center channel. The presence of plain water caused the qdots to precipitate and lose crystallinity, so I shifted to buffered solution in all channels.
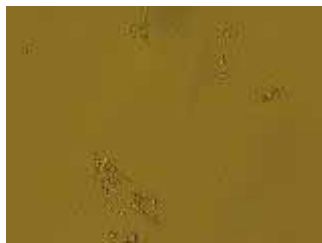
Figure 4.20 Quantum dots precipitate. When exposed to DI water, quantum dots lost their fluorescence and some precipitates were left behind.

This allowed focusing, through every attempt at drawing failed because the dots would coat the entire surface instead of just the focused spot area. Two effects are responsible – first, because of the flow profile in these channels, the flow is zero at the surface, which contributes to diffusional spreading. The second effect is the contribution of the bonding, which changes the rates constants – once a quantum dot is anchored to the surface, it is effectively taken out of the system. Moreover, in these miscible systems, the diffusion rate of quantum dots is of the order of 10 micron/s, so the dots can fill the channel in a few seconds if the solution is left standing without flow.
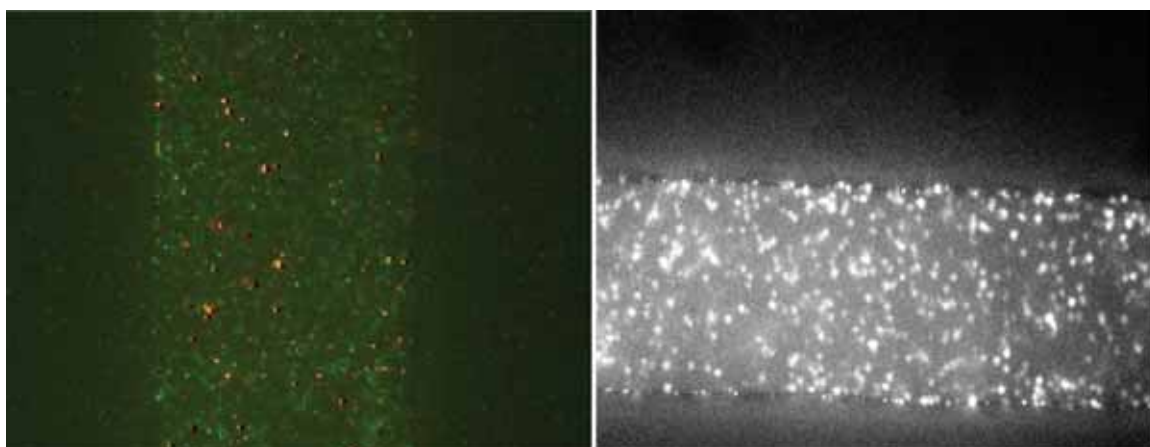
Figure 4.21 Quantum Dots on Surface. All attempts at focusing quantum dots left the entire surface coated with dots instead of a line

In light of this failure, I started to investigate 2-phase systems consisting of mineral oil in the side channels and buffered quantum dots in the main channel. This leads to a complicated set of flows, the phase space of which has been modeled previously[103]. The first flow without any surfactant tends to be fairly random, with the oil near the walls and buffered qdots near the center. With surfactant two phases were seen – a stratified phase and a "blob" phase.
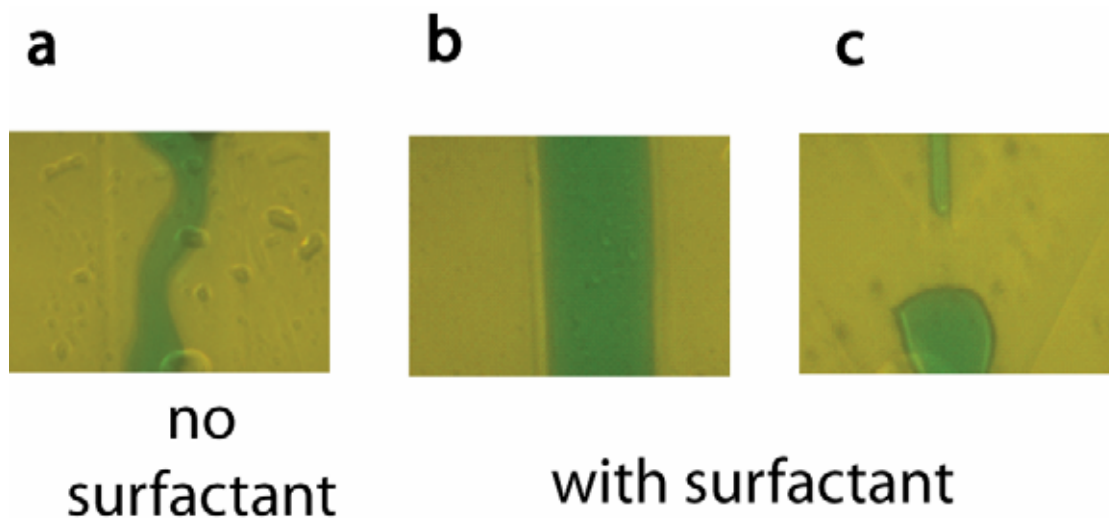
Figure 4.22 Two phase flows a) no surfactant
leads to random flows that change with time, with
surfactant we see b) stratified and c) blob phases.

These two phases are in line with the expectation of two phase flows previously seen. The surfactant we used was Dupont Fluorosurfactant FSN, in quantities less than its critical micelle concentrations. We were able to draw a thick line in the stratified phase.
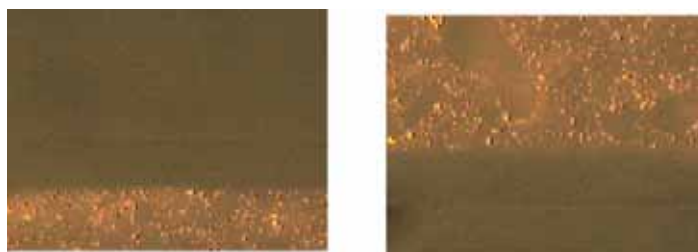
Figure 4.23 Thick Line using Two Phase Flows. A thick
quantum dot line written using oil/aquesous flow. The line is >100
microns wide

Finally I moved to liquid/air two phase flows, with air in the outer channels and buffered
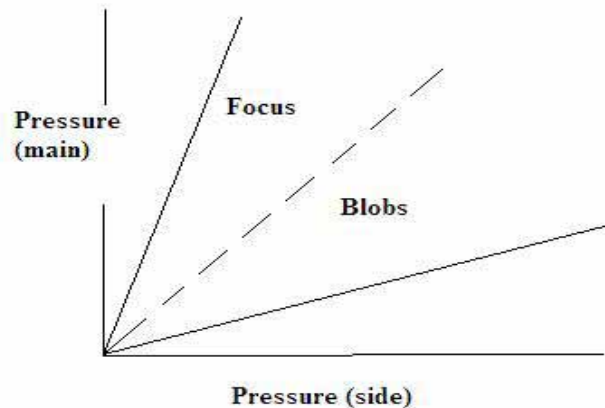
Figure 4.24 Phase diagram of air/liquid flows

quantum dots in the inner channels. Again, small amounts of surfactants were used to stabilize the flows. These flows are hard to control. Some pictures are shown in Figure 4.24. Air/liquid flows have the advantage that the quantum dots cannot cross the air/liquid boundary and must remain in the liquid. This allows us to change the focus, and even if there is no flow for a while, there is no diffusion to contend with. Again, there are two phases: a blob (or pearl) phase and a focus phase. Basically, there is a cutoff capillary number, Ca, where the flow switches. At low velocities of the liquid phase (low center pressures), Ca is small and surface tension wins leading to blob flow. As the flow speed increases, Ca increases and focus flow becomes viable. Surfactants reduce surface tension, changing the capillary number and thus changing the slope of the line dividing the two phases. We, of course, want to work in the focus flow phase and using it to draw a line. It is again possible to move the focused line by varying the side pressures.
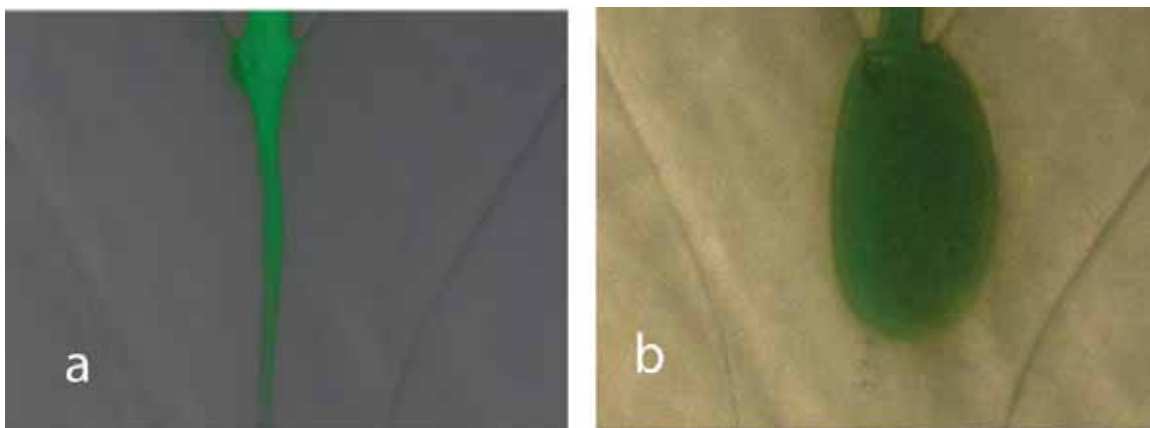
Figure 4.25 Pictures of Two Phase Air/Liquid Flows. Two cases are possible a) focused flow and b) "blob" flow. Focused Flow occurs at high flow rates of the central channel relative to the side channels. Surfactants can influence where exactly the change phase and occurs.

We were successful in writing a three-color barcode in a channel with these flows. Shown in **Figure 4.26** is an example of a 3-color line – essentially a 3-bit code.

Writing lines

605 nm

655 nm

565 nm
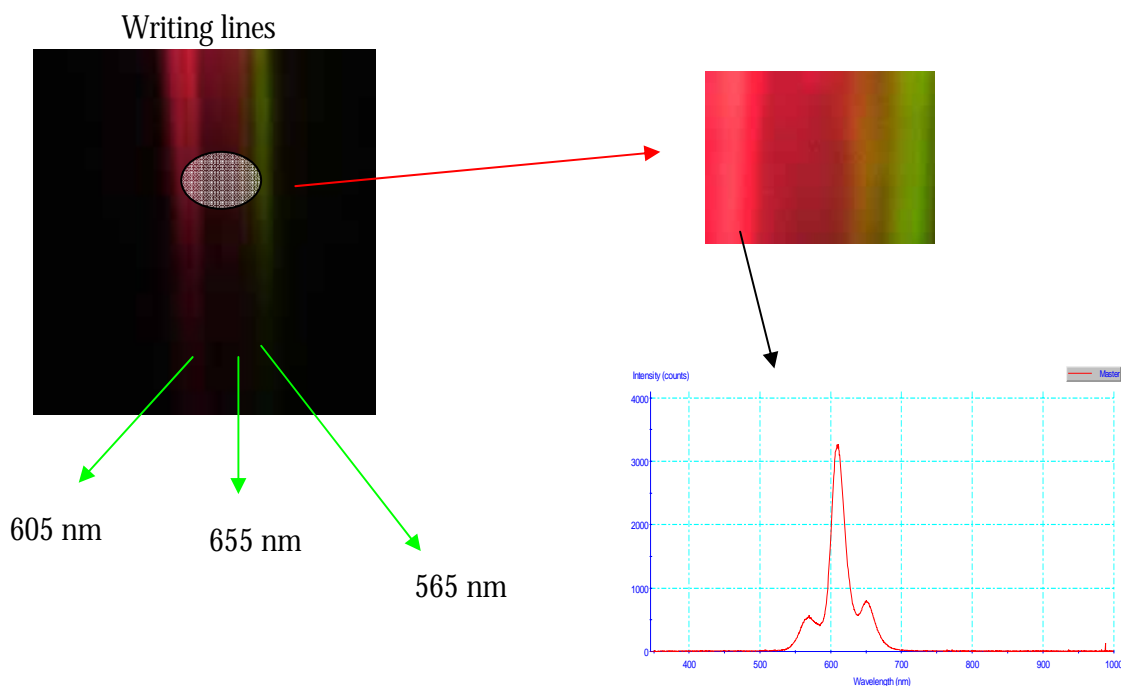
Figure 4.26 3 Color Line. Using three different colors of quantum dots and air – liquid flows, we were able to write the pattern.

4.11 Spectrofluidic Memory

Besides making these hydrodynamic flows, I also collaborated with the Psaltis group at Caltech, helping them to try and make memory devices out of quantum dots. We had only limited success with these, and a description is available in a conference paper[104]. I helped design the microfluidic chips for that work, a picture of which is shown below.
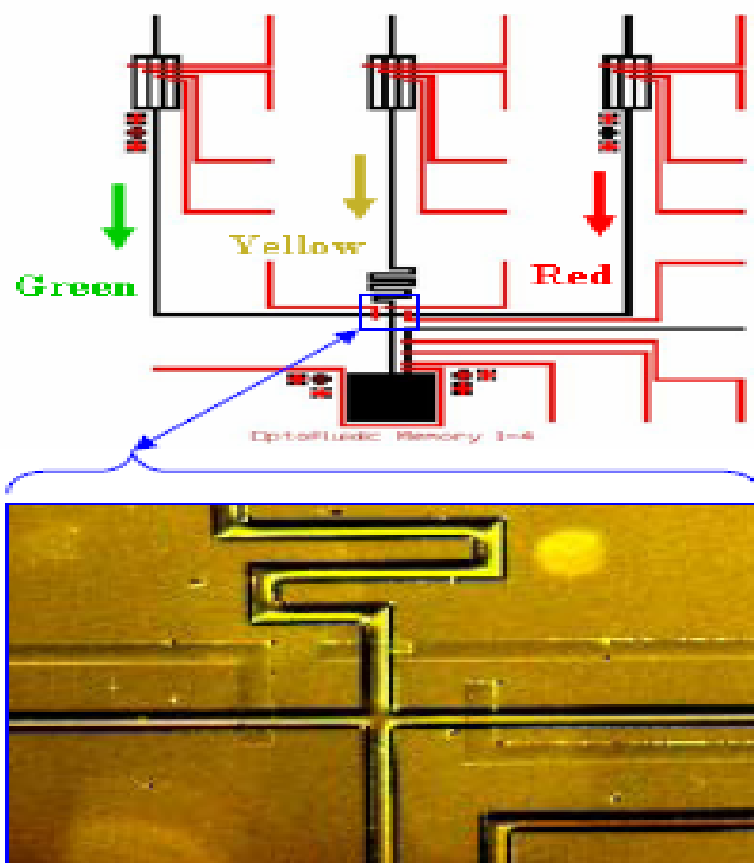
Figure 4.27 Quantum dot mixer A microfluidic chip allowing
the mixing of three quantum dots.

4.12 Conclusion and Acknowledgement

Opto-fluidics is a relatively new concept, though light and fluids have been combined together for many centuries, as anyone who has seen a musical fountain can attest. The combination of multilayer soft lithography chips that allow a simple way to have unprecedented control over fluids and photonic crystals or other photonic structures that allow unprecedented control over light is almost certain to result in novel devices in the future.

I would like to thank Aziel C. Epilepsia, who did a summer project on hydrodynamic focusing. Some initial results shown here came out of that collaboration. Thanks are due to Koichi Okamoto, who was instrumental in making me aware of surface plasmons. Collaboration with him led to the work on enhancing quantum dot emission. Brian Zhou, a summer undergrad student, worked with me on the quantum dot composites project.

Mohan Sankaran provided me with some Si quantum dots to perform experiments. Finally, members of Psaltis group including Baiyang Li, James Adleman and David Erikson collaborated with me on Optofluidics in general.

C h a p t e r   5

SELF ASSEMBLY: DNA PHOTONICS[*]

5.1 Introduction

In the murky, shallow depths of ponds and swamps, live purple bacteria, *Rhodopseudomonas acidophila*. This bacterium has evolved, over millions of years, to make use of the tiny amount of red and infra-red light that is able to penetrate through the algae films above it. The light is absorbed by a protein pigment complex that relays this energy to another ring, which funnels it into the main reaction center, providing energy for photosynthesis[105, 106]. These self-assembled machines rely on interactions involving protein conformational change, as well as energy and electron transfer. The light-harvesting complex II (LH2) of purple bacteria is about 30 nm wide and has a collection efficiency of 90%, vastly exceeding man-made designs[107]. In fact, every photosynthetic plant or bacteria has a variant of this light harvesting complex – without it, life as we know would not exist[108].
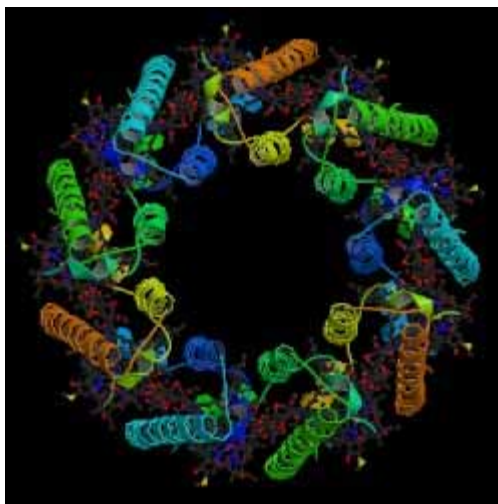
Figure 5.1 Light Harvesting Complex II of Purple Bacteria
(from Protein Data bank)

Can man-made devices replicate the light harvesting center? Unlike most man-made photonic devices, which rely on the classical Maxwell's equations of physics to propagate energy, natural designs rely more on quantum mechanics principles for energy transfer. Various attempts have been made at designing similar molecules in the form of porphorins or dendrimers[109]. Here, I describe an attempt to make waveguides using dyes and DNA that rely on an energy transfer principle called Fluorescence Resonance Energy Transfer (FRET).

5.2 FRET

FRET is a near field, radiation-less dipole–dipole interaction[110]. Two dyes – a donor dye and an acceptor dye in close proximity (<50 nm) - can interact via FRET with the donor dye, giving its energy to the acceptor dye. The exact form of the law was worked out by Thoreau Forster over fifty years ago. The energy transfer depends on the spectral overlap between donor and acceptor, the orientation and the quantum efficiency of the donor. The rate is proportional to:

$$ k \propto \frac{J\kappa^2 \Phi_D}{R^6} $$

[5.1]

Here, J is the overlap integral, R the distance between the two dyes (also called fluorphors), φ_D the donor quantum efficiency, and κ the orientation factor. The exact formula for each term is available in many references[111, 112].
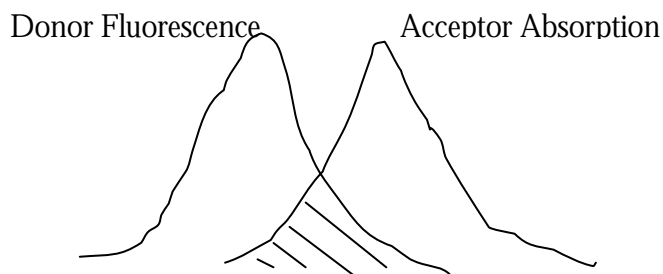
Figure 5.2 Spectral Overlap. Overlap between donor fluorescence and acceptor absorption

Acceptor

Donor
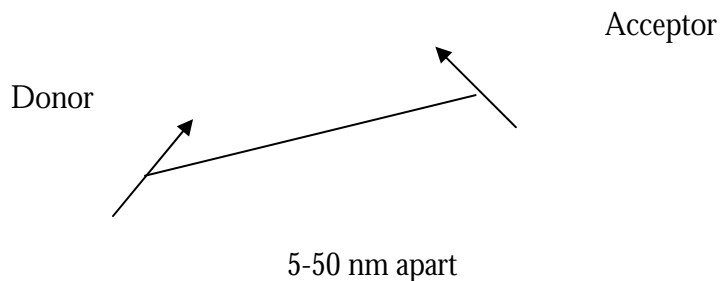
5-50 nm apart

Figure 5.3 Interactions between Dipoles. For FRET, the dye
molecules must be <50 nm and >5nm apart. The orientation of
molecules is important.

For any two dyes, a number called the Forster radius, R_0, can be calculated[112]. This gives
the distance at which the energy transfer is 50% efficient. Efficiency may be calculated for
any other distance, R, by the formula

$$\eta = \frac{1}{1 + (R/R_0)^6}$$ [5.2]

The efficiency of energy transfer falls off very rapidly as the distance between the dyes
increases. This explains why we consider FRET to be a near-field interaction. FRET has
been used as a spectroscopic ruler to measure small distances[113]. It is also clear from this
formula that in optimal conditions, FRET efficiency can approach 100%.
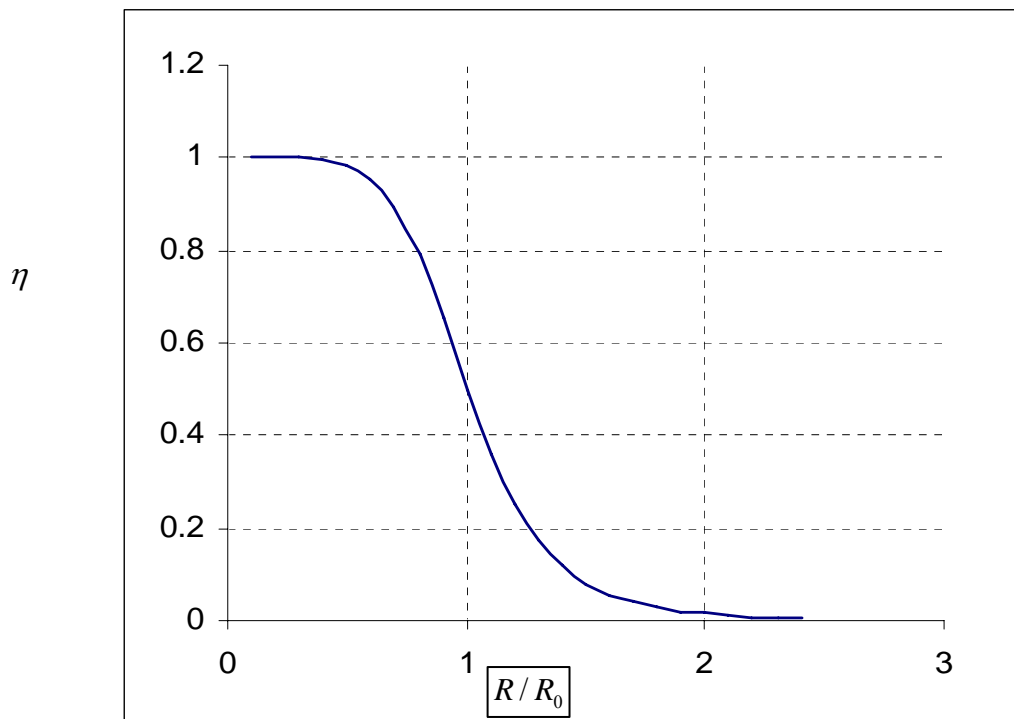
Figure 5.4 Change of Efficiency with Distance. The efficiency
of FRET falls with the sixth power of distance.

When the distance between the dyes becomes less than 5 nm, electron transfer is also possible. This is called Dexter transfer, and its efficiency falls off exponentially with distance, because it depends on the overlap between atomic orbitals[114]. When dyes are very close, the electrons could be considered localized over both of the dyes. In photosynthesis, both of these processes are important and work hand in hand.

5.3 DNA

DNA is a versatile molecule. As a polymer, it has a persistence length of 50 nm when double-stranded. Any sequence can be easily made in modern DNA synthesizers. In recent years, a variety of patterns have been made with DNA – including nano-cubes, octagons, smiley faces, tiles etc[115-118]. The recognition capabilities in-built in DNA make it possible to computationally design many structures that self-assemble. Conjugating dyes to DNA is also a mature field and hundreds of dyes can be conjugated to DNA. Thus, DNA is a versatile molecule for experimenting with molecular photonics.
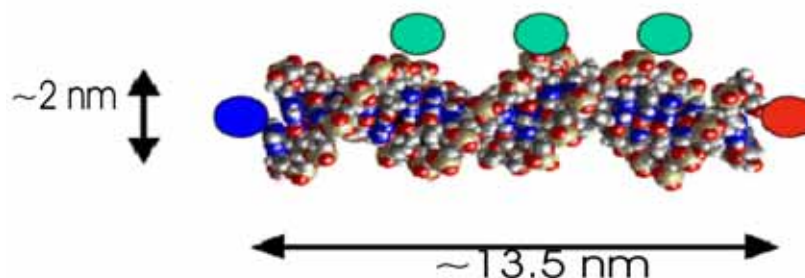
Figure 5.5 Molecular Photonic cascade. A cartoon representation of our DNA molecule with the dyes. The energy moves from left to right.

5.4 FRET measurements

FRET measurements can be done at the single molecule or, more conventionally, at the bulk level[119-121]. Despite many advances over the years, precise quantitative measurements are still difficult. The fluorescence of a dye depends on many factors like pH, salt concentration, the molecular entity it is conjugated with, temperature, presence of quenching agents, etc. Moreover, the FRET efficiency also depends on quantum yield and the orientation of the dye, which are hard to calibrate precisely. Thus, most measurements tend to be semi-quantitative. Measurements can be made of the increase in the acceptor fluorescence or the decrease in the donor fluorescence. The efficiency (η) can be directly measured by

$$\eta = 1 - \frac{F_{with\_acceptor}}{F_{no\_acceptor}} \qquad [5.3]$$

Here, F represents the fluorescence of the donor, and the subscript tells us if the acceptor is present of not. In general, the fluorescence from a dye depends on the concentration, extinction coefficient (how much light it absorbs) and its quantum yield (how efficiently

does it convert energy). Later in this chapter, we shall describe a simple model for multi-FRET systems. FRET is commonly used in biology as a marker for distance[122].

5.5 Bi-FRET 3-dye systems

Our design involved having an input dye, an output dye and a chain of dyes in-between to carry the signal. Previous work on this topic had involved using a set of unique dyes in a cascade. We realized that only three dyes are needed, because FRET can also occur back and forth between the same dye. The energy will move in one direction if there is a gradient at from start to end – and the input and output dyes provide this gradient.

Initial experiments were done with a 19-mer DNA sequence. We wanted to try to study 3 dye systems to confirm that input and output dyes functioned as expected. Similar work has been reported elsewhere with other dyes[123].The sequence was selected after checking to insure that DNA hairpins would not form. The sequence used was 5'
AAGGGAACCACTCAATGTC 3' (strand X) and its complement (strand X*). Three fluorphors were used Cy5, 6-FAM (6-carboxyfluorescein) and TAMRA ([6-tetramethylrhodamine-5(6)-carboxamide). The fluorphors were selected after checking to see for the spectral overlap required for FRET. All molecules and dyes were obtained from Trilink Biotech (San Diego, CA). Cy5 was attached to 5' end of X, 6-FAM to the 3' end of X*, and TAMRA to the 10th base of X*. The spacing between the dyes represents a compromise between optimal distances for FRET, and reducing the possibility of energy transfers that skip a dye. The spacing between DNA base pairs is about 3.4 nm, and this combined with the length of the spacer arm of the dyes gives an approximate value for the distance between dyes. The helical pitch of DNA is about 10 base pairs, so dyes are either on the same side or the opposite side of DNA, depending on which strand they are on. Due to problems with purifying DNA strands with dyes, we used DNA strands with a maximum of 2 unique dyes.

DNA single strands in STE buffer (0.1 M NaCl, 10 mM Tris.Cl, 1 mM EDTA, pH 8.0) were annealed in equimolar amounts using a rapid thermal cycler (PTC-150 Mini-Cycler MJ Research). The annealing was done by heating to 74^0 centigrade for 10 minutes and then slowly cooling to room temperature over 2-3 hours. The concentration selected was

such that inter-molecular FRET was negligible compared to the intra-molecular FRET – the final molecular concentration was 20 nM in 800 μl in a cuvette. A fluorimeter Shimadzu RS 5301PC was used to measure fluorescence. Absorbance measurements were also made using Shimadzu UV1601. However, the absorbance cannot be used as a quantitative tool to measure DNA concentration, because the presence of dyes interferes by adding noise to the absorption signal and makes it hard to calibrate the sample.

For a control experiment, we also made molecules with one or two dyes missing. In what follows, the molecules with all three dyes will be referred to as FTC; if a dye is missing we put a _ in its place. So, for instance, _TC has the FAM dye missing, whereas F_C has TAMRA missing. We used 480 nm as the excitation wavelength, and 665 nm as the detection wavelength.
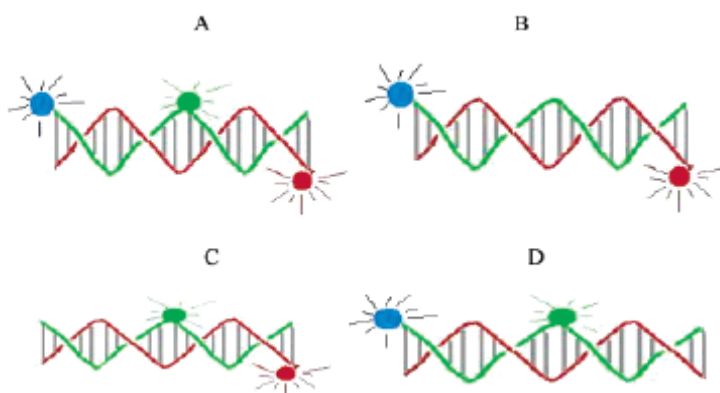
Figure 5.6 Bi-FRET molecules. Molecules were synthesized with A) all dyes present or one dye missing B) TAMRA dye missing C) FAM dye missing D) Cy5 dye missing

When FTC was excited by 480 nm light, a pronounced peak is seen was Cy5 emission. The peak was not seen if we used either _TC or F_C. Thus, the peak did not occur due to direct excitation or due to direct FRET between F and C, but transfer from F to C via T.
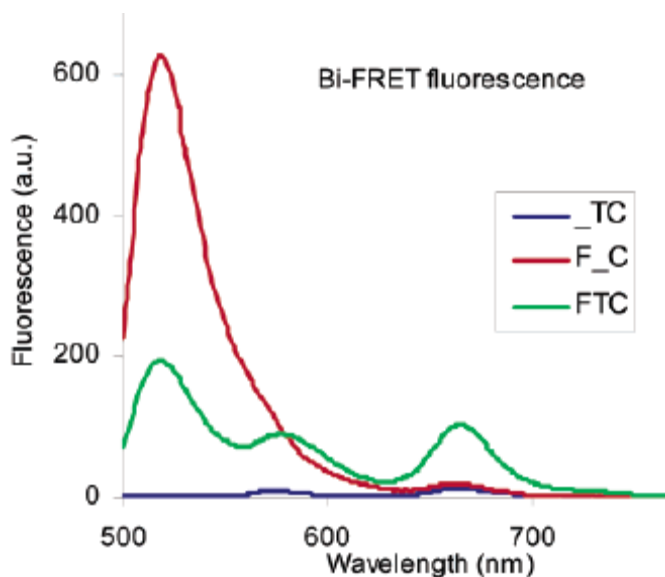
Figure 5.7 Bi-FRET Fluorescence. The molecules were excited at 480 nm. This experiment provides evidence that the energy is being transferred along the cascade via the center dye.

To make more quantitative measurements and determine the contribution of each dye, I fitted each dye's curve with a reference curve:

$$S(\lambda) = fF(\lambda) + tT(\lambda) + cC(\lambda) \qquad [5.4]$$

Where, S is the measured fluorescence that depends on the wavelength λ, and F, T and C represent the reference curves for 6-FAM, TAMRA and Cy5. A least square fitting method is used to fit the curves. The curve fitting has R values >0.99 in almost all cases.

On fitting the curve for TAMRA in FTC and FT_, we can determine the efficiency of TAMRA. To make these measurements, an excess of the X* strand (containing either no dye or Cy5) was added to the X strand. The measurements were made using 8 separate experiments for each molecule, and the results are shown in **Figure 5.8**. Error bars represent one standard deviation.
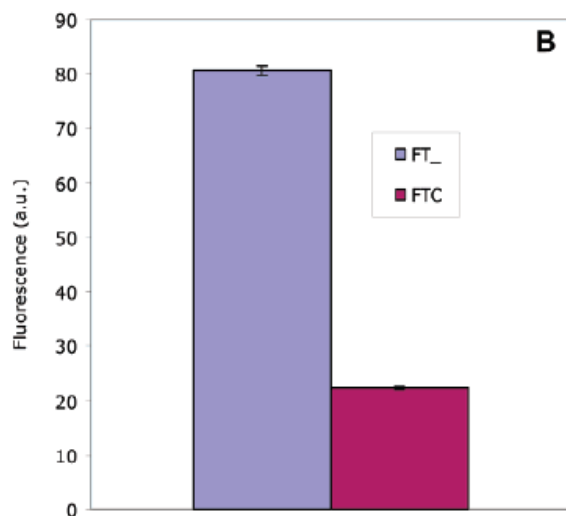
Figure 5.8 TAMRA Fluorescence in Bi-FRET molecules.
This graph summarizes 16 measurements done on FT_ and FTC
samples. The drop in fluorescence when the last dye is present is
clear and shows that energy is being transferred from F to T to C
rather than any other way.

This experiment provides further evidence that the transfer occurs from F to T to C dye and
other mechanisms are not very significant. IIya Fushman was able to take these molecules
and image them in his 2-color imaging system. The result is reproduced here from his
senior thesis.
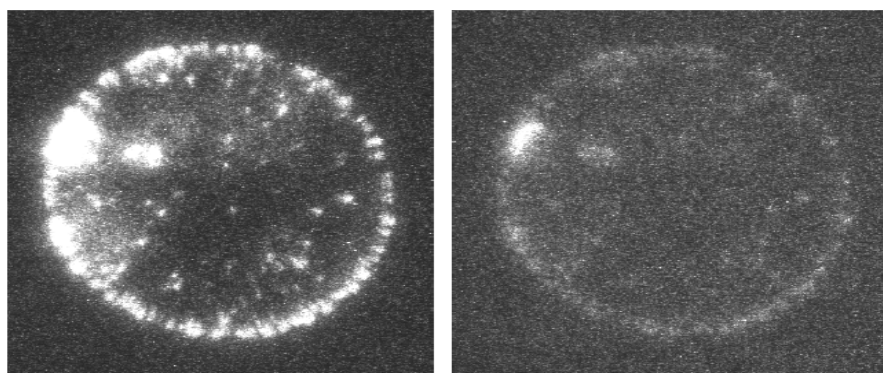
Figure 5.9 FTC Molecule Fluorescence in Two Colors. A drop
of FTC was put on a cover glass and imaged. Emission in 560-610
nm range windoe and 660-730nm window is shown on the left
and right resperctively (corresponding to TAMRA and Cy5)
Excitation wavelength was 473 nm (picture courtesy: Ilya
Fushman)

While 3 dyes are an interesting system, unless more dyes can be incorporated, the utility of the device will be limited. Using a dye cascade with a unique dye at every point is not a good solution because of the limited availability of dyes with correct spectral overlap, and the red-shift that occurs with every FRET transfer[124]. Instead, if we were to use the same dye the middle, there is no red-shift. With this idea, we decided to use multiple TAMRA units.

5.6 Multi-FRET

Experiments were done with 4-dyes systems – however, because they were done with a different set of dyes and not done by me (they were done by Keith M. Mathews) I shall not describe them. Recently, other authors have also shown similar results with a different set of dyes[125-127]. Instead, I will describe experiments with 5-dye or Quad-FRET systems that used the same dyes – 6-FAM, TAMRA and Cy5 as the Bi-FRET experiments. Here, we used a 40mer DNA strand 5′ TAGACAAGAAAGAGGACGAGTAACTGATAGGGACAACAT 3′ (strand Y) and its complement (Y*). Cy5 was attached to the first base pair of Y, and FAM to the 3' end of Y. TAMRA was attached to the 10th, 20th and 30th base of Y*. We also had some control DNA stands synthesized with a dye missing.
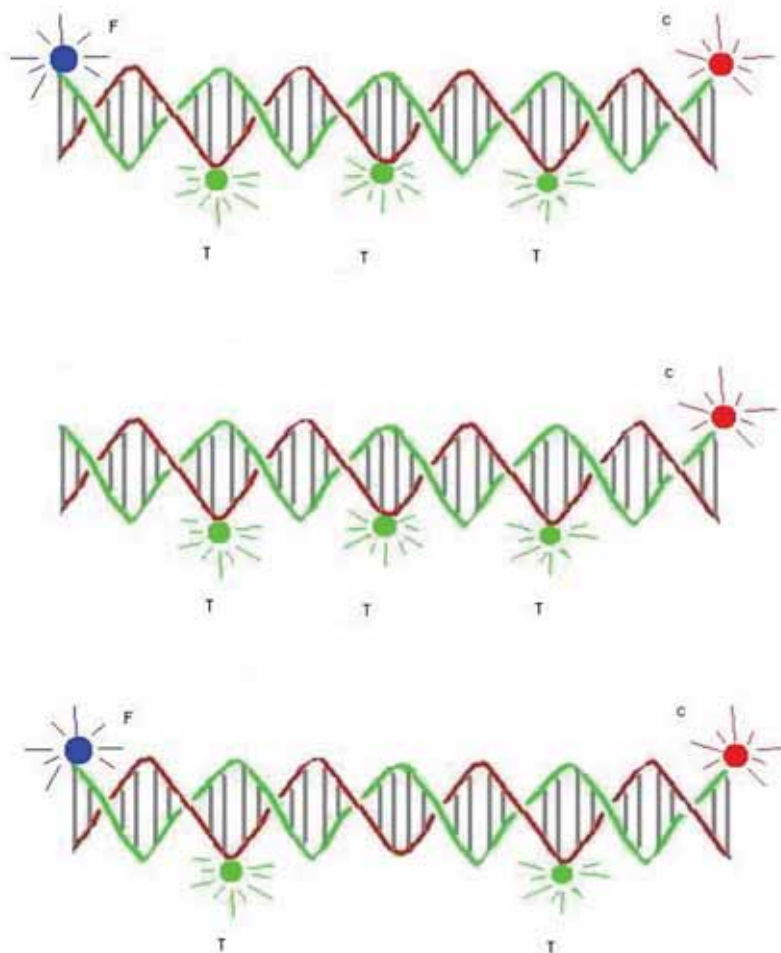
Figure 5.10 Quad-FRET Molecules. We synthesized DNA molecules with as many as 5 dye molecules. Control molecules with some dyes missing were also produced. The molecules are FTTTC, _TTTC and FT_TC.

In this molecule, we expect that the energy moves back and forth on the TAMRA dye. For three molecules FTTTC, FT_TC and _TTTC, the spectra is shown in **Figure 5.11.**
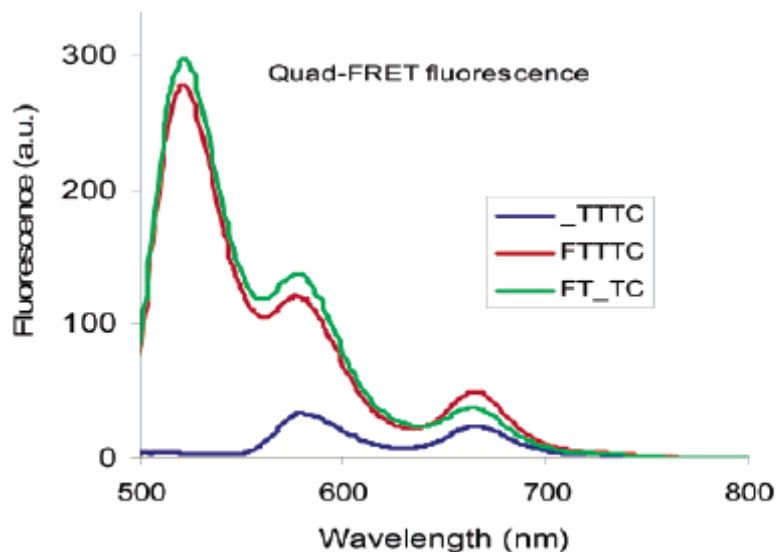
Figure5.11 Quad-FRET Fluorescence. The fluorescence from Cy5 dye is greatest in the molecule with all the dyes. Most of the fluorescence of Cy5 in _TTTC comes from T dyes. In FT_TC the transfer between T_T portion of the molecule is significant contributing to Cy5 fluorescence.

There is small shift <5nm in the case of the FAM spectra, which has also been noticed by others[128]. In the three molecules, FTTTC shows the largest amount of fluorescence for Cy5. In the case of _TTTC, the absence of F leads to a reduction in the fluorescence, indicating most of the fluorescence comes via multi-FRET transfers from F to T. When the middle T is missing in FT_TC the fluorescence is reduced; however, it still exists. We propose that this is due to transfers that skip a dye – the two T_T being close enough to have FRET. To more carefully analyze the spectra, we curve fitted Cy5's spectrum in 48 different samples, and the results are shown in **Figure 5.18.**
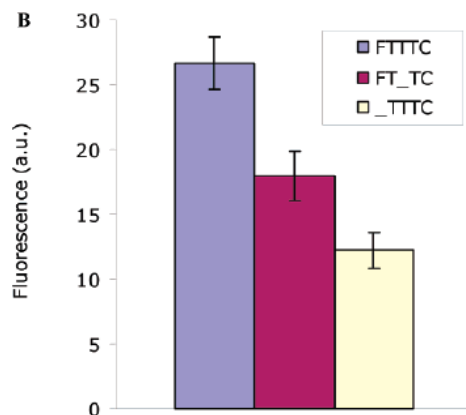
Figure 5.12 Cy5 Fluorescence. Data from a set of 48 experiments is shown here. The Cy5 fluorescence is obtained by curve fitting for dye's fluorescence.

The error bars are due mostly to the inaccuracies related to molecular concentrations. The results are consistent with our model of the process – energy transfer from F to C proceeds via a series of FRET hops from F to T to C. If F is absent, the fluorescence from C is reduced – most of the fluorescence seen is due to energy transfer from directly excited T, followed by transfer of energy to C.

5.7 Modeling

I developed a simple model that enables the calculation of FRET efficiencies between the dyes used. It uses a rate balance for excited fluorphors species X_n,

$$\frac{dX_n}{dt} = \varepsilon_n \Gamma - k_n X_n + \sum_{m=donor} k_{mn} X_m - \sum_{o=acceptor} k_{no} X_n \qquad [5.5]$$

Here ε_n = the extinction coefficient at the excitation wavelength, Γ = constant factor depending on excitation light and the geometry used, k_n = radiative and all other non-FRET decay rates (inter system crossing, quenching, internal conversion) and k_{mn} = FRET transfer from m (donor) to n (acceptor). $\varepsilon_n \Gamma$ gives the number of excited

fluorphor species created per unit time by excitation light. This model allows for the forward and backward transfer of energy in the TAMRA dyes. Using it, we can calculate the steady state efficiencies without having to resort to time-resolved spectroscopy. The detailed calculations are provided in the supplement to my paper[9].

From the model, we estimate that the TAMRA to Cy5 efficiency in Bi-FRET experiments, $\eta_{TC}^{bf} = 0.72 \pm 0.03$ and the FAM to TAMRA efficiency to be $\eta_{FT}^{bf} = 0.6\ 9 \pm 0.07$. Overall, this implies that about 40% of the energy reaches Cy5 from FAM. In the Quad-FRET experiments, the corresponding equations are non-linear and more difficult to solve. Here we found the TAMRA to Cy5 efficiency to be $\eta_{TC}^{qf} = 0.74 \pm 0.05$ and the FAM to TAMRA efficiency to be $\eta_{FT}^{qf} = 0.35 \pm 0.09$. The TAMRA to TAMRA efficiency was estimated to be $\eta_{TT}^{qf} = >0.95$. The lower value of η_{FT}^{qf} is a consequence of the two dyes being on opposite strands increasing the distance between them as compared to the Bi-FRET case. We also found that the fluorescence of Cy5 in FT_TC was greater than that in _TTTC. This is consistent with the high value of η_{TT}^{qf} that implies transfer of energy in the T_T part of the molecule – FRET even in the case where a dye is missing. These kinds of energy transfers were taken into account in the model – not including them in the model leads to non-physical results. The efficiencies indicate that about 20% of the energy from FAM reaches Cy5

5.8 Summary and Future outlook

The experiments we performed demonstrated the feasibility of multi-FRET transfers in artificially designed molecules[129]. With DNA and commonly available fluorphors, we were able to demonstrate for the first time a molecule in which at least 4 FRET events took place and 20% of the energy was eventually transferred. This should allow extending FRET as a ruler. Conventional FRET as a spectroscopic ruler is often used in biology; however, in practice it is a short ruler with limited dynamic range. Using multiple FRET transfers may allow extending its utility[130, 131]. The experiments also take us one step closer to being able to design artificial molecules to function as effectively as chlorophyll molecules.

5.9 Acknowledgements

C h a p t e r   6

SELF ASSEMBLY: CAPILLARY FLOWS[*]

6.1 Self Assembly by Surface Tension

If a drop of coffee is left to dry on a surface for a few hours, it leaves behind a circular stain. What forces were responsible for pushing the particles to the edge? In a paper written in 1997, the explanation was provided[132]. Pinning of the drop at the edge followed by surface-tension-driven flows pushes coffee particles to the edge, where they jam up to create a ring. This is a general phenomena depending only on capillary flows in conjunction with evaporation[133]. A burst of papers followed this paper, trying to use capillary driven flows to assemble rings in a variety of systems.

Pattern formation[134] by surface tension is also well known in other contexts – as bubbles and bubble rafts[135, 136], silica skeletons of radiolarians, finger patterns in Hale-Shaw cells [137]and in DNA combing[138]. Self-assembly by itself has seen a surge in interest – all biological systems self-assemble – and chemists are slowly learning how to harness this for useful structures[8, 139, 140].
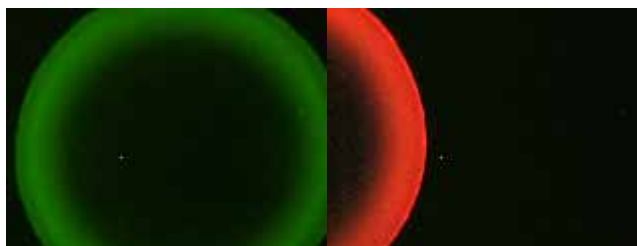
Figure 6.1 Ring Stains by Evaporating Drop. Here quantum dots in an evaporating solution leave behind ring stains.

---

[*] Part of this chapter are reproduced with permission from Vyawahare, S., Craig, K. M. & Scherer, A. Patterning lines by capillary flows. Nano Letters 6, 271-276 (2006). Copyright 2006 by American Chemical Society.

As mentioned in the second chapter, when we scale down to microns and nanometers, surface tension forces dominate every other force by orders of magnitude. Because the force scales so well, the ability to manipulate it practically could allow for the building and manipulation of things in miniature systems where other forces simply become too small to use[141].

The ability to self-assemble rings is by itself of limited use unless we can expand the range of patterns possible. In this chapter, I shall describe a new phenomena that I discovered which could be used to create fine lines in a controlled way, and explore the physics behind it.

6.2 Experiments with BSA

The experiments started with an accidental discovery that a solution of quantum dots between two cover slides left for a few hours results in the picture shown in **Figure 6.2.**
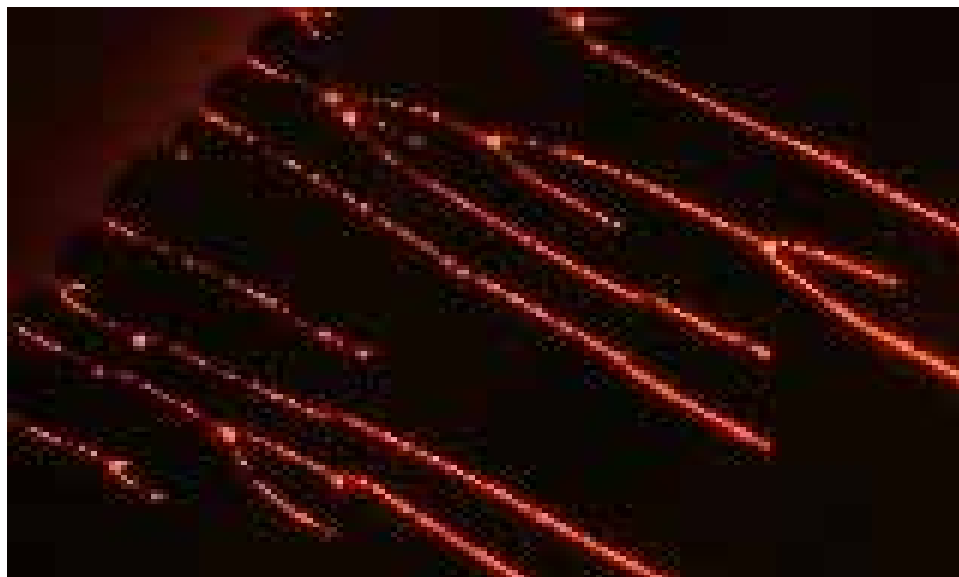
Figure 6.2 Lines forming. As the quantum dot solution recedes, it leaves lines of quantum dots behind.

The quantum dots had self assembled into a line that grew perpendicular to the contact line (the three phase boundary between the retreating liquid, air and the solid). The lines were

1-2 microns wide and extended for many millimeters and shone brightly because of the quantum dots seemed to concentrate there.
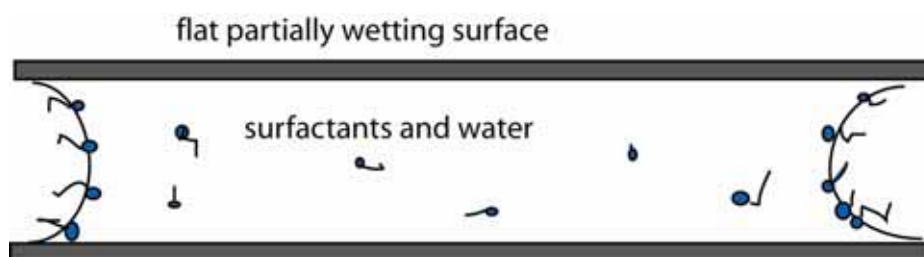
Figure 6.3 2D Geometry of the System

Since the mixture was a complicated one, components were removed one by one until the minimum required mixture to create the line was found. It turned out that a protein in the buffer bovine serum albumin (BSA) was the culprit. Solutions of BSA over a wide range of concentrations (in borate buffer at pH 8), 10nM to 10 mM, formed these lines.

BSA belongs to a class of proteins, called albumins, found in blood serum and milk in large quantities. It is a sticky protein and is often used along with biological buffers to prevent non-specific sticking of other proteins, or to stabilize proteins. Its heart-shaped structure is shown in **Figure 6.4**. The function of the protein is to transport fat molecules.
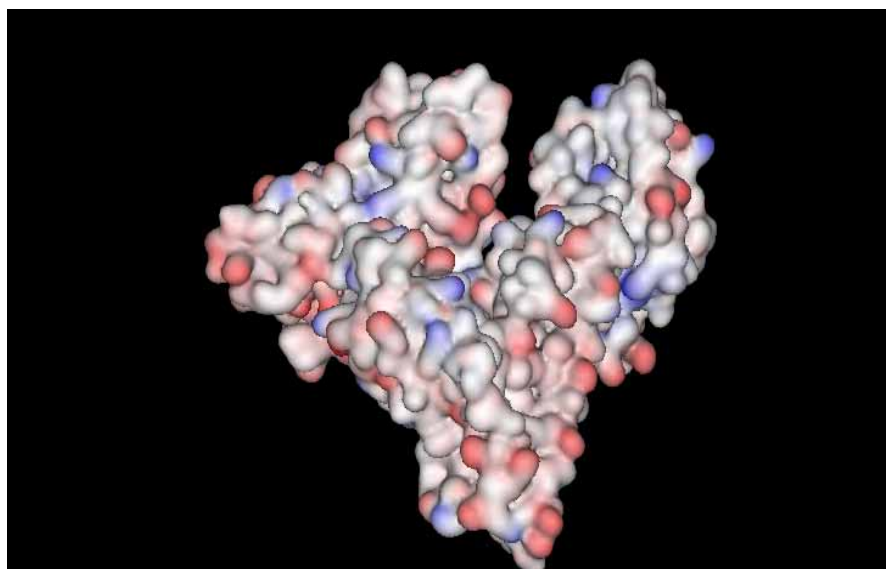
Figure 6.4 BSA Molecule

We notice that the end of every line had pinning.

BSA in solution tends, like the coffee drop, to collect at the edges and can form a gel. This gel creates a pinning point, an inhomogenity in the surface tension that immobilizes the contact line[142]. As the solution evaporates and the contact lines moves backward, it leaves a thin liquid line behind. This self-pinning by BSA in not the only requirement – BSA itself is also needed to stabilize the line.
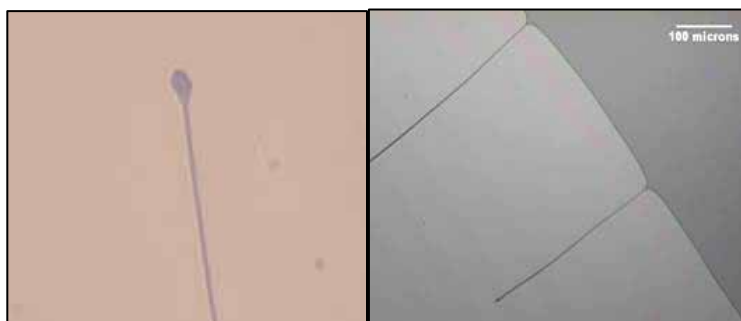
Figure 6.5 BSA Pinning Points and Lines. The picture on the left shows a BSA pinning point. The picture on the right shows the (darker) receding liquid leaving behind a line

We also saw the breaking of lines if another piece of BSA was near the contact line. These pinning points exert a force on the contact line.

Figure 6.6 Breaking of a BSA line. Two pinning points can compete for lines. This shows that a force is exerted by a pinning point

When the line breaks, it seems to leave a thin film behind. The line itself dries up and does not break into drops, which may be expected from Rayleigh Plateau instability[143].

6.3 Imaging with Quantum Dots and Dyes

Fluorescent dyes and dots in the solution enable visualization of the flow pattern. We used quantum dots (brought from Quantum dots corporation) and fluorescently-tagged BSA (from Sigma Aldrich, St. Lois, MO) to visualize the flow pattern and the shape of the contact line in the vicinity.

The flow is the result of the combination of evaporation and capillary driven flows[144]. The shape of the contact line in the vicinity of a line fits a parabola (or a catenary) well. The radius of curvature of the line seems to depend on the evaporation rate.
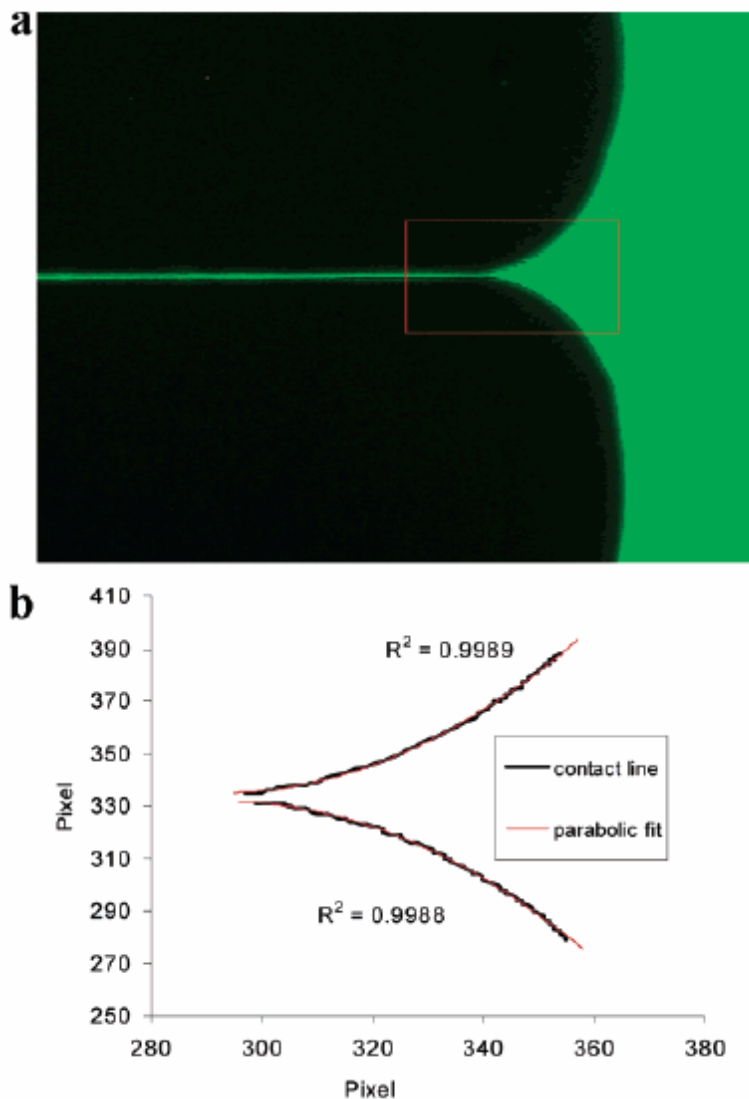
Figure 6.7 Parabolic Fit. The junction between line and boundary a) can be fit to a parabolic curve shown in b). Fluorescent BSA was used to get a clearly defined line

The curved shape is very likely a minimum shape similar to that found in soap bubble films and is a result of two competing tendencies – the force due to the pinning holding the line, and the surface area minimizing surface tension. Unlike the three-dimensional case of a pinned drop, the shape in not exponential[145, 146].

The curved shape of the contact line caused a negative Laplace pressure inside. This pressure is given by:

$$\Delta P = \gamma \left(\frac{1}{R_1} + \frac{1}{R_2} \right)$$

Here, γ is the surface tension of the fluid, and R_1 and R_2 are the principle curvatures of the
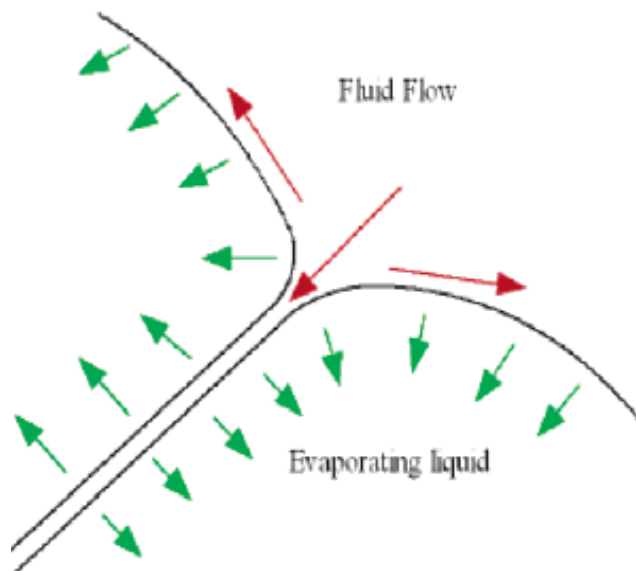
Figure 6.8 Fluid Flows. The flow is a combination of evaporation and capillary driven flows. As the contact line recedes the fluid has to move to make way. At the same time the curvature of the contact line pushes fluid into the line

surface at the point being considered, with the positive direction taken to be into the fluid being considered. Since the curvature here is negative (one principle curvature goes from infinity to something negative as we move from to from the fluid line, to the point of its attachment, to the receding contact line), it tends to suck in particles. At the same time, evaporation moves the contact line backward, causing a fluid flow along the contact line and away from the fluid line. In the line itself, liquid is evaporating from the sides; however, this is compensated by the sucking-in effect of the curved contact line. The combined effect is that small particles can get sucked into the line and concentrate there. A video of this process is available in the supplement of my paper[10].

6.4 Other shapes

Besides lines, we did see other shapes occasionally. The lines always grow locally perpendicular to the receding contact line. However, if the contact line is evaporating non-uniformly, two lines may be drawn towards each other. The resulting shape is that of a prong, as shown in **Figure 6.9**. The angle between the prong was found to be usually close to 120 degrees. This is probably an energy-minimizing value - the least curvature at a 3-line junction.
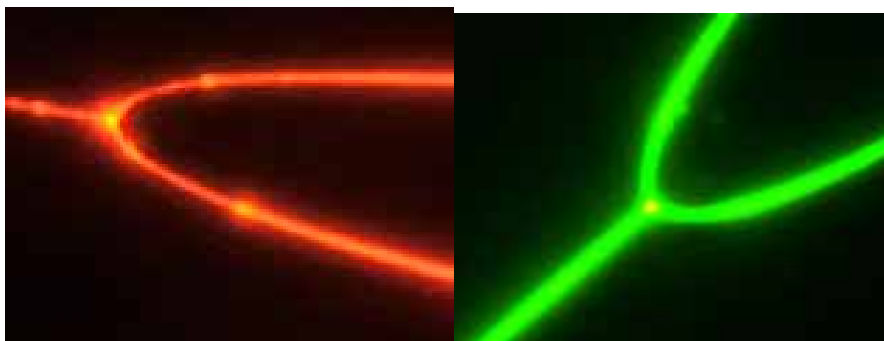
Figure 6.9 Prong Formation. I used green and red quantum dots to show prong formation – when two line meet. These lines are about ~1 micron wide.

We also saw the creation of "lollipop"-like structures if there was an air-bubble at the edge of a contact line. A sequence of pictures is shown.
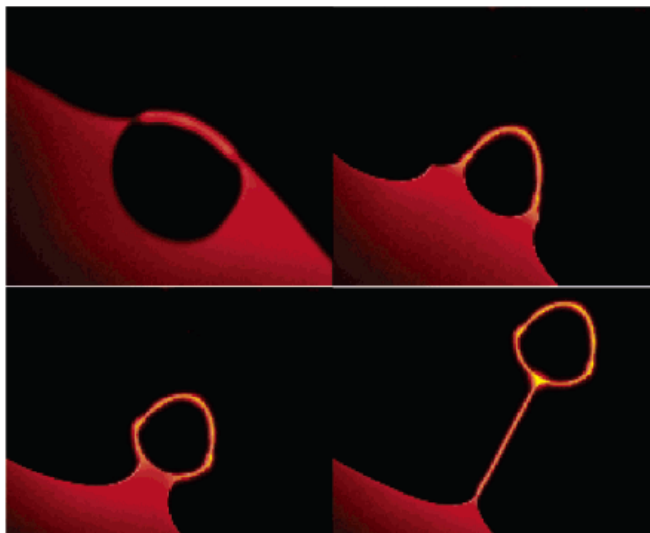
Figure 6.10 "Lollipop" A bubble in the solution results in the
shape shown. These pictures were taken every 9 minutes.

6.5 SEM Imaging

The BSA line can be imaged under a scanning electron microscope (SEM). We use a FEI
Sirion SEM. The images show that the dries up BSA lines are made up of a tall wall and a
thin film, which appears somewhat darker in the image. The imaging was possible because
the two parallel plates can be stripped apart, leaving a line on each surface. This line was
imaged at 20 degrees.
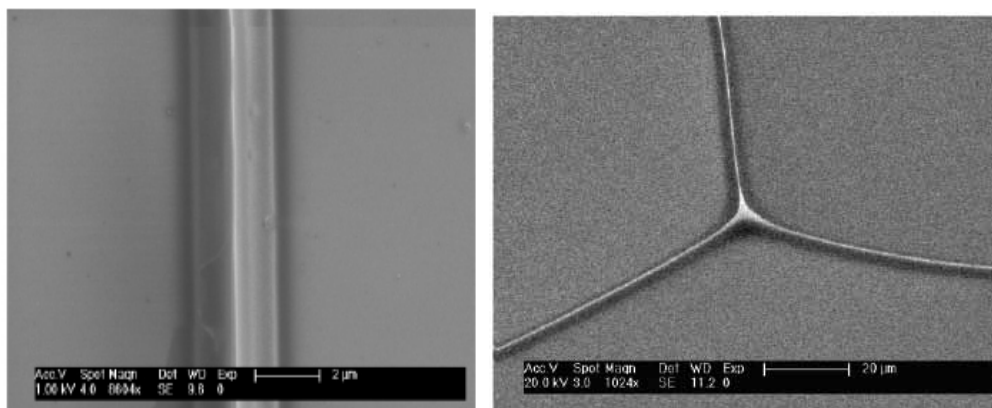
Figure 6.11 SEM images of BSA Line and Junction. Shape of
the line seems to be a tall wall with a thin film at the surface.

The ability to have access to the lines directly improves the usefulness of the technique. Shown in **Figure 6.11** are two SEM images of a BSA line and a junction. The peeling process may perturb the shape of the final line; however, the smooth edges indicates that the break of the tall wall-like structure is smooth and happens at the weakest point, right at the center of the two plates where the BSA line is the thinnest. Near the surface, there is a film of BSA.

6.6 Conditions for Line formation

A number of experiments established the conditions needed for stable, repeatable line formation with BSA:

1) A partially wetting surface – surfaces that wet completely or did not wet at all did not seem to form consistent lines[147]. Untreated Si wafer or cover-glass worked well.

2) Pinning points – the presence of a speck or BSA gel or other impurity acting like a pinning point was necessary for line formation.

3) 2-dimensional system – Our attempts at dip-coating[148] failed – the lines only formed if the fluid was sandwiched between two plates, creating a two dimensional fluid.

6.7 Why are lines formed?

What special properties does BSA have that enable line formation, and will other substances do the same? The key turns out to be the foaming properties[149] of BSA.

BSA is a foaming surfactant – it stabilizes bubbles and surfaces. BSA, like other surfactants tends to collect at surfaces and changes the interfacial properties of water - in particular, the surface tension[143]. The surface tension of water is about 72 dynes/cm. This is reduced by half on addition of BSA. The presence of BSA at the surface stabilizes the surface. Foaming surfactants also stabilize the thin fluid lines by the poorly understood Gibbs Marangoni effect[150-152].

The line formation is analogous to the formation of "foam plateau" studies over 200 years ago. There are many similarities between these lines and the junction formed between two

bubbles[153, 154]. The fluid flow at a line junction is very similar to flow at a bubble plateau where liquid is sucked into the plateau from the lamellae. A video is available a supplement to my paper[10].

Surfactants stabilize by changing the contact line elasticity E, which is given by

$$E = \frac{d\gamma}{d \ln A}$$

where γ is the surface tension and A the area. Like soap films, these lines are meta-stable. Their stability is increased by increased viscosity. BSA does increase the viscosity of solutions.

Because the line properties are not specifically dependent on BSA's chemical properties but its physical ones, one should expect that other substances should also be able to form thin lines in similar geometries. This is exactly what we found, and it is described next.

6.8 Other Surfactants and Artificial Pinning points.

We worked with other foaming surfactants including sodium oleate, sodium dodecyl sulphate[155] (SDS) Triton X100 (octyl phenol ethoxylate), Dupont fluoro-surfactants like FSN and FS300. In each case, we observed line formation. Even with coffee, we saw coffee lines! In these cases, we had to create artificial pinning points using photo-resist SU8 2025 (Microchem).

The shape of the pinning point did not seem to matter – all shapes led to a single line. This line was usually smaller than the pinning point itself. This is an advantage because it allows for the creation of thin lines despite large pinning points. The pinning points afford us better control of where the lines form and allow for the precise placement of lines.
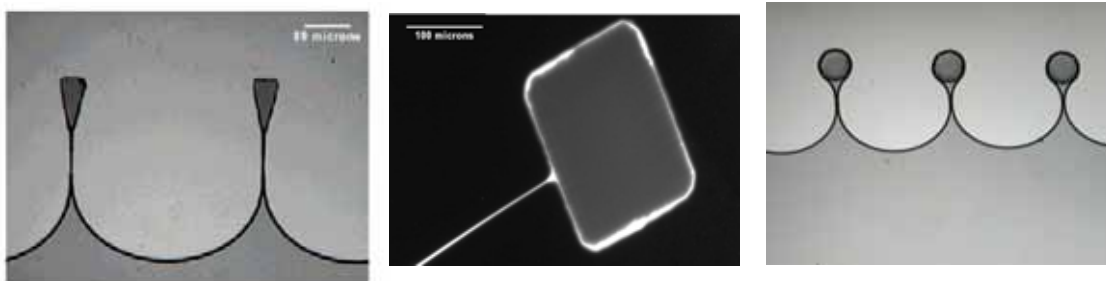
Figure 6.12 Pinning Points of Various Shapes. Here we used
Triton X100 in the first picture, BSA and qdots in the second and
Triton X100 again in the third.

Pinning points can also be created for BSA solutions, instead of relying on random self-pinning points. Photo-resist structures can also be designed to control evaporation and steer it in any direction we want.

l
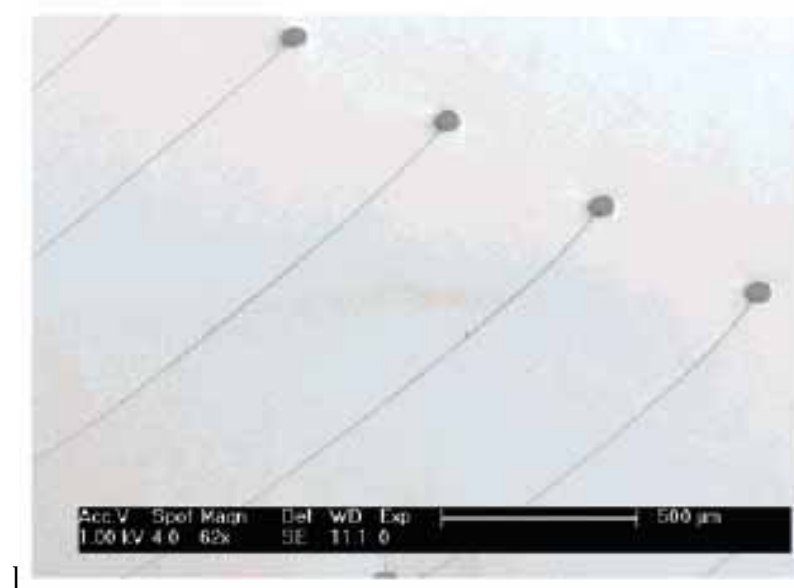
Figure 6.13 Photo-resist Circles and BSA Lines

We found that these other surfactants generally produced lines that changed width with time – generally, they became smaller with time. Eventually, if the flow stopped, a series of drops were created, this being the result of the Rayleigh-Plateau instability[143, 156]. This is unlike the BSA case, where the lines were of constant width.

Figure 6.14 Drop Formation. In non-rigid surfactant the lines break into drops when cut off from the flow. This is in accordance with the Rayleigh-Plateau theory

This leads us to hypothesize that there are two types of surfactants – rigid ones like BSA and fluid ones like most of the others we have seen[157]. Protein surfactants like BSA probably have conformational changes at the surface, and their sticky nature insures that the lines are rigid.

Another interesting phenomenon occurs if the contact line recedes crossing two pinning points - it leaves a fluid line behind. This opens the possibility of creating inter-connect wires.
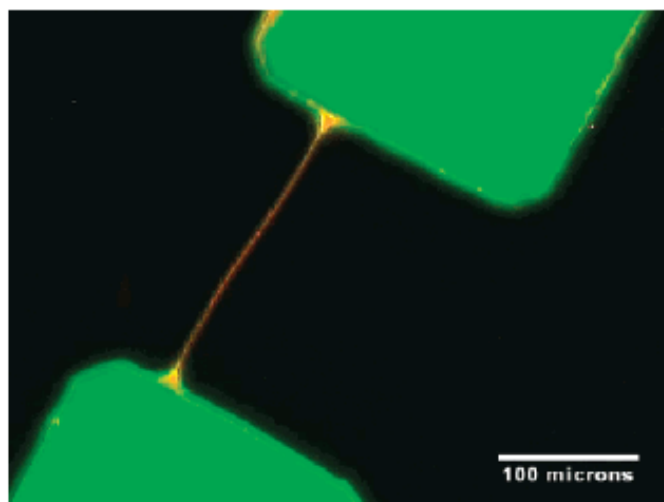
Figure 6.15 Line between Two Pinning Points. A quantum dot line has been created by steering evaporation, so that the contact line moves over two pinning points.

We also tried measuring the rate of line growth, and found it to be linear with time – most likely just dependent on the evaporation rate which is constant, at constant temperature, for short time periods (i.e. not long enough for the concentration to change appreciably).
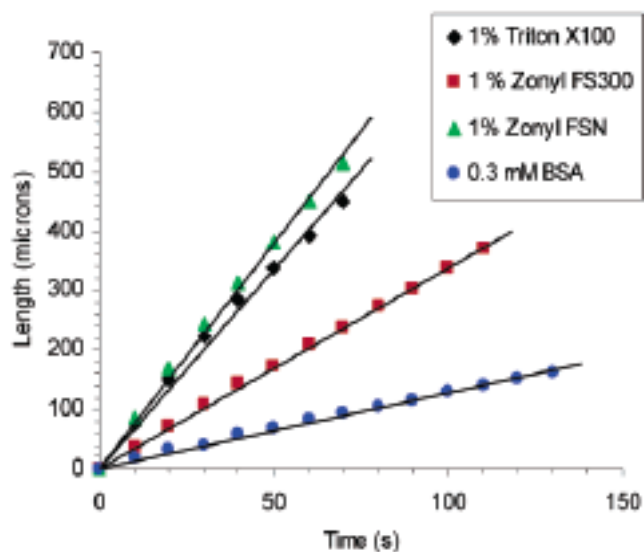
Figure 6.16 Line Growth. Growth of lines is linear for many surfactants depending only on the evaporation rate which is constant for short time periods

6.9 Adding particles

We can easily add micro-bead particles to the solution. This leads to their self-assembly into lines. These lines are fairly ordered, though there are also many defects. Larger particles (>1 micron) tend to assembled better than smaller ones (<500 nm). Smaller particles tend to get out of the solutions, and only a few get into the lines. It is well-known that smaller particles act like anti-foaming agents and this may be the reason[158, 159]. Also, larger particles may by themselves act like surfactants, aiding the process[160].
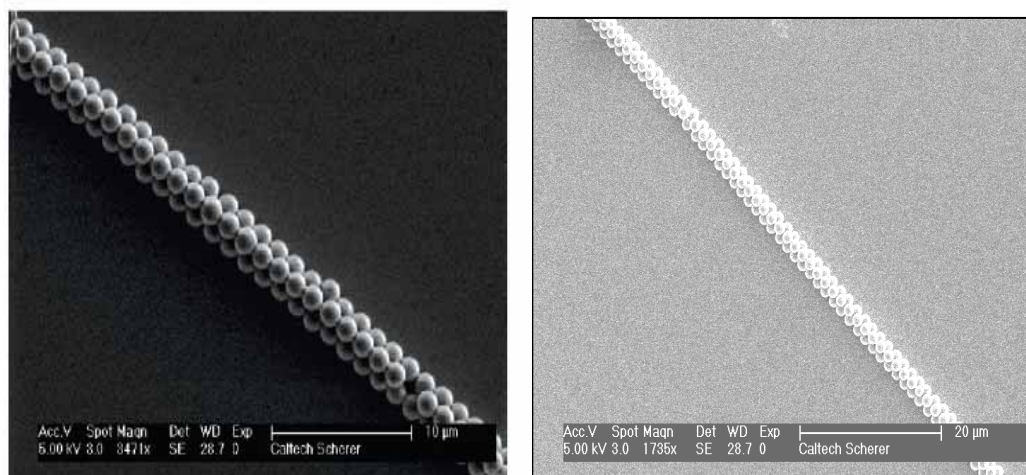
Figure 6.17 Micro-spheres assemble into Lines. In both of these
cases, we used FSN surfactant. The particles are 2 micron in
diameter

Smaller particles that get into lines tend to form pinning points by themselves, leading to
bridges that can be quite small < 100nm in the **Figure 6.18**:

Figure 6.18 Smaller Spheres and Smaller Lines. Notice a line
between the two spheres < 100nm in width. We used BSA in this
case.

Self-assembly of micro-particles has seen an extensive amount of work recently[161]. My
method for creating lines provides a new tool for self-assembly. The method is not
restricted to micro-spheres; any kind of nano-particle may be used, including protein, nano-
tubes, metal particles etc[162].

6.10 Discussion

These lines are a new way to use capillary forces to self-assemble small particles, proteins and quantum dots. This phenomenon may be used to create a variety of shapes. It is compatible with any foaming surfactant. We believe that this method could find use in many future nano- and micro-fabrication schemes.

Recently, I also realized that there may be a link between these lines and certain biological processes called tunneling nano-tubes. These tunneling nano-tubes are nanometer scale tubes formed by lipid molecules. They form both in vivo and in vitro and have been observed between human immune T cells called immunological nano-tubes. It is intriguing to suggest that the mechanism of their formation is related to the phenomena mentioned in this chapter. The main difference is that those systems have no evaporation and take place inside a fluid media, with the corresponding amphiphilic molecules being lipids. However, these are just speculations and we have no experimental evidence at this moment.

6.11 Acknowledgements

A p p e n d i x

DESIGNING AN ELASTOMERIC MICROFLUIDIC CHIP

This section describes the procedure involved in designing an elastomeric microfluidic chip. The information comes from teaching micro-fluidics to grad students in Caltech course APh109 and my own research. This is also the procedure needed to use the **Caltech Microfluidic Foundry** (http://www.kni.caltech.edu/foundry)

First, two caveats – one, no one should assume that they can learn microfluidic chip fabrication from reading, any more than you can learn to ride a bi-cycle by reading a book. And two, this tutorial is restricted to designing multi-layer soft lithography planar chips made of PDMS. Other kinds of microfluidic chips are possible, but are not covered here.

The microfluidic chip-making process can be broken down into four steps:

1) Make a design and print a photo-mask.

2) Create photolithography molds.

3) Replica molding, alignment and bonding of PDMS layers.

4) Test the devices.

Here, I will concentrate exclusively on Step 1 because detailed procedures for the other steps are available elsewhere.

Mask Design

Mask Design is done using AutoCAD or other CAD software. We shall describe the procedure for AutoCAD and transparency laser printout from www.outputcity.com. The procedure can be modified for other software (Tanner, Cadence etc.) and other printout (for example, using a laser chrome mask printer).

Let's say you have a new idea for chip - it's a single layer T- junction and you draw it on paper. You want to split a fluid stream into 2. What dimensions should it be? Let's make the channels 100 microns wide. The height could then be selected to be ~10 microns, so that the aspect ratio is about 1:10. An aspect ratio of 1:10 will work fine, but an aspect ratio exceeding 1:20 usually results in collapse with PDMS, unless there are pillars to hold the channel up.

T junction
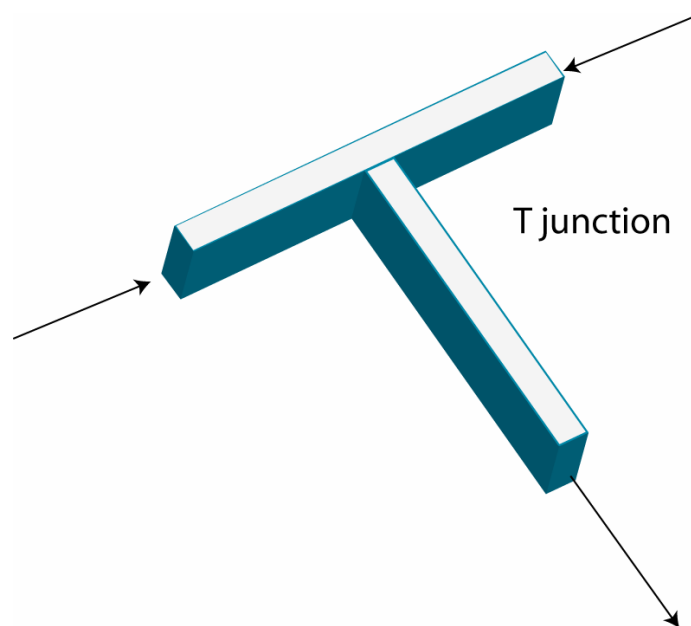
We will assume some very basic familiarity with AutoCAD. You can probably get used to it in 15 minutes. Open AutoCAD (any version beyond AutoCAD 2000). The following rules must be followed:

1) Select microns as the unit with 0 precision (→Format →Units)

2) Everything must be drawn using CLOSED POLYLINES.

3) Draw everything on a layer different from ZERO layer. Select a new layer and use it for drawing (→Format →Layer). Let's call out layer FLUID. Choose a color for the layer.

Three functions may be useful for your drawing ORTHO, SNAP and GRID. Find out about them. A circle of a square or a polygon IS a closed polyline in AutoCAD. Normally, the printing software will do the "hatching" for you – i.e. fill the polyline. Note these possibilities for conversion:
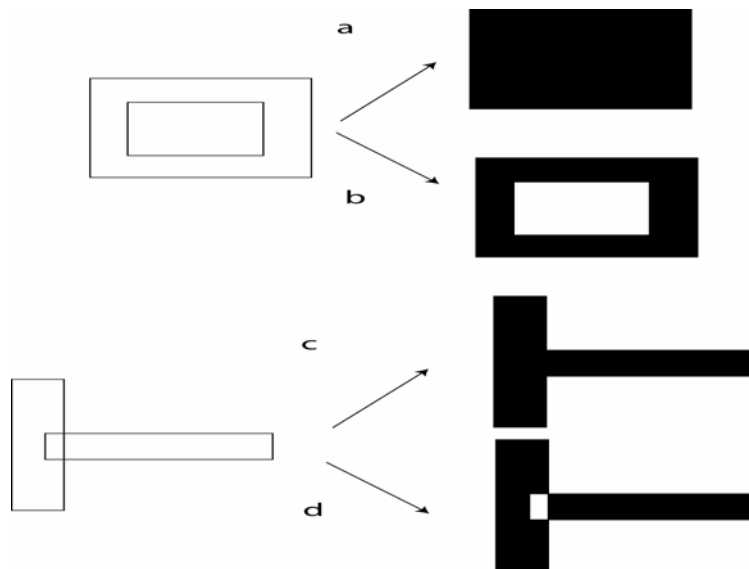
The software for printing that we use does b) and c) – but you need to confirm for your specific case. It is good practice to draw a border around the diagram. Let us make a boundary of 24000 micron x 24000 micron (fitting an inch square).We use a double-square to the correct hatching. Also, a good practice is to put identification marks on the chip. Find out what type of marks are allowed by your mask printing software. Finally, you might have (not to scale):

my first chip
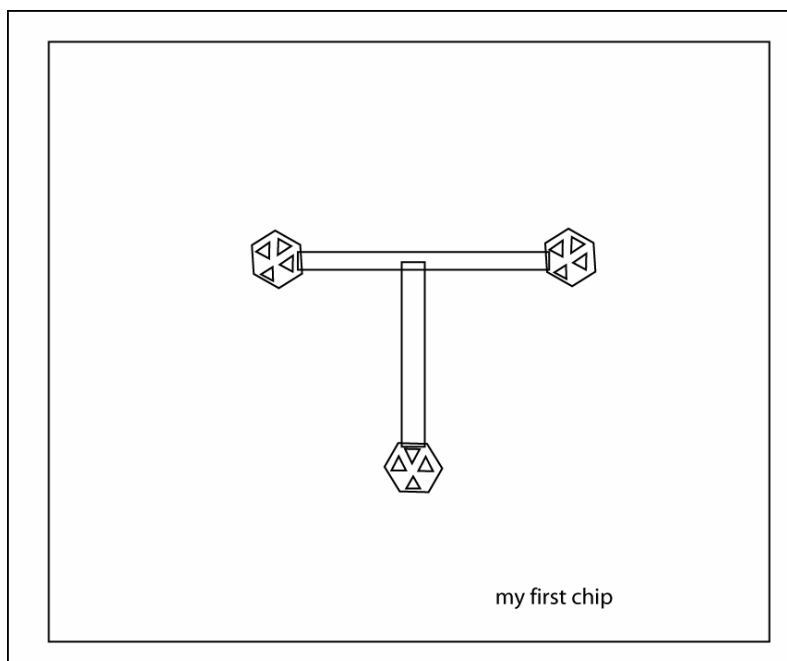
Note that because the lines are fairly thin, we will need to put some ports at the end of the line where hollow metal pins can poke through the PDMS and connect put fluids into and out of the chip. That is the larger structure at the end of each line. We put in some triangular posts to prevent collapse.

You will also have to decide whether this is to be printed negative or positive. If printed positive, it will be used with positive photo-resists, and if negative it will use a negative photo-resist. (Negative means that the channels you made will be transparent, and the rest will be dark like a negative of a photograph.) The photo-resist spinning speed during the molding determines the height of the channels, while the design determines the width and length of channels.

Now say you change your mind, and want to make a multilayer device with valves at the two inlet channels. A valve is created when two channels in different layers overlap (with one on top of the other), and a thin membrane separates them. This is done by molding either the fluidic or control channels in a thin sheet of PDMS, and then the other layer can be stacked on top of it.
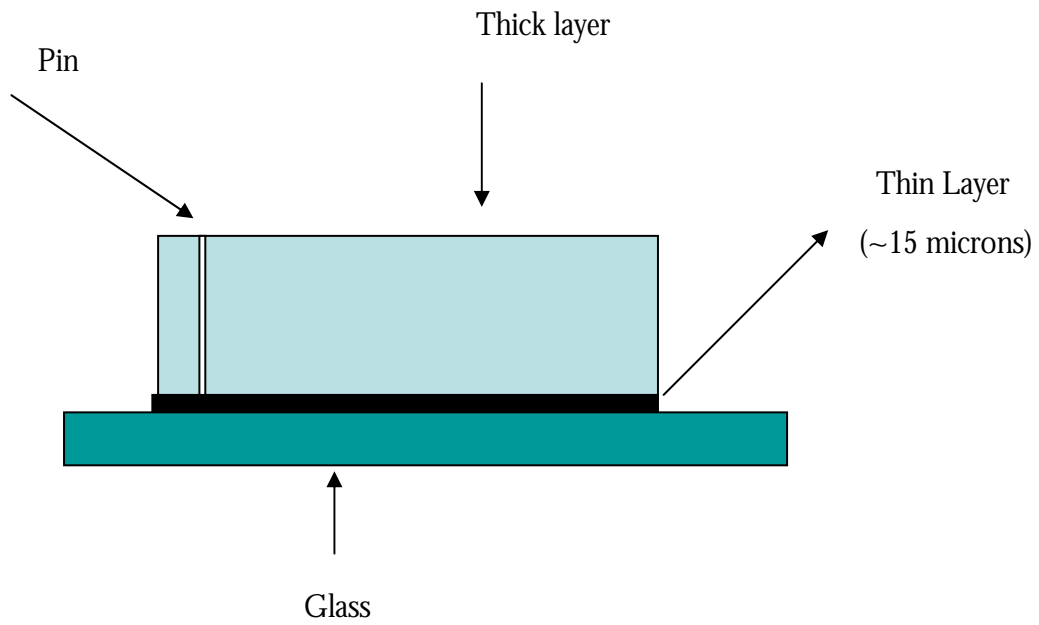
A new layer must be drawn on a separate layer – lets call this CONTROL and give it a new color. In AutoCAD it might look like this (not drawn to scale):
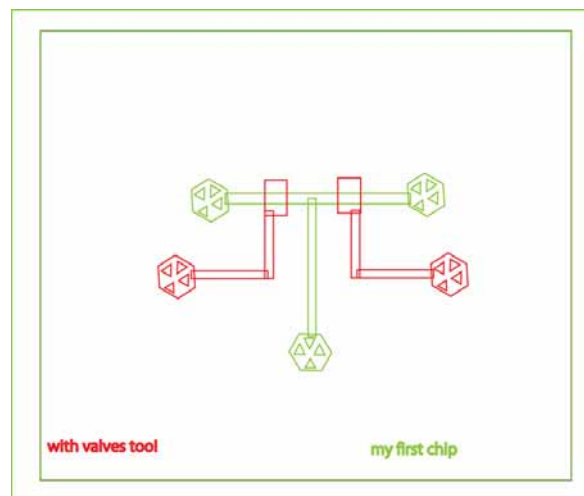
Note that with the control layer, we put a boundary (not seen in picture), ports, and identification marks. Also note how we increased the overlap area where we wanted a valve. This is a common strategy that helps lowering the actuation pressures.

It is essential that the ports be separated as far as possible from each other and other channels – at least 2 mm away from all other channels (except the one it connects to. of course!) and ports is a good rule of thumb. Since we need to poke pins into the ports and there is an element of error involved, this minimizes the chance of the pin rupturing another channel or port and ruining your device.

Finally, we need to separate the control and flow layers, make allowances for polymer shrinkage and arrange them to be put on a wafer. We use 3" silicon wafer so that 4 chips of the type drawn can fit into it.   So we can separate them as shown and put them on separate files. Here, we will plan to make the FLUID layer to be the thin layer. This is called the top-down geometry, because the valve functions by a thin membrane moving down. The other geometry is the bottom-up geometry, with the control channel below the flow channels.
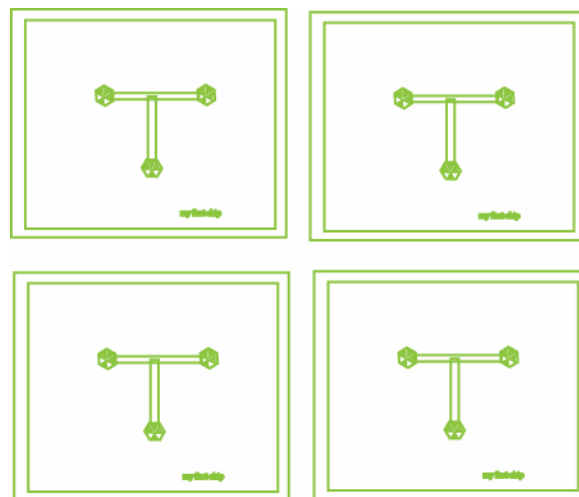
The thick layer must be EXPANDED by ~1.5 % to compensate for the shrinkage in the fabrication. Expand the control layer using the SCALE command by 1.015 and put it in the same format:
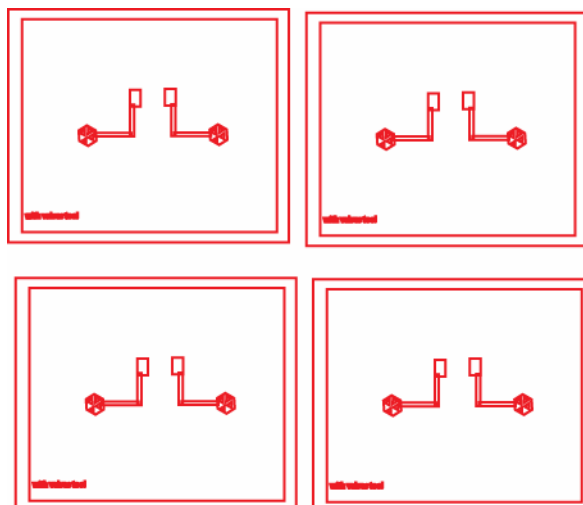
Normally, the flow channels are made with POSITIVE resists because we need to make them rounded, and this done by re-flow (square $\rightarrow$ parabolic) At present, we only know of positive resists that may be rounded. This is because a square cross-section will have its ends stick out when the valve action is done, preventing full closing of a valve (a leaky valve may be a good thing for cases where we want to just trap some large particles but allow flow through). The control channels may be printed negative.

At this stage you can simply hand your design to the **_Caltech Microfluidic Foundry_** (http://www.kni.caltech.edu/foundry) and they will make the chips for you!

REFERENCES

1. Jensen, K. F. Microchemical Systems: Status, Challenges, and Opportunities. AIChE journal 45, 2051 (1999).
2. Jensen, K. F. Microreaction engineering -- is small better? Chemical Engineering Science 56, 293-303 (2001).
3. Quake, S. R. & Scherer, A. From micro- to nanofabrication with soft materials. Science 290, 1536-1540 (2000).
4. Lee, J. N., Park, C. & Whitesides, G. M. Solvent compatibility of poly(dimethylsiloxane)-based microfluidic devices. Analytical Chemistry 75, 6544-6554 (2003).
5. Rolland, J. P., Van Dam, R. M., Schorzman, D. A., Quake, S. R. & DeSimone, J. M. Solvent resistant photocurable "liquid teflon" for microfluidic device fabrication (vol 126, pg 2322, 2004). Journal of the American Chemical Society 126, 8349-8349 (2004).
6. Adams, M. L., Enzelberger, M., Quake, S. & Scherer, A. Microfluidic integration on detector arrays for absorption and fluorescence micro-spectrometers. Sensors and Actuators~A 104, 25-31 (2003).
7. http://www.optofluidics.caltech.edu
8. Whitesides, G. M. & Grzybowski, B. Self-assembly at all scales. Science 295, 2418-2421 (2002).
9. Vyawahare, S., Eyal, S., Mathews, K. D. & Quake, S. R. Nanometer-scale fluorescence resonance optical waveguides. Nano Letters 4, 1035-1039 (2004).
10. Vyawahare, S., Craig, K. M. & Scherer, A. Patterning lines by capillary flows. Nano Letters 6, 271-276 (2006).
11. Maltezos, G., Vyawahare, S. & Scherer, A. (USA, 2006).
12. Erikson, D. et al. Spectrographic Microfluidic Memory. Proceedings of the ICMM2005 (2005).
13. Okamoto, K. K., Vyawahare, S. & Scherer, A. Surface plasmon enhanced bright emission from CdSe quantum dot nanocrystals. JOSA B (in press) (2006).
14. Kamholz, A. E. A. E. Proliferation of microfluidics in literature and intellectual property. Lab on a chip 4, 16N-20N (2004).
15. 32 review papers published in 2005 were found using SciFinder Scholar using "microfluidic" in the title.
16. Manz, A. I. Miniaturized Total Chemical-Analysis Systems - A Novel Concept for Chemical Sensing. Sensors and actuators. B, Chemical 1, 244-248 (1990).
17. Xia, Y. S. R. Soft lithography. Angewandte Chemie 37, 550 (1998).
18. Unger, M. A., Chou, H. P., Thorsen, T., Scherer, A. & Quake, S. R. Monolithic microfabricated valves and pumps by multilayer soft lithography. Science 288, 113-116 (2000).
19. Thorsen, T., Maerkl, S. J. & Quake, S. R. Microfluidic large-scale integration. Science 298, 580-584 (2002).
20. http://www.conferences.jp/microtas2006/
21. www.rsc.org/loc
22. Beebe, D. J., Mensing, G. A. & Walker, G. M. Physics and Applications of Microfluidics in Biology. Annual Review of Biomedical Engineering 4, 261-286 (2002).

23.	Stone, H. A., Stroock, A. D. & Ajdari, A. Engineering Flows in Small Devices. Annual Review of Fluid Mechanics 36, 381-411 (2004).
24.	Squires, T. M. & Quake, S. R. Microfluidics: Fluid physics at the nanoliter scale. Reviews of Modern Physics 77, 977-1026 (2005).
25.	Purcell, E. M. Life at Low Reynolds-number. American journal of physics 45, 3-11 (1977).
26.	Trimmer, W. S. N. Microrobots and Micromechanical Systems. Sensors and actuators 19, 267-287 (1989).
27.	Brody, J. P. Biotechnology at low Reynolds numbers. Biophysical journal 71, 3430-3441 (1996).
28.	www.caliper.com
29.	www.biocompare.com/videoview.asp?id=112
30.	Mitchell, P. P. Microfluidics--downsizing large-scale biology. Nature biotechnology 19, 717-721 (2001).
31.	personal communication, Balagadde, F.
32.	Maltezos, G., Johnston, M. & Scherer, A. Thermal management in microfluidics using micro-Peltier junctions. Applied Physics Letters 87 (2005).
33.	Balagadde, F. K., You, L. C., Hansen, C. L., Arnold, F. H. & Quake, S. R. Long-term monitoring of bacteria undergoing programmed population control in a microchemostat. Science 309, 137-140 (2005).
34.	Fu, A. Y. An integrated microfabricated cell sorter. Analytical chemistry 74, 2451-2457 (2002).
35.	Marcus, J. S., Anderson, W. F. & Quake, S. R. Parallel picoliter RT-PCR assays using microfluidics. Analytical Chemistry 78, 956-958 (2006).
36.	Lee, C.-C. et al. Multistep Synthesis of a Radiolabeled Imaging Probe Using Integrated Microfluidics. Science 310, 1793-1796 (2005).
37.	Hansen, C. L., Skordalakes, E., Berger, J. M. & Quake, S. R. A robust and scalable microfluidic metering method that allows protein crystal growth by free interface diffusion. PNAS 99, 16531-16536 (2002).
38.	Duffy, D. C., McDonald, J. C., Schueller, O. J. A. & Whitesides, G. M. Rapid Prototyping of Microfluidic Systems in Poly(dimethylsiloxane). Anal. Chem. 70, 4974-4984 (1998).
39.	McDonald, J. C. Poly (dimethylsiloxane) as a Material for Fabricating Microfluidic Devices. Accounts of chemical research 35, 491 (2002).
40.	Mark, J. E. Polymer data handbook.
41.	Hong, J. W. & Quake, S. R. Integrated nanoliter systems. Nature Biotechnology 21, 1179-1183 (2003).
42.	Studer, V. et al. Scaling properties of a low-actuation pressure microfluidic valve. Journal of Applied Physics 95, 393-398 (2004).
43.	N. Futai, W. G. S. T. Rapid Prototyping of Microstructures with Bell-Shaped Cross-Sections and Its Application to Deformation-Based Microfluidic Valves. Advanced Materials 16, 1320-1323 (2004).
44.	Liu, J. J., Hansen, C. C. & Quake, S. R. S. R. Solving the "world-to-chip" interface problem with a microfluidic matrix. Analytical chemistry 75, 4718-4723 (2003).
45.	Van-Dam, M. (California Institute of Technology, 2005).
46.	Kanai, M. et al. in Proceedings of the 7th International Conference on Miniaturized Chemical and Biochemical Analysis Systems 429-432 (Squaw Valley, CA, USA, 2003).

47.   Logothetis, A. L. Chemistry of Fluorocarbon Elastomers. Progress in Polymer Science 14, 251-296 (1989).

48.   personal communication, Prof. Robert Grubbs

49.   Anolick, C., Hrivnak, J. A. & Wheland, R. C. Soluble perfluoropolymers. Advanced Materials 10, 1211-+ (1998).

50.   Zhao, Y. Y. A new generation of high performance fluoropolymers. Su liao 19, 40 (1990).

51.   Matsumoto, Y., Yoshida, K. & Ishida, M. A novel deposition technique for fluorocarbon films and its applications for bulk- and surface-micromachined devices. Sensors and Actuators a-Physical 66, 308-314 (1998).

52.   Arcella, V., Ghielmi, A. & Tommasi, G. High Performance Perfluoropolymer Films and Membranes. Ann NY Acad Sci 984, 226-244 (2003).

53.   Wang, S. H. & Legare, J. M. Perfluoroelastomer and fluoroelastomer seals for semiconductor wafer processing equipment. Abstracts of Papers of the American Chemical Society 224, U548-U549 (2002).

54.   Heller, M., Legare, J., Wang, S. H. & Fukuhara, S. Thermal stability and sealing performance of perfluoroelastomer seals as a function of crosslinking chemistry. Journal of Vacuum Science & Technology a-Vacuum Surfaces and Films 17, 2119-2124 (1999).

55.   Rolland, J. P., Van Dam, R. M., Schorzman, D. A., Quake, S. R. & DeSimone, J. M. Solvent-resistant photocurable "liquid teflon" for microfluidic device fabrication. Journal of the American Chemical Society 126, 2322-2323 (2004).

56.   www.liquidia.com

57.   Waksman, L. K., Hirofumi; Sato, Shin-ichi; Tarumi, Yasuo (ed.) The Evolution of Fluoroelastomer: SIFEL, A New Class of Easily Processed High Performance Elastomer, Adhesive and Sealant (SAE, 2001).

58.   Anderson, J. R. et al. Fabrication of topologically complex three-dimensional microfluidic systems in PDMS by rapid prototyping. Analytical Chemistry 72, 3158-3164 (2000).

59.   Xue, Y. A review of rapid prototyping technologies and systems. Computer aided design 28, 307 (1996).

60.   McDonald, J. C. et al. Prototyping of Microfluidic Devices in Poly(dimethylsiloxane) Using Solid-Object Printing. Anal. Chem. 74, 1537-1545 (2002).

61.   Kim, B.-G., Kim, J.-H. & Yoon, E. in 7th International Conference on Miniaturized Chemical and Biochemical Analysis Systems 627-630 (Squaw Valley, California, USA, 2003).

62.   Kim, J. Y., Baek, J. Y., Lee, K. A. & Lee, S. H. Automatic aligning and bonding system of PDMS layer for the fabrication of 3D microfluidic channels. Sensors and Actuators~A 119, 593-598 (2005).

63.   Chen, C. C., Hirdes, D. & Folch, A. Gray-scale photolithography using microfluidic photomasks. Proceedings of the National Academy of Sciences of the United States of America 100, 1499-1504 (2003).

64.   Anderson, J. R. et al. Fabrication of topologically complex three-dimensional microfluidic systems in PDMS by rapid prototyping. Analytical Chemistry 72, 3158-3164 (2000).

65.   Kartalov

66.   Matthias, S. & Muller, F. Asymmetric pores in a silicon membrane acting as massively parallel brownian ratchets. Nature 424, 53-57 (2003).

67.   Mathias, S., personal communication
68.   Efros, A. L. & Efros, A. L. Interband absorption of light in a semiconductor sphere. Soviet Physics - Semiconductors 16, 772-775 (1982).
69.   Reed. Quantum Dots. Scientific American 268, 118 (1993).
70.   Murray, C. B., Kagan, C. R. & Bawendi, M. G. Synthesis and Characterization of Monodisperse Nanocrystals and Close-packed Nanocrystal Assemblies. Annual Review of Materials Science 30, 545-610 (2000).
71.   personal communication, Paul Alivasatos
72.   Medintz, I. L. I. L., Uyeda, H. T. H. T., Goldman, E. R. E. R. & Mattoussi, H. H. Quantum dot bioconjugates for imaging, labelling and sensing. Nature materials 4, 435-446 (2005).
73.   Klimov, V. I. et al. Optical Gain and Stimulated Emission in Nanocrystal Quantum Dots. Science 290, 314-317 (2000).
74.   Rosenthal, S. S. J. Bar-coding biomolecules with fluorescent nanocrystals. Nature biotechnology 19, 621-622 (2001).
75.   Han, M. Quantum-dot-tagged microbeads for multiplexed optical coding of biomolecules. Nature biotechnology 19, 631 (2001).
76.   Chan, W. C. W. Luminescent quantum dots for multiplexed biological detection and imaging. Current opinion in biotechnology 13, 40 (2002).
77.   Chan, Y. et al. Incorporation of luminescent nanocrystals into monodisperse core-shell silica microspheres. Advanced Materials 16, 2092-+ (2004).
78.   Van Blaaderen, A. Synthesis and characterization of colloidal dispersions of fluorescent, monodisperse silica spheres. Langmuir 8, 2921 (1992).
79.   Gryczynski, I. et al. Surface-Plasmon-Coupled Emission of Quantum Dots. J. Phys. Chem. B 109, 1088-1093 (2005).
80.   Ozbay, E. E. Plasmonics: merging photonics and electronics at nanoscale dimensions. Science 311, 189-193 (2006).
81.   Maier, S. A. Plasmonics: Localization and guiding of electromagnetic energy in metal/dielectric structures. Journal of applied physics 98 (2005).
82.   Aslan, K., Lakowicz, J. R. & Geddes, C. D. Plasmon light scattering in biology and medicine: new sensing approaches, visions and perspectives. Current Opinion in Chemical Biology 9, 538-544 (2005).
83.   Okamoto, K. K. et al. Surface-plasmon-enhanced light emitters based on InGaN quantum wells. Nature materials 3, 601-605 (2004).
84.   Neal, T. L. Surface plasmon enhanced emission from dye doped polymer layers. Optics express 13, 5522 (2005).
85.   Lakowicz, J. R. Radiative Decay Engineering: Biophysical and Biomedical Applications. Analytical Biochemistry 298, 1-24 (2001).
86.   Lakowicz, J. R. Radiative decay engineering 5: metal-enhanced fluorescence and plasmon emission. Analytical Biochemistry 337, 171-194 (2005).
87.   Kulakovich, O. et al. Enhanced Luminescence of CdSe Quantum Dots on Gold Colloids. Nano Lett. 2, 1449-1452 (2002).
88.   Song, J. H., Atay, T., Shi, S., Urabe, H. & Nurmikko, A. V. Large Enhancement of Fluorescence Efficiency from CdSe/ZnS Quantum Dots Induced by Resonant Coupling to Spatially Controlled Surface Plasmons. Nano Lett. 5, 1557-1561 (2005).
89.   Hacskaylo, M. Dielectric Anomaly in ZnS Films. Journal of applied physics 33, 3042 (1962).

90. Jensen, B. L. Refractive index of hexagonal II- VI compounds CdSe, CdS, and CdSeS sub 1 sub- sub x. Journal of the Optical Society of America. B, Optical physics 3, 857 (1986).

91. Sankaran, R. M. R. M., Holunga, D. D., Flagan, R. C. R. C. & Giapis, K. P. K. P. Synthesis of blue luminescent si nanoparticles using atmospheric-pressure microdischarges. Nano letters 5, 537-541 (2005).

92. Yao, J., Larson, D. R., Vishwasrao, H. D., Zipfel, W. R. & Webb, W. W. Blinking and nonradiant dark fraction of water-soluble quantum dots in aqueous solution. PNAS 102, 14284-14289 (2005).

93. Hohng, S. S. & Ha, T. T. Near-complete suppression of quantum dot blinking in ambient conditions. Journal of the American Chemical Society 126, 1324-1325 (2004).

94. V. Hessel, S. H. H. L. F. S. Laminar mixing in different interdigital micromixers: I. Experimental characterization. AIChE Journal 49, 566-577 (2003).

95. Knight, J. B. Hydrodynamic Focusing on a Silicon Chip: Mixing Nanoliters in Microseconds. Physical review letters 80, 3863 (1998).

96. Song, H. H. & Ismagilov, R. F. R. F. Millisecond kinetics on a microfluidic chip using nanoliters of reagents. Journal of the American Chemical Society 125, 14613-14619 (2003).

97. Jahn, A. A., Vreeland, W. N. W. N., Gaitan, M. M. & Locascio, L. E. L. E. Controlled vesicle self-assembly in microfluidic channels with hydrodynamic focusing. Journal of the American Chemical Society 126, 2674-2675 (2004).

98. Demas, J. N. Fluorescence Detection in Hydrodynamically Focused Sample Streams: Reduction of Diffusional Defocusing by Association of Analyte with High-Molecular-Weight Species. Applied spectroscopy 52, 755 (1998).

99. Lee, G.-B., Hwei, B.-H. & Huang, G.-R. Micromachined pre-focused M x N flow switches for continuous multi-sample injection. Journal of Micromechanics and Microengineering 11, 654-661 (2001).

100. Sundararajan, N., Pio, M. S., Lee, L. P. & Berlin, A. A. Three-dimensional hydrodynamic focusing in polydimethylsiloxane (PDMS) microchannels. Microelectromechanical Systems, Journal of 13, 559-567 (2004).

101. Kamholz, A. A. E., Weigl, B. B. H., Finlayson, B. B. A. & Yager, P. P. Quantitative analysis of molecular interaction in a microfluidic channel: the T-sensor. Analytical chemistry 71, 5340-5347 (1999).

102. Ismagilov, R. F. Experimental and theoretical scaling laws for transverse diffusive broadening in two-phase laminar flows in microchannels. Applied physics letters 76, 2376 (2000).

103. Dreyfus, R. R., Tabeling, P. P. & Willaime, H. H. Ordered and disordered patterns in two-phase flows in microchannels. Physical review letters 90, 144505-144505 (2003).

104. David Erikson, B. L., James R. Adleman, Saurabh Vyawahare,Stephen Quake, Demetri Psaltis. Spectrographic Microfluidic Memory. Proceedings of the ICMM2005 (2005).

105. Thorsten Ritz, A. D., cacute & Schulten, K. The Quantum Physics of Photosynthesis. ChemPhysChem 3, 243-248 (2002).

106. Fleming, G. R. The primary steps of photosynthesis. Physics today 47, 48 (1994).

107. McDermott, G. et al. Crystal structure of an integral membrane light-harvesting complex from photosynthetic bacteria. Nature 374, 517-521 (1995).

108. Cogdell, R. J. et al. How Photosynthetic Bacteria Harvest Solar Energy. J. Bacteriol. 181, 3869-3879 (1999).

109. María F. García-Parajó, J. H., Gabriel Sanchez Mosteiro, Jacob P. Hoogenboom, Erik M., H. P. van Dijk, Niek F. van Hulst. Energy Transfer in Single-Molecule Photonic Wires. ChemPhysChem 6, 819-827 (2005).
110. Berney, C. C. & Danuser, G. G. FRET or no FRET: a quantitative comparison. Biophysical journal 84, 3992-4010 (2003).
111. Stryer, L. Fluorescence Energy Transfer as a Spectroscopic Ruler. Annual Review of Biochemistry 47, 819-846 (1978).
112. Clegg, R. M. Fluorescence Resonance Energy-Transfer and Nucleic-Acids. Methods in Enzymology 211, 353-388 (1992).
113. Stryer, L. & Haugland, R. P. Energy Transfer - a Spectroscopic Ruler. Proceedings of the National Academy of Sciences of the United States of America 58, 719-& (1967).
114. Faure, S., Stern, C., Guilard, R. & Harvey, P. D. Role of the spacer in the singlet-singlet energy transfer mechanism (Forster vs Dexter) in cofacial bisporphyrins. Journal of the American Chemical Society 126, 1253-1261 (2004).
115. Seeman, N. C. Nucleic acid nanostructures and topology. Angewandte Chemie-International Edition 37, 3220-3238 (1998).
116. Rothemund, P. W. K. Folding DNA to create nanoscale shapes and patterns. Nature 440, 297-302 (2006).
117. Seeman, N. C. DNA in a material world. Nature 421, 427-431 (2003).
118. Seeman, N. C. From genes to machines: DNA nanomechanical devices. Trends in Biochemical Sciences 30, 119-125 (2005).
119. Ambrose, W. P. et al. Single molecule fluorescence spectroscopy at ambient temperature. Chemical Reviews 99, 2929-2956 (1999).
120. Ha, T. Single-Molecule Fluorescence Resonance Energy Transfer. Methods 25, 78-86 (2001).
121. Jares-Erijman, E. A. & Jovin, T. M. FRET imaging. Nat Biotech 21, 1387-1395 (2003).
122. Selvin, P. R. The renaissance of fluorescence resonance energy transfer. Nat Struct Mol Biol 7, 730-734 (2000).
123. Tong, A. K. et al. Triple fluorescence energy transfer in covalently trichromophore-labeled DNA. Journal of the American Chemical Society 123, 12923-12924 (2001).
124. Shchepinov, M. S. & Korshun, V. A. Design of multidye systems for FRET-based applications. Nucleosides Nucleotides & Nucleic Acids 20, 369-374 (2001).
125. Ohya, Y., Yabuki, K., Hashimoto, M., Nakajima, A. & Ouchi, T. Multistep fluorescence resonance energy transfer in sequential chromophore array constructed on oligo-DNA assemblies. Bioconjugate Chemistry 14, 1057-1066 (2003).
126. Kawahara, S., Uchimaru, T. & Murata, S. Sequential multistep energy transfer: enhancement of efficiency of long-range fluorescence resonance energy transfer. Chemical Communications, 563-564 (1999).
127. Ohya, Y., Yabuki, K., Tokuyama, M. & Ouchi, T. Construction and energy transfer behavior of sequential chromophore arrays on an oligo-DNA assembly. Supramolecular Chemistry 15, 45-54 (2003).
128. Sjoback, R., Nygren, J. & Kubista, M. Characterization of fluorescein-oligonucleotide conjugates and measurement of local electrostatic potential. Biopolymers 46, 445-453 (1998).
129. Philip Tinnefeld, M. H. M. S. Design of Molecular Photonic Wires Based on Multistep Electronic Excitation Transfer. ChemPhysChem 6, 217-222 (2005).
130. Watrob, H. M., Pan, C. P. & Barkley, M. D. Two-step FRET as a structural tool. Journal of the American Chemical Society 125, 7336-7343 (2003).

131. Philip Tinnefeld, M. S. Branching Out of Single-Molecule Fluorescence Spectroscopy: Challenges for Chemistry and Influence on Biology. Angewandte Chemie International Edition 44, 2642-2671 (2005).
132. Deegan, R. D. Capillary flow as the cause of ring stains from dried liquid drops. Nature 389, 827 (1997).
133. Deegan, R. D. Pattern formation in drying drops. Physical Review E 61, 475-485 (2000).
134. Cross, M. C. & Hohenberg, P. C. Pattern-Formation Outside of Equilibrium. Reviews of Modern Physics 65, 851-1112 (1993).
135. Magnasco, M. O. 2-Dimensional Bubble Rafts. Philosophical Magazine B-Physics of Condensed Matter Statistical Mechanics Electronic Optical and Magnetic Properties 65, 895-920 (1992).
136. Almgren, F. J. & Taylor, J. E. Geometry of Soap Films and Soap Bubbles. Scientific American 235, 82-93 (1976).
137. Cazabat, A. M., Heslot, F., Troian, S. M. & Carles, P. Fingering Instability of Thin Spreading Films Driven by Temperature-Gradients. Nature 346, 824-826 (1990).
138. Bensimon, A. et al. Alignment and Sensitive Detection of DNA by a Moving Interface. Science 265, 2096-2098 (1994).
139. Bowden, N., Bowden, N., Terfort, A., Carbeck, J. & Whitesides, G. M. 233 (1997).
140. Whitesides, G. G. M., Mathias, J. J. P. & Seto, C. C. T. Molecular self-assembly and nanochemistry: a chemical strategy for the synthesis of nanostructures. Science 254, 1312-1319 (1991).
141. Syms, R. R. A. Surface tension-powered self-assembly of micro structures - The state-of-the-art. Journal of microelectromechanical systems 12, 387-417 (2003).
142. Dussan, E. B. Spreading of Liquids on Solid-Surfaces - Static and Dynamic Contact Lines. Annual Review of Fluid Mechanics 11, 371-400 (1979).
143. Pierre-Gilles de Gennes, F. B.-W., David Quere. Capillarity and Wetting Phenomena : Drops, Bubbles, Pearls, Waves (Springer, 2003).
144. V V Krotov, A. I. R. Physicochemical Hydrodynamics of Capillary Systems (Imperial College Press, 1999).
145. Joanny, J. F. & Robbins, M. O. Motion of a Contact Line on a Heterogeneous Surface. Journal of Chemical Physics 92, 3206-3212 (1990).
146. Brochard, F. & Degennes, P. G. Collective Modes of a Contact Line. Langmuir 7, 3216-3218 (1991).
147. de Gennes, P. G. Wetting: statics and dynamics. Reviews of Modern Physics 57 (1985).
148. Darhuber, A. A., Troian, S. M., Davis, J. M., Miller, S. M. & Wagner, S. Selective dip-coating of chemically micropatterned surfaces. Journal of Applied Physics 88, 5119-5126 (2000).
149. Dennis Weaire, S. H. The Physics of Foams (Oxford University Press, 1999).
150. Velarde, M. G. Drops, liquid layers and the Marangoni effect. Philosophical Transactions of the Royal Society of London Series a-Mathematical Physical and Engineering Sciences 356, 829-843 (1998).
151. Scriven, L. E. & Sternling, C. V. Marangoni Effects. Nature 187, 186-188 (1960).
152. Brian, P. L. T. Effect of Gibbs Adsorption on Marangoni Instability. Aiche Journal 17, 765-& (1971).
153. Mysels, K. S., K; Frankel, S. Soap Films, Studies of their Thinning (Pergamon Press, New York, 1959).

154. Isenberg, C. The Science of Soap Films and Soap Bubbles (Dover Publications, Inc. (originally printed by Tieto, Ltd. Clevedon, Avon, England), New York, 1992).
155. Djuve, J., Pugh, R. J. & Sjoblom, J. Foaming and dynamic surface tension of aqueous polymer/surfactants solutions 1: ethyl(hydroxyethyl) cellulose and sodium dodecyl sulphate. Colloids and Surfaces a-Physicochemical and Engineering Aspects 186, 189-202 (2001).
156. Rayleigh. Scientific Papers (Cambridge Press, Cambridge, UK, 1964).
157. Berg, S., Adelizzi, E. A. & Troian, S. M. Experimental study of entrainment and drainage flows in microscale soap films. Langmuir 21, 3867-3876 (2005).
158. Pugh, R. J. Foaming, foam films, antifoaming and defoaming. Advances in Colloid and Interface Science 64, 67-142 (1996).
159. Murray, B. S. & Ettelaie, R. Foam stability: proteins and nanoparticles. Current Opinion in Colloid & Interface Science 9, 314-320 (2004).
160. Binks, B. P. Particles as surfactants - similarities and differences. Current Opinion in Colloid & Interface Science 7, 21-41 (2002).
161. Fan, F. Q. & Stebe, K. J. Assembly of colloidal particles by evaporation on surfaces with patterned hydrophobicity. Langmuir 20, 3062-3067 (2004).
162. Gerdes, S., Ondarcuhu, T., Cholet, S. & Joachim, C. Combing a carbon nanotube on a flat metal-insulator-metal nanojunction. Europhysics Letters 48, 292-298 (1999).